Magnetically induced directed Cell Migration as a new Approach for Therapy of *Glioblastoma multiforme*

Dissertation

zur Erlangung des Doktorgrades
des Fachbereichs Chemie
der Fakultät für Mathematik,
Informatik und Naturwissenschaften
der Universität Hamburg

vorgelegt von

Birte Mucha

Hamburg

2011

Dissertation

Gutachter 1:
Prof. Dr. Ulrich Hahn

Gutachter 2:
Prof. Dr. Regine Willumeit

Disputation
04.November 2011
Gutachter 1:
Prof. Dr. Ulrich Hahn

Gutachter 2:
Prof. Dr. Alf Mews

Gutachter 3:
PD Dr. Edzard Spillner

Gott gebe mir die Gelassenheit
Dinge hinzunehmen,
die ich nicht ändern kann,
den Mut Dinge zu ändern,
die ich ändern kann
und die Weisheit
das Eine vom Anderen zu unterscheiden.

Friedrich Christoph Oetinger

Content

I Introduction

Several works exist in the field of treatment for Glioblastoma. This work has developed a new approach, using interdisciplinary methods. The following chapters present an overview regarding cells in brain, as well as defining the astrocytes and glioblastoma cells used in this study. In focus is glioblastoma, a grade IV tumor, for which there is at present no successful therapeutic treatment.

I.1 Overview of the Cells of the central nervous system (CNS):

- Neurons: electrical signalling
- Neuroglia
  - Astrocytes: communicating with neurons and feeding of neurons
  - Oligodendrocytes: electrical isolation of neurons by myelin
  - Ependymal cells: cell layer of the ventricle system and the central canal
  - Plexus epithelial cells: excretion of Liquor cerebrospinalis
- Radialglia: leading structure during brain development, in adult brain structure in retina (muellerglia)
- Microglia: residential macrophage

I.2 The role of Astrocytes in the brain:

Fifty percent of all glia cells in the brain are astrocytes. These cells were chosen as a standard control as they represent healthy cells of the brain and because they are easier to handle within in vitro studies compared to neurons.

Astrocytes have a specific role in the brain: they clasp with their long excrescences the abluminal surfaces of capillary endothelial cells and they regulated the blood flow in the brain areas after neuronal stimulation (Wolf and Kirchhoff, 2008). Here the

diffusion of soluble reagents is blocked. In other words astrocytes act as “door-keepers”. Hence these cells are able to control the transport of metabolites between the blood and the neuropil area. Other brain cells are also well protected against toxic metals like lead and mercury.

To act as door keepers, the cells need a good protection to stand the glycolysis and neurotransmission (Benarroch, 2005, Ralph Dringen 2003) caused by toxic metals. Astrocytes are able to import and export iron actively and they are most likely involved in the transfer of iron from the periphery in the neuropil (Ralph Dringen, 2007).

Iron is essential for life (*e.g.* as a component of the haem groups or as an iron-sulphite reservoir in proteins), high iron depletion or increase can be lethal for cells. Unbound iron can catalyze the accumulation of toxic reactive oxygen species (ROS). Therefore iron transport and storage is a finely tuned process. The toxicity of iron is founded in its redox attribute. In the Fenton reaction H_2O_2 is reduced to a hydroxyl radical and a hydroxyl anion, while Fe^{2+} is oxidized to Fe^{3+}. The Fe^{3+} of this reaction can then be reduced again to Fe^{2+} by superoxide. This reduced agent (Fe^{2+}) is omnipresent and H_2O_2 is constantly produced during the cellular oxygen metabolism.

The formation of cytotoxic hydroxyl radicals is a potential risk which can damage proteins via hydration. Cells minimize this risk by storing the iron in a redox inactive form: Ferritin and by rapidly transforming H_2O_2 into water via the enzymes catalase and gluthathione peroxidase (Dringen, 2006).

Astrocytes that incorporate *in vitro* larger amounts of iron very rapidly reach their storage capacity. As a consequence they become more sensitive to oxidative stress (Hoepken, 2004). This manifestation of reactive oxygen species can lead to cellular protection dysfunction but also to iron-dependent process damage. Normally astrocytes efficiently detoxify peroxides via glutathione peroxidases (Liddell and Liddell, 2006). Additionally they are able to absorb and store large amounts of iron, normally as ferritin (*in vitro*; Torti, 2002).

Ferritin is a globular protein complex consisting of 24 protein sub-units, made up of light and heavy chains (19 kDA and 21 kDA respectively) and which is able to store 4500 iron atoms. The heavy chain performs a ferroxidase activity function, which can transform bivalent iron to trivalent iron, thus it can be stored in a redox inactive form.

Kirschvink *et al.* (1992) found that magnetic particles from the maghemite-magnetite family are present in the human brain, with a very similar structure to the crystal

morphology of magnetotatic bacteria and fish. They found a minimum of 5 million crystals per gram and a maximum of more than 100 million per gram. In fresh tissue (shock frozen) the iron content is 4 to 10 times higher (Dobson and Grassi, 1995; Banaclocha, 2009). It is suggested that astrocytes like neurons are involved in the magnetic-based storage of memory (Fredrik Stormer, 2009). Kobayashi *et al.* (1997) suggested that natural magnetite crystals in the brain and tumours are formed by Ferritin, but not spontaneously.

I.3 Gliomas:

Accounting for more than 40% of all brain tumors, gliomas are the most common primary tumors to occur in adults. Based on their aggressiveness and malignancy, these neoplasms can be categorized into three histo-pathological (specific type of cell) subgroups: ependymomas (ependymal cells), oligendendrogliomas (oligodendrocytes), and astrocytomas (astrocytes).
The World Health Organization (WHO) ratified a comprehensive classification of neoplasms affecting the central nervous system (Louis DN *et al.* 2007). According to this classification, ependymomas which usually grow slowly and are well delineated from the adjacent brain structures (but not often totally resected by neurosurgeons, de Hauwer *et al.* 1997) belong to the grade I (least aggressive), *i.e*., tumours which are slow-growing, non-malignant, and associated with long-term survival.

The oligodendrogliomas are also slowly growing tumours but are difficult to remove. This is because they have a tendency to infiltrate neighbouring brain structures and hence their histopathologic grading is controversial. Oligodendrogliomas are generally dichotomized into grade II (low grade) and grade III (high grade) tumours. Astrocytic tumours (astrocytomas) are very heterogeneous (see figure 1) on a pathologic as well as on the genetic level and are characterized by their diffuse infiltration of the surrounding brain parenchyma. Astrocytomas can be low- or high-graded tumours (Kleihues *et al.* 1993).

I.3.1 Glioblastoma multiforme:

Malignant gliomas are the most common and deadly brain tumours (van Meir et al 2010). Between 12 and 15% of all brain tumors are glioblastoma. The survival time for patients suffering from glioblastoma multiforme (the most aggressive form; WHO classification grade IV) has been extended from 10 months up to 14 months in the last five years, given better diagnosis and current standard proedures including aggressive surgery, radiation and chemotherapy (Van Meir *et al.* 2010).
Up to now no adequate / efficient therapy exists for malignant gliomas. This is mainly due to the fact that the cells are extremely mobile and infiltrate the brain by forming metastases (De Hauwer 1997). The metastases are always found to have spread within the brain and not to other tissues types.

I.3.2 Pathogenesis:

More often low grade astrocytic tumours progress during growth to higher levels of malignancy (anaplastic astrocytomas and glioblastomas see table 1; De Hauwer, 1997; Kleihues *et al.* 1995) then ependymomas or oligendendrogliomas. Hence astrocytomas represent the most aggressive form of gliomas (Mc Black 1991; Kleihues 1992). The pathogenesis of glioblastoma multiforme can be therefore *de novo* or as result of the progression of lower grade astrocytomas after therapy.

Some investigators have postulated a viral cause for malignant glioma, possibly SV40 (Miller 2009).In the studies of Regis *et al.* (2003) it was found that SV40 had a significant association with brain tumors, bone cancers, malignant mesothelioma (cancer of the mesothelium) and non-Hodgkin's lymphoma (a form of blood cancer). Another hypothesis is that the Anopheles mosquito transmit a virus, which then leads to brain tumour formation (Lehrer 2010).

WHO Grade	WHO designation	St. Anne/Mayo	Histopathology	Associated genetic alterations
I	Pilocytic astrocytoma	Pilocytic astrocytoma	Bipolar, “piloid” cells, Rosenthal fibers, eosinophilic granular bodies	Accumulation of P53 (>50%) Deletion of 17q/NF1 (<20%)
II	Ependymomas are Low grade astrocytoma	Astrocytoma Grade 1 and 2	Neoplastic fibrillary, or gemistocystic astroyctes; nuclear atypia	P53 accumulation *(>40%), p53* mutation (>25%), LOH 17p (>20%)
III	Anaplastic astrocytoma	Astrocytoma Grade 3	Neoplastic fibrillary, or gemistocystic astrocytes; nuclear atypia, mitotic activity	P53 accumulation (>50%), *p53* mutation (>30%), LOH 17p *(40%), p16 deletion (>30%), LOH 10 (>15%, 17p (25%))*
IV	Glioblastoma multifome	Astrocytoma Grade 4	Cellular anaplasia, nuclear atypia, mitoses, vascular proliferation, necrosis	P53 accumulation *(40%),p53* mutation (>25%), LOH 10 *(>60%),* 17p (25%) 19q (24%),p16 deletion (>60%)E, GF-R (>30%) and CDK4 (70%) amplification

Table1: Comparison of the World Health Organization (WHO) and St. Anne/Mayo grading system for astrocytomas -

Modified from Kleihues *et al.* 1993

I.3.3 Pathology:

The macroscopic aspect of glioblastoma multiforme is characterized by its inhomogeneous and multiple appearance: the tumour cross section often demonstrates single and multiple haemorrhage with yellowish necrosis (Kleihues 1995). Glioblastoma multiforme are histological astrocytic sophisticated tumours. The cells have multi-polar fine fibric- astrocytic differentiated appendages, or they show a fatted cellular differentiation with foamed cytoplasm. Giant cells with bizarre nuclei or minor cellular areas with less expanded cytoplasm are also possible. Here the nuclei are mostly rich in chromatin and polymorph (Cavenee 2000).
The preferential location for glioblastomas to form is within the fronto-temporal region of the brain, but the parietal lobes are also frequently affected. Typically is a rapid spreading along compact myelinated pathways is observed, similar to butterfly gliomas: a bilateral symmetric lesion after an infiltration through the corpus callosum with extension in their contralateral hemisphere (Kleihues 1995).

I.3.4 Therapy:

The standard and actual therapy for glioblastoma multiforme is a combination of aggressive surgery with chemotherapy and radiation. It is hoped that new therapies / methodologies can be developed within the next 10 years will improve the current poor prognosis for treating this form of cancer.
Radiotherapy for example, a standard tool in the therapy of such lesions, has improved in its ability to focus the beam, to better tailor it to the irregular structures of brain tumours. This has been achieved via the modulation of intensity, side effects and dose, so that damage to nearby critical structures is minimized (Stieber 2007). For some patients a new local chemotherapy with biodegradable *GLIADEL*® Wafer (polifeprosan 20 with carmustine implant; Gliadel; Eisai Inc, Woodcliff Lake, NJ) used after surgical resection of newly diagnosed glioblastomas and recurrent malignant gliomas has extended the time line of disease progression and overall survival chances (Westphal 2003; Brem 1995).
Temozolomide, is a chemotherapeutical agent with a lower toxicity profile than older agents (e.g. carmustine) that is used in conjunction with radiotherapy. Following

chemotherapy this combination has clearly improved the overall survival and due to its relatively simple administration it has the advantage of wide applicability (Stupp).
The therapeutic effect of temozolomide depends on its ability to alkylate / methylate DNA, which mostly occurs at the N-7 or O-6 positions of guanine residues, thus generating DNA damages and methylation and activating thereby the death of tumour cells (Jacinto 2007).

In the first tests performed using magnetic nanoparticles they were bound with BCNU (carmustine) to concentrate the chemotherapeutics on targeted sites in vitro and in vivo using an external magnet. When applied to brain tumours, magnetic targeting increased the concentration and retention of bound – BCNU-3 (Hua *et al.* 2010).
Biodegradable polymer fibre carriers were tested in vitro as a direct drug delivery system due to their ability to deliver BCNU over longer periods, the intension was to improve the therapeutic efficacy and reduce toxicity effects (Xux *et al.* 2006; Seong 2003). To further enhance the efficiency of anti-cancer drug-based therapies, micro-electromechanical devices (Li *et al.* 2004) and polymeric microchips (Grayson *et al.* 2003) have been designed.
Another approach is a therapy employing bevacuzimab, an antibody targeted against vascular endothelial growth factor (VEGF). This targeted therapy has found its way into clinical practice for the treatment of recurrent or progressive glioblastomas (Norden 2008).

I.3.5 Problems in therapy:

Beside the problem that most agents are unable to cross the blood brain barrier (BBB) (Lawson 2007; Groothuis 2000) and thus achieve therapeutic concentrations, most therapeutic concentrations of any drug within the central nervous system (CNS) increases the risk of systemic toxicity (Sampath 1998). Additionally, enthusiasm raised by good results obtained from new drugs must be viewed critically; because of the ability such tumours have to become resistant to such therapies (Van Meir 2010). This resistance can be explained by the high proliferation ability of cancer stem cells for self-renewal and therefore sustained tumour growth (Clarke *et al.* 2006), coupled with their resistance to conventional radiation and pharmacological treatments (Bao

et al.; Liu *et al.* 2006). Most chemotherapeutics are alkylating agents which damage the DNA primarily by pairing of O^6methylguanine with thymine during replication, leading to point mutation from guanine : cytosine to adenine : thymine (Coulondre 1977). Beside their point mutagenic potential, O^6methylguanine residues are also re-combinogenic and cytotoxic (Rasouli – Nia *et al.* 1994). As such this can lead to mutation of healthy cells and induce cancer.

Additionally, Temozolomide is a standard alkylating agent, inducing DNA damage that can be repaired by repair enzymes, such as methylguanylmethyltransferase (MGMT) for example (Hegi 2005). It has been shown that the survival times for patients are elongated if they have an MGMT non expressing tumour and if the therapy is combined with radiation (Stupp *et al.* 2005).

However the biggest problem during glioblastoma therapy is related to their mobility characteristics. The cells can migrate very rapidly, leading to high invasiveness (Demuth 2004). It is well known that cell motility is not a *de novo* feature emerging coincident to carcinogenesis, several cell types migrate actively during the stages of embryonic development, or macrophages as course of immune response (Demuth 2004). The motile behaviour of all cells is strictly controlled (refer chapter I.6), suggesting that the reappearance of a motile phenotype in cancer cells is a result of loosing of normal inhibitor controls or the cessations of these (Graham 1994), leading to high invasiveness of this tumors. Part of this invasiveness is the increased expression of proteases of the glioblastoma cells digesting the intracellular matrix. The proteases ADAMTS4 and ADMTS5 were identified as such candidates (Held-Feindt 2006). Demuth et.al. (2008) found an up regulation of the CTGF (connective tissue growth factor) in migratory glioma cell lines, but less is known about the different gene expressions. The most studies about glioblastoma cell migration want to identify involved genes using them as target for therapy. This is because the migration behaviour, in combination with a very fast growth rate, is what makes such tumours so dangerous.

Prior to, and also as a consequence of treatment, patients can exhibit the following symptoms: Aphasia, a change of personality, partial disorders or paralysis of the respiratory centre.

In standard therapies only the main tumours can be treated and removed, thus leaving many invasive cells in the surrounding tissue after surgery. This always leads to a recurrence of the tumor.

I.4 Magnetic nanoparticles in medicine:

One of the most critical points in the treatment of cancer is its imaging (*i.e*., detection of small tumours and metastases) because only early detection allows for successful treatment (Grodzinski 2006). One method to improve the resolution of imaging has been through the introduction of super-paramagnetic iron oxide nanoparticles in Magnetic Resonance Imaging (MRI) (Morawski 2005). Commercial products like Sinerem®, Resovist®, Combidex®, or Endorem® consist of carbohydrate-polymer (dextran) coated magnetite and maghemite nanoparticles diluted in water (Alexiou 2006). Using such products it is possible to detect pathological alterations in many tissues, e.g. spleen, liver, lymph nodes and brain (Stark 1988; Suzuki 1996).

Apart from their use as contrast agents magnetic nanoparticles could more widely be employed in the field of biomedical applications and techniques, for example in magnetic separation (cell and macromolecule separation and purification), immunoassays, controlled drug release, gene therapy, hyperthermia or as a magnetically guidable carrier e.g. in drug delivery systems (Alexiou 2006; Babincova 2009).

This has led to many different types of small particles being developed including magnetic microparticles, magnetoliposomes (Kubo 2000; Kückelhaus 2004) and various magnetic nanoparticles.

Several studies approaches have focused on specific nanoparticles that have been designed to be able to target different types of cancer, such as for breast cancer for example (Li X 2009).

Depending on the approach employed, different types of magnetic fields (homogeneous, alternating and inhomogeneous), magnetic strengths and magnetic gradients are required. Another important parameter is the size of the nanoparticles. Particles with a hydrodynamic diameter of about 100nm seem to be most suitable; these consist of conglomerates made up of single domain particles of 10-15nm diameter (Alexiou 2006) and are super paramagnetic. Larger particles rather than smaller one are incorporated by the Mononuclear Phagocyte System (MPS) (Sachdeva 1998).

I.5 Magnetotaxis in Bacteria

Magnetic orientated migration of single cells is known for some prokaryotes, they use biomagnetic functions to orientate themselves.

Several types of bacteria originating from different families are classified as magnetic bacteria e.g. Desulfovibrio magneticus RS-1 (Sakaguchi *et al.* 2002) Magnetobacterium bavaricum (Spring 1995), Magnetotactic multicellular Prokaryote (MMB) (Greenberg 2005), Marine magnetotactic coccus (Frankel 1997), Magnetospirillum gryphiswaldense (Schultheiss 2004) and Magnetospirillum magneticum AMB-1. As it is possible to cultivate Magnetospirillum magneticum AMB-1 under in vitro conditions, it has been relatively well studied.

Magnetotactic bacteria contain so called magnetosomes: Intracellular single domain magnetic crystals surrounded by phospholipid membranes (Gorby *et al*. 1988). Transmission electron microscopy studies have shown that the magnetite crystals (50-100nm in diameter) are enveloped by a bilayer membrane of approximately 2-4 nm in thickness (Matsunaga 2003).
The magnetosomes are structured in chain-lines perpendicular to the cell axis (Matsunaga 2003). The result here is rather like a compass needle.
This results in a structure somewehat like a compass needle and allows the cell to migrate along the Earth's geomagnetic field lines, positioning the bacteria within the boundary of the oxic-anoxic transition zone (OATZ) (Bazylinski 1999). This magnetic sensing is coupled with an aerotactic sensory mechanism (Frankel 1997). Magnetotactic bacteria use this guidance after exposure to oxidative stress to reach habitats with low or no oxygen and/ or redox gradients (Frankel 1997). In the northern hemisphere the cells swim parallel to the Earth's magnetic field (north-seeking motility) whereas bacteria in the southern hemisphere swim in the opposite direction (south-seeking motility). This results in the bacteria migrating along the downward or upward- inclined geomagnetic field lines in the respective hemispheres (Blakemore *et al.* 1980).

Prokaryotes have potential for use as a model system to gain a better understanding of the magnetotaxis of more highly organized forms of life e.g. vertebrates or

eukaryote cells, and to optimize culture conditions for industrial–scale production of biotechnological processes (Mastunaga1996). One example is in the use of natural magnetite crystals for biomedical therapies like hyperthermia. Because the magnetosomes are produced by a living organism and not artificial it should be possible via genetic engineering to design special natural biomimetic nanoparticles for different applications. Another idea is to use induced magneto taxis for cancer treatment.

I.6 Principle of Cell Migration

n mammals most cells move via crawling, with one exception being sperm that swims. During embryogenesis the structure of an animal is organized by the migration of single cells (Lauffenburger 1996), which define the location and the coordinated migration of whole epithelial layers. Long distance migration is needed, for example, in the construction of the full nervous system. Here actin-rich growth cones that form on the leading edge of a newly built axon must find their way to their synaptic goal. This is achieved through a combination of soluble and on cell surfaces and matrix bound signals (Dent 2003).
Unfortunately the issue of cell migration is very important for certain cancer types. If cells of a primary tumour for example infiltrate neighbouring tissues (e.g. glioblastoma) or / and pass into the blood and lymph system (e.g. breast cancer), they can move to different locations within the body and thus build metastases in these regions. The movement of the cells is a highly complex integrated process, consisting of the actin-rich cortex under a plasma membrane (see figure 2, Alberts 2011). This moving process can be well organized and fluent with no observable change of phenotype (e.g. keratinocytes of a fish), while in other cells like fibroblasts the movement activities are independent of each other, leading to a jerky movement (Wen Tien Chen 1981).

Depending on cell type the type of built movement structure will differ, e.g. filopodia, lammelipodia or pseudopodia.

Filopodia: Are a one dimensional long and thin structure with a long core of bundled actin filaments, formed by moving leading edges and some fibroblasts.

Lamellipodia: Are two dimensional structures similar in form to leaves, with an orthogonal Network of actin filaments, most of them parallel to the subsoil. These structures are formed by epithelial cells, fibroblast and some nerve cells such as astrocytes.

Pseudopodia: Are three dimensional short structures filled with a gel of actin filaments, formed by amoeba and neutrophile cells.

Best known is the structure of lammelipodia and hence it is primarily used as an example of actin nucleation and resulting cell migration.
The actin filaments in this lammelipodia are orientated into plus (forward) and minus (to cell nucleus). The minus ends are hidden by the Arp2/3 (actin related protein) complex; this protects degradation of the actin filament and assists the nucleation of the actin at the plus end (forward) (Millard 2004). Arp2/3 are linked to other actin filaments building a two dimensional network (see figure 3).

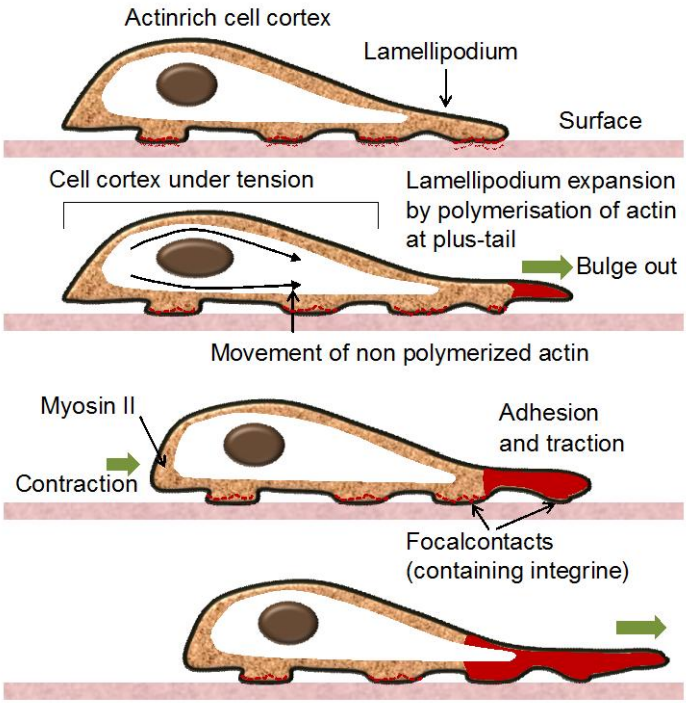

Figure 1: Model of cell movement

Three different processes are involved: excrescence, whereby actin-rich structures at the top of the cells stretch out;
Adhesion, in this state the actin cytoskeleton is connected with the subsoil through the plasma membrane, and tension which pulls the cytoplasm forward (adapted from Alberts 2011, Molekulare Zellbiologie, Wiley VCH, chapter 16).

The tractive forces created by a moving cell transmit considerable tension on the substrate. Contrariwise is generated mechanical tension and distension in cells responsible for building stress fibres and focal adhesions such that the cell becomes more contractile (Harris 1980). Although poorly understood, it is thought that the mechanical interaction between cells and their real environment is a fundamental factor in the self organisation of mammal tissue. For locomotion a cell initially needs a polarisation (definition of front, back etc.) to achieve a defined direction of movement.

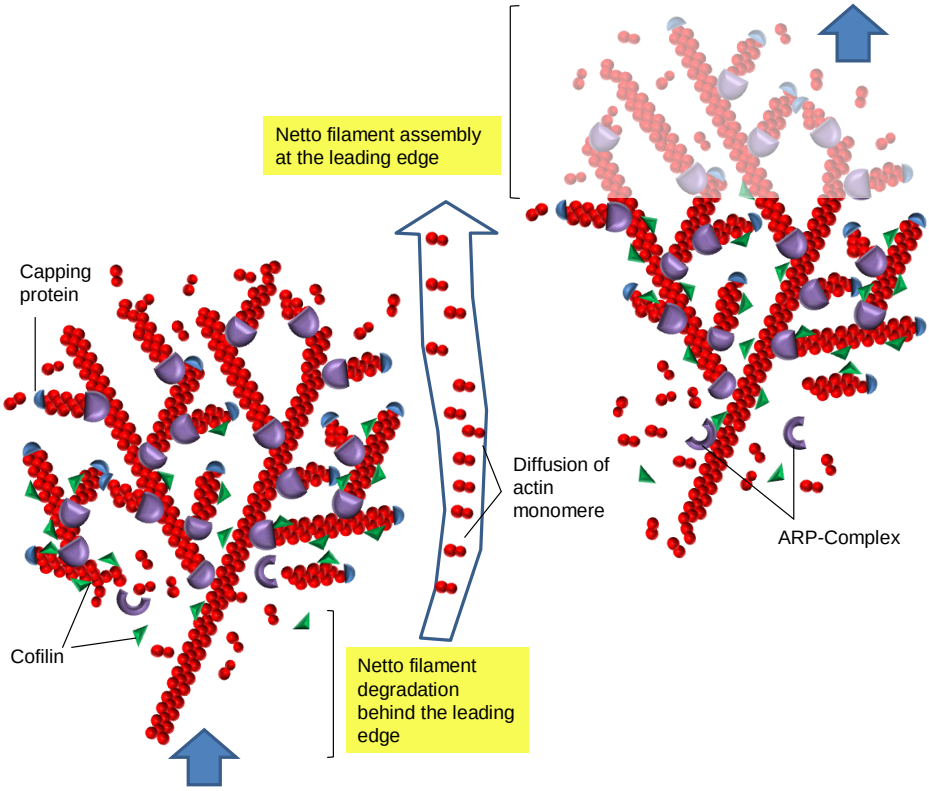

Figure 2: Model of the forward movement of actin network at the leading edge. (adapted from Molekularbiologie der Zelle, 2011, Wiley VCH)

Presented is the time interval of a forward movement of a lamellipodia (new structures bright colour). Germ building is mediated by the Arp2/3 complex at the front. Newly built actin filaments are linked to the network in an angle of 70 degrees. Via the elongation of the actin filaments the plasma membrane is pushed forwards, because the retrial network acts as an anchor. With consistent speed the plus ends of the actin filaments are capped. After hydrolysis of ATP in the new branches, the retrial network can be depolymerised by cofilin. This cycle causes regional disconnection between the netto-filament degradation and netto filament.

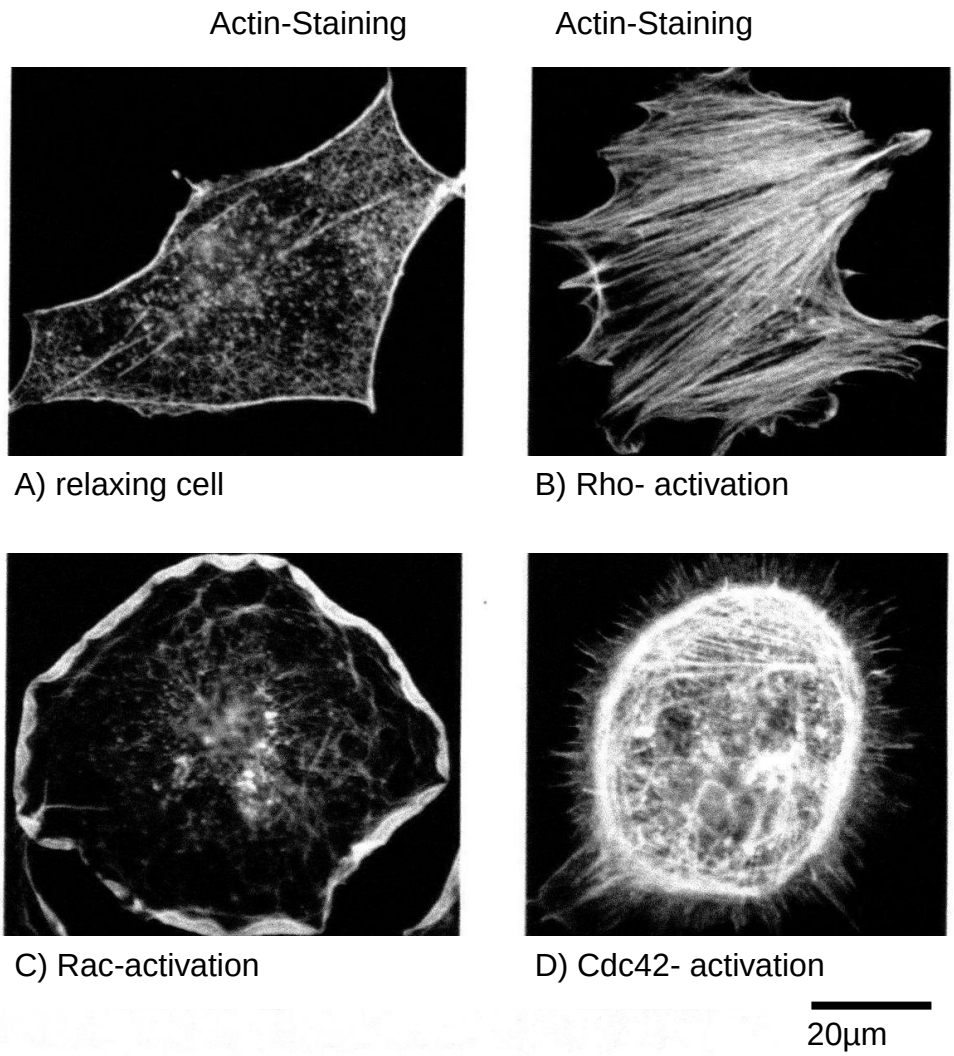

Figure 3: Effects of Rac, Rho and Cdc42 to the actin organisation of Fibroblasts

Staining of the actin filaments with the fluorescent marker phalloidin.

A) Fibroblast, incubated without Serum, showing actin filaments mainly at the cell cortex and relatively low stress fibres. B) Micro-injection of a constitutive activated form of Rho resulting in a fast building of many stress fibres. C) Micro-injection of a constitutive activated form of Rac, a monomere GTPase (Rho family), resulting in the formation of a large lamellipodium surrounding the whole cell. D) Micro-injection of a constitutive activated form of Cdc42 (as well Rho family) resulting in the formation of many small filopodia at the cell surface. The different effects of these three GTPases on the organisation of the cytoskeleton are mediated by many other proteins and regulated by other GTPases. N-WASP and other proteins named in this chapter belonging to these cytoskeleton organisation proteins (pictures: Hall 1998, text adapted from Alberts 2011).

Later it was found that human Scar binds to the Arp2/3 complex and that this interaction stimulates the actin filament nucleation activity of the complex (Machesky 1999; Machesky 1998).
Rohatgi et. al (1999) demonstrating that binding of N-WASP with an active form of Cdc42 enhances the ability of the protein to activate Arp2/3. So for the first time a signalling pathway for actin nucleation was identified.

Nucleation process with Arp2/3 drives locomotion forward and is regulated by WASP (Wiskott Aldrich Syndrom Protein) family members.polymerisation at the front (Pollard 2003), resulting in a forward movement by stationary filaments to the substrate.

In Mammals five WASP family members have been identified:
WASP, N-WASP (Neural WASP), Scar/WAVE1, Scar/WAVE2 and Scar/WAVE3 (Miki 1998).
In connection with Cdc42 (cell division cycle protein 42; see figure 4), a small GTPase known as an important actin regulator (Symons 1996), WASP was originally described as a protein that could induce actin polymerisation.
Changes of the main structures of cytoskeletons are mediated by some GTPases (Hall 1998), all members of the Rho family (see figure 4). In the case of Cdc42 the cell shows a high activity with the building of many Filopodia, the cell migrates. Because Cdc42 is interacting close with N-WASP to activate actin nucleation, this was a focal point for this work. Because Cdc42 also regulates signalling pathways controlling diverse cellular functions e.g. cell morphology, endocytosis, migration and cell cycle progression, for this thesis an analysis for the activity of the N-WASP was more suitable.

I.7 Aim of this thesis

Fundamental to this study has been the invasive migratory nature of *Glioblastoma multiforme* tumor cells and the fact that currently there are insufficient therapy approaches to remove these from regions surrounding a tumor. This has led to the idea of making use of the otherwise poor migratory behaviour of tumour cells in combination with the magnetic properties of nanoparticles, creating thereby a new therapeutic model for medically handling of such aggressive cancers.

The aim of this thesis was to develop a new therapy whereby nanoparticle loaded cells are polarized in an external magnetic field and thereby activated through magnetically induced gradients to purposefully migrate.
This therapy, if applied to patients in the future, should make it possible to collect the invasive and inaccessible cells from the region of the brain adjacent to the tumor and purposely migrate these cells to a pre-defined location for further medical treatment.

I.7.1 Open questions at the beginning of the thesis:

Since at the start of this work no parameters were known the work has concentrated itself on answering the following fundamental questions:

Are the nanoparticles incorporated by the cells and do they have toxic properties?
What form must the magnetic field take for basic in vitro research studies and how strong must the magnetic field be?
If the cells incorporate the nanoparticles, where are the nanoparticles located in the cells and how high must the iron content be within a cell for it to be moved in a magnetic field?
Last but not least if it’s possible to achieve a directed movement of the cells, which biochemical changes can be detected in the cells?

II Materials and Methods

II.1 Materials

II.1.1 Consumables:

6 Well-Plates	Greiner Bio-One GmbH, D
12 Well-Plates	Greiner, Nürtingen, D
Nonreturnable Pipettes	TPP,Trasadingen, Ch
15ml+ 50ml Polypropylentubes	Greiner Bio-one GmbH, D
Cryo Tank	MVE Inc. Bloomington, USA
Mini Tubes	Eppendorf AG, Hamburg, D
Pipette Tips	Eppendorf AG, Hamburg, D
Cell culture flasks	NalgeNunc International, NY, USA
Cryotube	NalgeNunc International, NY, USA
Chamber Slides (Lab-Tek)	NalgeNunc International, NY, USA
Chambered Coverglasses (Lab-TekII)	NalgeNunc International, NY, USA
T 75 cell culture flasks blue filter cap	NalgeNunc International, NY, USA

II.1.2 Chemicals:

Anti N-WASP phospho-specific	Millipore, D
Bisbenzimide Hoechst 33342	Sigma Aldrich, USA
Counter Isoton II Diluent	Beckman Coulter Inc, USA
DMEM®	Invitrogen™, Grand Island, N.Y., USA
DMSO	Sigma Aldrich, USA
Cell mask (membrane)	Invitrogen™, Grand Island, N.Y., USA
ER Tracker	Invitrogen™, Grand Island, N.Y., USA
Fetal Calf Serum (FCS)	PAA Laboratories GmbH, Austria
37% Formaldehyd	Sigma Aldrich, USA

HP-Sätze H 301, 311, 314, 317, 331, 351

P 260, 280.1-3,7, 301+310, 303+361+353, 304+340, 305+351+338, 308+313, 403+233

Eosin B	Sigma Aldrich, USA
100% Ethanol	Merck KgaA, Darmstadt, D

HP-Sätze H 225 P 210, 403+233

Hydrochloric acid fuming (37% HCl)	Merck KgaA, Darmstadt, D

HP-Sätze H 314, 335 P 260, 280.1-3+7, 301+330+331, 303+361+353, 305+351+338, 310

IgG (H+L) goat anti rabbit	Dianova
KCl	Merck KgaA, Darmstadt, D
KH_2PO_4	Merck KgaA, Darmstadt, D
LIVE/DEAD® (Viability/Cytotoxicity Kit for mammalian cells)	Invitrogen™, Grand Island, N.Y., USA
Lyso Tracker Yellow	Invitrogen™, Grand Island, N.Y., USA
Lyso Tracker Red	Invitrogen™, Grand Island, N.Y., USA
NaCl	Merck KgaA, Darmstadt, D
Na_2HPO_4	Merck KgaA, Darmstadt, D
Nitric acid Suprapure	Sigma Aldrich, USA

HP-Sätze H 272, 314 P 220, 260, 280.1-3+7, 303+361+353, 304+340, 305+351+338, 310

Nanoparticles solutions	Academy-Timisoara Devision, Romania
Paraffin-oil	Sigma Aldrich, USA
Penicillin/Streptomycin	Gibco, invitrogen, NY, USA
Potassium ferrocyanide trihydrate	Sigma Aldrich, USA

HP-Sätze H 412 P 273

RNA Later	Applied Biosystems
Trypsin-EDTA (0,05%)	Gibco, invitrogen, NY, USA
Yttrium Standard for ICPMS	Merck KgaA, Darmstadt, D

II.1.3 Kits

iScript RT-qPCR Sample Preparation Reagent	Biorad, D
iScript cDNA Synthesis Kit	Biorad, D

II.1.4 Buffer and solutions

Actin-Staining solution	1 mL 1x PBS 25 µL phalloidin 10 µL DAPI –solution 1% BSA
Antibody Solution 1	Anti N-WASP 1:1000 diluted in Blocking solution
Antibody Solution 2	Texas Red marked Antibody 1:100 in Blocking solution
Blocking Solution	1xPBS 1% Triton X100 2% BSA
DAPI-Stock solution	5 mg DAPI 10 mL ddH_2O Store at 2-8°C
DAPI-Working solution	1 µL DAPI stock solution 49 µL ddH_2O (=1 µg/µL)
Life-Dead-Staining-Solution	2 µL Calcein AM 5 µL Ethidiumhomodimer-1 5 mL PBS
Fibronectin solution	100 µL Fibronectin Stocksolution (100ng/mL) 900 µL PBS
3.7% Formaldehyde solution	1 mL Formaldehyde (37%) 9 mL PBS

10% Formaldehyde solution	10mL Formaldehyde (37%) 27 mL dH_2O
20% hydrochloric acid	20 mL HCl (37%) 17mL dH_2O
PBS (Phosphate buffered saline) .	8.00 g NaCl 0.20 g KCl 1.44 g Na_2HPO_4 0.24 g KH_2PO_4 1L ddH_2O pH 7.4 with 10 M NaOH
10% Potassium ferrocyanide solution	10 g Potassium ferrocyanide trihydrate Filled up to 100 mL with dH_2O

II.1.5 Media

DMEM GlutaMAX-I:
Gibco® DMEM(1x)(+)Glucose 4,5 g/L(+)GlutaMAX™(+)Pyruvat (GlutaMAX)
For the cultivation of cells the medium was completed with Fetal Calf Serum (FCS).
Media for the cultivation of Glioblastoma multiforme:

GlutaMAX-I +10% (V/V) FCS

Media for the cultivation of human primary Astrocytes:

GlutaMAX-I + 15% (V/V) FCS

II.1.6 Human cells

Glioblastoma multiforme: G44, G55, G112, G122
Primary Astrocytes1

The cancer cells used for this thesis were provided by Professor Katrin Lamszus (Neurosurgery, University Clinical Eppendorf, Hamburg, Germany).

The cells were chosen due to their efficient migration behaviour. Primary astrocytes, represent 50% of normal brain tissue. Therefore, they were chosen as the control in this study.

II.1.7 Equipment

Incubator	Thermo Scientific BBD 6220, Heraeus CO_2/O_2 Heracell 150i incubator Heraeus instruments™
Pipettes	Eppendorf™
Microscope	Axiovert 25, Zeiss™
Clean Bench Cl.2	Hera Save, Heraeus instruments™ ; Scanlaf cell culture bench
Water bath	Fa. Memmert
Ice machine	Scotsman AF-80
Flüssigstickstoffbehälter	MVE SC20/20, CHART/MVE
Cell counter	Particle count & analyzer Z_2, Coulter™
Centrifuge (15ml+ 50ml tubes)	Labofuge 400R, Heraeus instruments™
Table-Centrifuge (Minitubes)	Heraeus Biofuge Pico
Cooling Centrifuge (Minitubes)	Eppendorf centrifuge 5415C
Rotoshake Genie	Scientific Industries, Bohemia, NY
Cold room (4°C)	Viessmann
N_2-container	SC20/20
- 80°C freezer	Viessmann
- 25°C freezer	National Lab
Fridge	Bosch
Ultrasonic bath (small)	SONOREX
Microscope	Nikon TIS Eclipse, Nikon, Japan
Microwave	Severin MW7800 microwave
Dishwasher	Miele

Autoclave	Gössner GVA 4.6
Magnet stirrer	IKAMAG RCT
Analyse balance	Scaltech SBA 32
Vortex Genie 2	Scientific Industries, Bohemia, NY
Mastercycler Personel	Eppendorf
Real time PCR	C1000 Thermo Cycler CFX96, Biorad
pH-meter	Hannah pH 211

II.2 Methods:

II.2.1 Preparation of nanoparticles:

Two different magnetic ferrofluids (Bica 2007) were used in the study, synthesized by Doina Bica. They consisted of magnetite nanoparticles, that were stabilized by coating with a double layer of two types of fatty acid (NP-MA = double layer of myristic acid and NP-LA = double layer of lauric acid).
The nanoparticles were synthesized through chemical co-precipitation followed by sterical stabilization in a water carrier of the resulting magnetic nanoparticles.

The main steps of the preparation route are given below:
215mL of 1M $FeSO_4$ solution and 130mL of 2.8M $FeCl_3$ solution were applied under atmospheric conditions resulting in a Fe^{3+}/Fe^{2+} factor of 1.7. The reaction mixture was heated to 80-82°C under continuous stirring, and 300mL of NaOH(6N) was then added.
After co-precipitation the magnetite nanoparticles were coated by a surfactant via the addition of 24g of myristic or lauric acid at 80°C. The phases were separated after 20min by decantation, the resulting magnetic organosol was washed with distilled water to eliminate any residual salts.
The nanoparticles that had been coated with a double layer of fatty acid were dispersed in a weak solution of NaOH or NH_4OH to obtain the required pH. At least 100 mL of the resulting magnetic fluids were purified by magnetic decantation / filtration with a saturation magnetization of 12kA/m.
The mean diameter of the nanoparticles determined using TEM analysis was 4.3 ± 0.08 nm with a standard deviation of 1.3 ± 0.07nm for NP-MA particles and a mean diameter of 6.1 ± 0.15 nm with a standard deviation of 2.4 ± 0.13 nm for NP-LA particles.
Structural characterisation of the nanoparticle containg solutions was carried out by small-angle scattering with polarized neutrons (Feoktystov 2009).
The iron content of the ferrofluids for biological purposes was analyzed after sterile filtration (0.22 µm pore size) using ICPMS.

II.2.2 Cell culture methods:

II.2.2.1 Thawing of cells:

The cells were gently warmed to room temperature. Two cell culture flasks with preheated DMEM Glutamax I media containing 10% FCS (fetal calf serum) for Glioblastoma cells and 15% FCS for astrocytes (4mL, 10 mL or 25 mL for small, medium or large sized flasks) were prepared.

The thawed cell suspension was gently mixed by pipetting up and down.

The suspension was divided into two prepared cell culture flasks in which the cells were incubated at 37°C with 90% relative humidity and 5% CO_2.

In order to remove any dead cells and DMSO the media was changed on the following day.

II.2.2.2 Cultivation of cells

The cells were grown to a confluence of 80%. As stated above the environment consisted of a temperature of 37°C with a relative humidity of 90% and 5% CO_2.

The medium was changed every two or three days. If and when the cells reached 90% confluence, they were divided.

II.2.2.3 Splitting procedure

Normally the denseness of the cells should measure approximately 80% confluence. If the density however increased beyond this limit the cells were split. Here the medium was removed and the cells were washed once with 1x PBS (phosphate buffered saline). After removing the PBS the flasks were filled with 2mL, 4mL or 6 mL Trypsin (for small, medium or large sized flasks).

Small flask	Middle flask	Big flask
2ml Trypsin	4ml Trypsin	6ml Trypsin
+ 4ml medium	+ 6ml medium	+10ml medium

To detach the cells from the surface of the flasks, the flasks were incubated for 3min at 37°C. After this incubation time the cells were loosened by gently knocking on the

flask. To stop the enzymatic reaction, the cell – trypsin suspension was mixed with medium containing FCS.

To get a homogeneous cell suspension with single cells, the mixture was gently pipetted up and down and transferred into a 15mL or 50mL polypropylentube. A sample of 50µL was retained for cell counting and transferred into 10mL of cell coulter solution (or CASY solution). Cell counting was performed at Cell Coulter or CASY.

The polypropylentubes with the cell suspension were centrifuged for 5min at 1500rpm to pellet the cells. After centrifuging the supernatant was removed and the cells were resuspended in fresh medium containing FCS.

For a large cell culture flask, 500.000 cells of Glioblastoma or 300.000 cells of astrocytes were cultivated in 25mL complete medium. The cells were used for experiments or grown at 37°C, 90% relative humidity and 5% CO_2 in the incubator.

II.2.2.4 Cryopreservation

For long-term storage the cells were frozen. Here the cells were first trypsinized, see II.2.2.3. After pelleting the cells using centrifuging, the supernatant was removed and the cells were washed with 3mL 1x PBS. The cells were then once again centrifuged for 5min at 1500rpm. After removing the supernatant the cells were resuspended in FCS containing 10% DMSO for a final concentration of 1Mio/mL.

The cell suspension was filled in a cryo tube up to a maximum of 1mL. The cryo tubes were transferred into a freezing box filled with isopropanol (room temperature), thereafter the box was placed into a freezer at -80°C.

Isopropanol cools at a constant rate of -1°C/min , thus avoiding the formation of ice crystals within the cells. For long-term storage the cryo tubes were transferred after 24h into a nitrogen container (-175°C).

II.2.2.5 Measurement of cell proliferation

- The cells were grown to 70% confluence. After removing from the media, the cells were washed with 1x PBS and trypsinized (37°C, 3 min). The Trypsin reaction was stopped by adding a media containing FBS. 50µl of the cell suspension was transferred into 10mL of coulter solution and counted with the cell coulter.

  The remaining cells were pelletised by centrifuging for 5min at 1,500 rpm. Subsequently the supernatant was discarded and the cells resuspended in an adequate volume of fresh culture medium to reach a concentration of 1 Mio/mL.

- Five 12-well plates were prepared by adding 2 mL of: culture media (*i. e*., 4 wells), culture media complemented with 0.25 µL/mL (21 µg Fe/mL) of nanoparticle containing solution (*i. e*., 4 wells), and culture media complemented with 0.5 µL/mL (42 µg Fe/mL) of nanoparticle containing solution (*i. e*., 4 wells).

  In every well 20,000 cells were seeded and incubated for 1 to 5 days at 37°C. On the third day, 500 µL of fresh medium was added (“to feed the cells”).

- One plate was analyzed each day. Here, the cells were washed with 2 mL 1x PBS and then treated with 500 µL trypsine (37°C, 3min). The reaction was stopped with 2mL of a cell specific medium and homogenized via pipetting thoroughly. 50 µL of this suspension was used for cell counting. Furthermore quadruplicate cell numbers for every concentration per day could be achieved by applying this procedure.

II.2.3 Immunochemical and Biochemical Investigations

II.2.3.1 Berliner Blue Staining

Berliner blue staining was conducted to show that the cells incorporated the nanoparticles. The reaction is iron dependent and builds a blue color complex. Protocol is modified by Perls (1867).

20,000 cells were seeded in 12 well plates or chamber-slides and incubated at 37°C overnight with different concentrations of nanoparticles in the media (0; 21 µg Fe/mL and 42 µg Fe/mL). After 48 h the media were soaked and the cells were washed with 1x PBS and afterwards fixed with 10% formaldehyde (1h).

To remove formaldehyde deposits the cell were washed 3 times with 1x 1mL PBS for 1 min. After 5min pre-incubation with potassium ferrocyanide trihydrate solution (1mL; 10%), 1mL of 20% hydrochloric acid was added and incubation took place for a further 30 min. After washing four times with dH_2O for 5 min, 1 mL eosin B was added and incubated for 30 min. Thereafter the cells were again washed twice for 5 min and then dried with ethanol as outlined below:

- 2min ethanol 60%
- 2min ethanol 70%
- 2min ethanol 80%
- 2min ethanol 96%

The cells were covered with paraffin-oil (1 mL/well; if using a well plate) or with DAKO mounting medium (one drop; if a chamber-slide had been used) and a cover-glass.

II.2.3.2 Live Dead Staining

Calcein AM and Ethidiumhomodimer-1 must always to be stored at **-20°C**. After preparation of the staining solution this solutions was immediately returned to the refrigerator. Additionally to avoid hydrolyses of calcein AM the staining solution was always prepared directly prior to staining.

The cells were seeded in the first two wells of chamber cover glasses (20,000 cells/well) which contained 400µL medium supplemented with nanoparticles-solution to final concentrations of 21µg Fe/mL and 42µg Fe/mL, or zero (this was performed twice) for two days. After an incubation time of 48h the media was then removed and the cells were washed with 1x PBS.

400µL of fresh medium containing no nanoparticles was added to each well. Thereafter half of the chamber cover glasses were placed in a magnetic field. The other half were used as the control group, not having undergone exposure to the magnetic field. The cells were incubated again for 24h at 37°C, 90% relative humidity and 5% CO_2.
For the staining procedure the media was removed and the cells washed with 1x PBS. In each well 50µL of LIVE- DEAD staining solution was added and incubated for 20min at 37°C in total darkness. On approaching the end of the incubation time the staining solution was replaced with PBS. Micrographs were immediately taken to identify living cells. (Invitrogen)

II.2.3.3 Actin Staining including immunhistochemical experiment

The actin staining was performed with Alexa Fluor 488 phalloidin, a toxin from the fungus Death Cap against F-actin marked with a green fluorescence dye. For staining of the nuclei DAPI was used.
Antibody 1 (Anti N-Wasp, rabbit anti human) is an antibody against the phospho specific form (active form) of N-WASP, a protein involved in the nucleation process of F-actin.
Antibody 2 is an IgG (H+L) goat anti rabbit Texas Red conjugate.
In the first two wells of chamber cover glasses 400µL of cell culture media (DMEM Glutamax-I) containing zero, 0.25µL/mL (21µg Fe/mL) or 0.5µL/mL (42µg Fe/mL) of nanoparticles and 5000 cells were added.
The cells were incubated at 37°C in the incubator for 2 days.

After incubation the cells were washed with 1x PBS and further incubated for 24h within a nanoparticle free media in a magnetic field. For the control a chamber cover glass with cells having undergone the same pre-incubation were again incubated without exposure to the magnetic field.

The cells were washed with 1xPBS and fixed with 3.7% formaldehyde for 10min, then washed twice with 1xPBS. Thereafter the fixed cells were incubated for 2h with

a blocking solution. The solution was then removed and antibody solution 1 was added and this was then incubated for 1h in a relative humidity of 90%.
The cells were washed again three times with 1x PBS for 5min, then incubated with antibody solution 2 for 1h. Again the cells were washed three times with 1xPBS for 5min.

Counterstaining

200 µL actin –staining solution was further added to each well. The lids from each chamber cover glass were closed and these then stored in darkness at room temperature for 20min.
Staining was completed after this incubation step. Prior to proceeding with microscopy and storage, the cells were washed once with 1x PBS and covered with 400 µL 1x PBS.

Microscopy:

3D Photographs were taken in fluorescence modus using a Nikon Ti-S microscope with an automated Prior Maerzhaueser xy- table and z-drive at 100x magnification.

II.2.3.4 Cell Organelle Staining

In the first two wells of chamber cover glasses, 400 µL cell culture media (DMEM Glutamax-I) containing zero, 0.25µL/mL (21µg Fe/mL) or 0.5µL/mL (42µg Fe/mL) nanoparticles and 5000 cells were added.
The cells were incubated at 37°C in the incubator for 2 days.
Thereafter the cells were washed with 1x PBS and incubated for 24h with nanoparticle free media within a magnetic field. As a control, a chamber cover glass with cells having the same pre-incubation was incubated without exposure to the magnetic field.

To proceed with the cell organelle staining the cells were washed with pre-warmed 1x PBS. Here 200µL of PBS per well was added that contained DAPI, Lyso Tracker Red and ER-Tracker as indicated below in the given concentrations.

Staining solution	Ex	Em	Filter	Concentration
Lyso Tracker Red	577	590	Texas Red	50mM in PBS
ER-Tracker	504	511	FITC	1µM in PBS
DAPI	340	465	DAPI	1µL /mL in PBS

Table 2: Filter and concentration set ups for cell organelle staining

The cells were incubated for 30min at 37°C in total darkness. For longterm storage the cells were fixed in 3.7% Formaldehyde for 5min.

II.2.4 Physio-chemical Methods

II.2.4.1 Iron quantification using Inductively Coupled Plasma Mass Spectrometry (ICP-MS)

Inductively coupled plasma mass spectrometry (ICP-MS) represents an important method for the parallel quantitative determination of multiple elements in various sample matrixes. Depending on the sample introduction system; liquid, gaseous or solid samples can be analyzed.

The main advantages of this technique is its high sensitivity (normally in the low ng L^{-1} range for most elements) as well as the possibility of analyzing nearly all elements of the periodic table with only a few exceptions. Figure 4 indicates the elements detectable by ICP-MS.

Preparation of the consumables

Three polypropylene tubes for each sample, +10 (calibration) were prepared ???.

To each 15mL polypropylene tube 1mL nitric acid and 9ml ddH2O were added. The closed polypropylene tubes were gently shaken and incubated for two days under the extractor hood. The acid solution was discarded in the appropriate acid waste. The tubes were washed twice with ddH_2O and air-dried under a clean-bench. The dried tubes were closed and stored in a plastic bag until required.

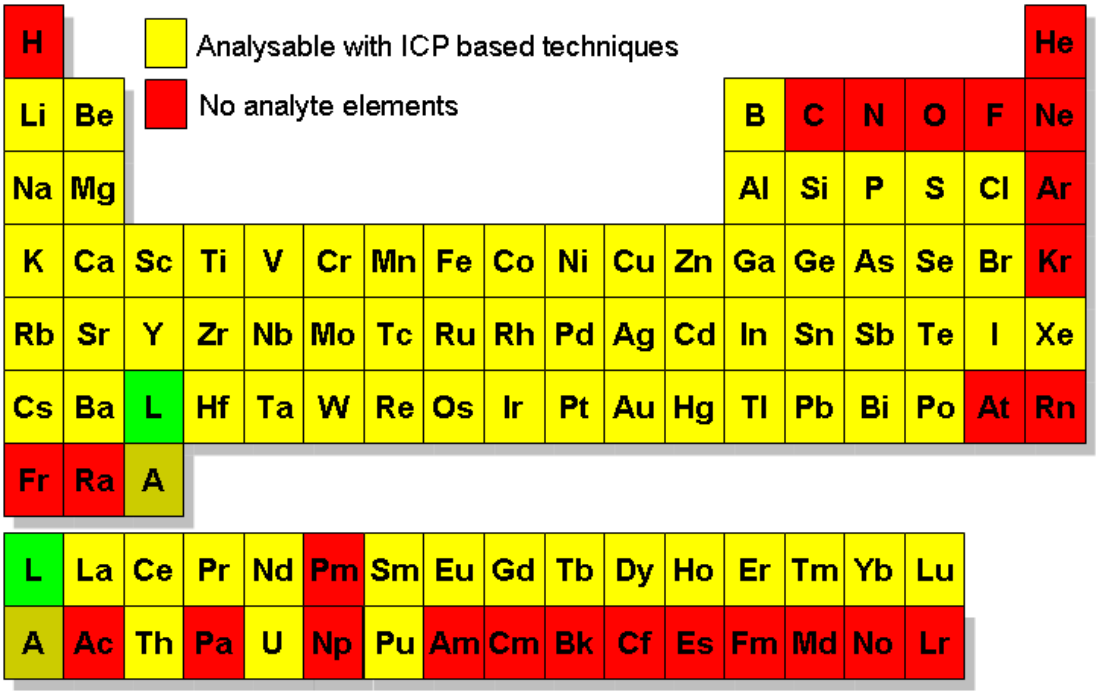

Figure 4: Schematic view of the periodic table indicating ICP-MS detectable elements.

Experimental procedure

1. The cells were trypsinized, counted and pelletised by centrifugation. The cells were then resuspended to obtain a final concentration of cells per mL media of 2Mio/mL.

Three T75 cell culture flasks were filled with 10mL media containing zero, 0.25µL/mL (21µg Fe/mL) and 0.5µl/ml nanoparticles (42µg Fe/mL) of NP-MA or NP-LA. Thereafter 750µL cells (1,5Mio) were added and then incubated at 37°C for two days. The cells were then trypsinized, counted and pelletised.

The pre-incubated cells were used for different experiments in the following matter:

As a base line sample cells were resuspended in media to a final concentration of 2Mio/mL.

a. Magnetically directed migration

50,000 cells per chamber-slide and sample were used.

(Description in results: Development of the magnetic field and magnetically directed migration assay)

2. The remaining cells (minimum 400,000) were centrifuged, removed from the supernatants, washed with 1x PBS and centrifuged again. The supernatants were discarded and the cells resuspended in ddH_2O to a final concentration of 1mio cells /mL. The samples were collected and stored at -20°C until step 3.

3. The samples were ultrasonically homogenised for 2min at 15°C.
Each sample was split into three: 100µL into each of the prepared falcons, where 50µL of the Yttrium standard solution and 900µL of sub boiled nitric acid (65%) were added. The samples were incubated overnight at room temperature under the extractor hood.

4. On the following day 8,950µL of ddH_2O was added to a total volume of 10mL. This was carefully homogenised by shaking and then measured for iron concentration on an Agilent 7500cs ICP-MS detector system using the experimental conditions indicated in Table 3.

ICP-MS Agilent 7500c	
RF power	1500 W
Carrier gas	0.84 L min^{-1}
Makeup gas	0.28 L min^{-1}
Extraction lens 1	5 V
Extraction lens 2	- 180 V
Octopole bias	- 18 V
Quadrupole bias	- 16 V
Cell gas	5 mL min^{-1} H_2
Spray chamber Temperature	4 °C
Measured isotopes	^{54}Fe, ^{56}Fe, ^{57}Fe, ^{89}Y, ^{115}I
Dwell time	0.1 s

Table 3: Instrumental conditions used for measurements.

The analysis of iron using ICP-MS is hampered due to the formation of polyatomic ions such as $^{40}Ar^{16}O^{+}$, which are formed inside the plasma. To overcome this problem an ICP-MS system with an octopole collision and reaction cell has been

used. It features an off-axis octopole ion guide operated in an RF-only mode, which helps reduce the abundance of interfering polyatomic ions via the introduction of different gases, into the cell.
For the reduction of interferences on the main isotope ^{56}Fe, H_2 efficiently reduces interfering polyatoms due to a proton and charge transfer reactions as given below:

(1) $^{40}Ar^{16}O^{+} + H_2 \rightarrow {}^{40}Ar^{16}O^{1}H^{+} + H$

(2) $^{40}Ar^{16}O^{+} + H_2 \rightarrow {}^{40}Ar^{16}O + H_2^{+}$

In addition kinetic energy discrimination obtained by the settings of the octopole and quadrupole bias was applied to further reduce the background on the main iron isotope.

II.2.4.2 Magnetically directed Migration assay

Preparations:
For the migration experiment Chamber slides (NUNC) with a glass surface were used and were coated with fibronectin. Therefore 2mL 1x PBS (phosphate buffered saline) with 10ng fibronectin /mL were transferred in the chamber slides and rotated softly for one hour. Afterwards this slides were stored (closed with parafilm) at 4°C.
For the migration assay the cells collected from the ICP-MS preparation were used and 50 µL (1 Mio/mL) were transferred to a marked area on the prepared chamber slides. The cells were incubated for 6h at 37°C to adhere. Afterwards the cells were washed with prewarmed media and sucked of to extract loose cells from the chamber slide. Than 2mL of nanoparticles free media was added and the chamber slides were placed into the magnetic field (+B) or without (-B) in the cell culture incubator for 24h. Pictures were taken with a Nikon Microscope TiS at point 0 (start) and after 24h.

II.2.5 Statistic

Statistic was performed with the program Sigma Plot 11.0 using One Way ANOVA and the Holm Sidak method.

III Results:

At the beginning of this study two different types of nanoparticles were made available. Both possess a core of magnetite and are covered by fatty acids. The nanoparticles are designated as NP-LA and NP-MA. NP-LA is characterized by a bilayer coating of lauric acid, while the other variant NP-MA contains myristic acid as its coating. Initially it was unknown whether these particles were biocompatible and if they would be taken up by the investigated cancer cells.

III.1 Nanoparticle uptake

In order to develop a methodology to direct migrating cells in a magnetic field it was extremely important to select nanoparticles that could be successfully incorporated into the cells in a pre-determined concentration and that the nanoparticles show none or very low levels of toxicity.
In order to investigate these aspects different imaging and analytical procedures within the cells, and Inductively Coupled Plasma Mass Spectrometry (ICP-MS) enabled the measurement of the iron content within the cells.

III.1.1 Berliner Blue Staining

BBS is a staining method based on a reaction of potassium ferrocyanide with iron contained in the ferrofluids of a blue dye complex (the natural iron content of the cells can be detected using this method.) The presence and rough location of iron within the cells were determined after staining using microscope based techniques.

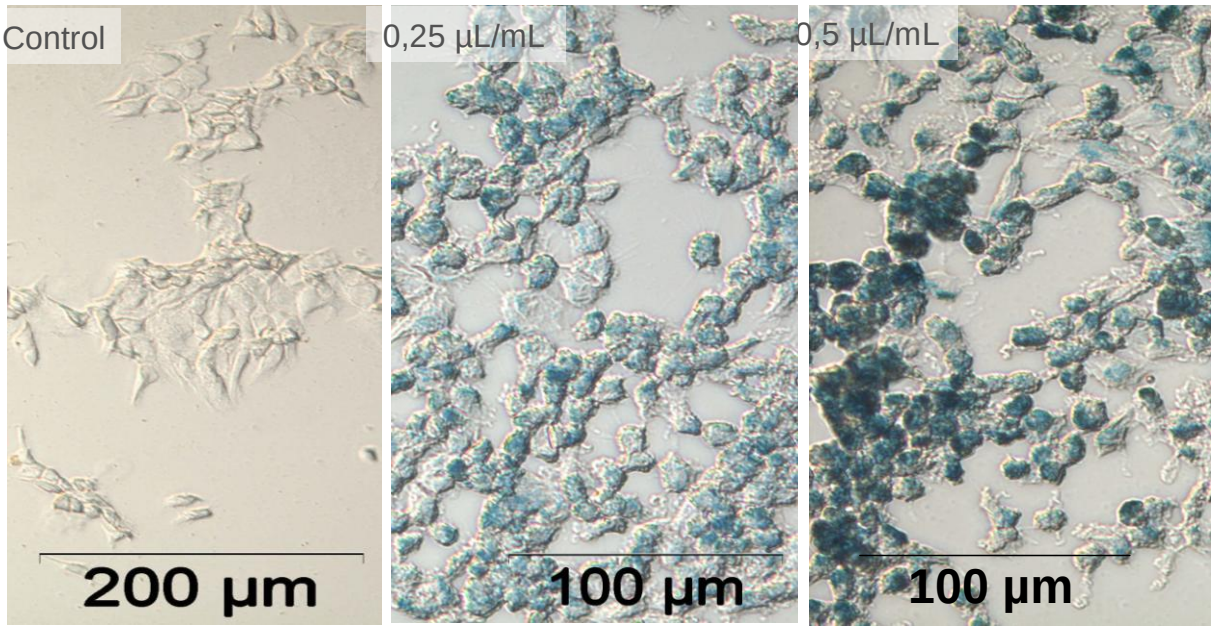

Figure 5: Microscope investigation of iron deposition (NP-MA) and their position in glioblastoma cells. Cells were treated with normal media (control) or with media containing 0.25µL/mL or 0.5µL/mL NP-MA nanoparticle solution (see II.2.3.1) for 48h. The glioblastoma cells were analyzed using an Olympus microscope (20x magnification).

Figure 6:Microscope investigation of iron deposits (NP-LA) and their position in glioblastoma cells after treatment with different concentrations of nanoparticle containing solutions. Glioblastoma cells treated with media containing 0.25 µL/mL or 0.5 µL/mL NP-LA nanoparticles for 48h.

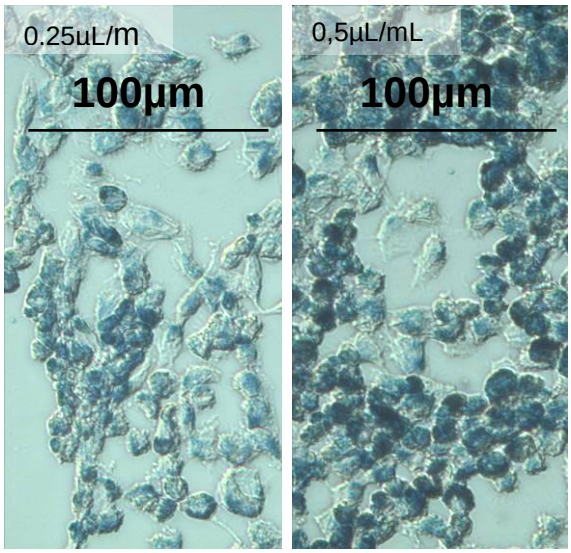

The results of Glioblastoma cells G55 stained with potassium ferrocyanid after a treatment with NP-MA and NP-LA are shown in figures 5 and 6. Both the NP-MA and NP-LA nanoparticles were well absorbed into the cells. Additionally, the iron content within the cells directly correlated with the concentration of nanoparticles used. Cells treated with the low concentration (0.25 µL/mL) of nanoparticle containing media, exhibited a light blue colour next to the cell nuclei, see figures 5 and 6. In the

micrographs for cells treated with the high concentration (0.5 µL/mL NP-MA and 0.5 µL/mL NP-LA) of nanoparticles; most of the cells are completely blue.

III.1.2 Measurement of the Iron content in cells using ICP-MS

The use of BBS enables only a subjective representation of nanoparticle uptake by the cells. This is because it is not capable of discerning to what extent the different components of the particles affect colouring, hence only coarse differences in iron uptake can be identified. This was overcome by employing an ICP-MS to make iron content measurements. Due to its high sensitivity, the ICP-MS made it possible to precisely measure the iron content of cells within very small sample volumes (100 µL a100, 000 cells). This was performed after a 2-day incubation period.

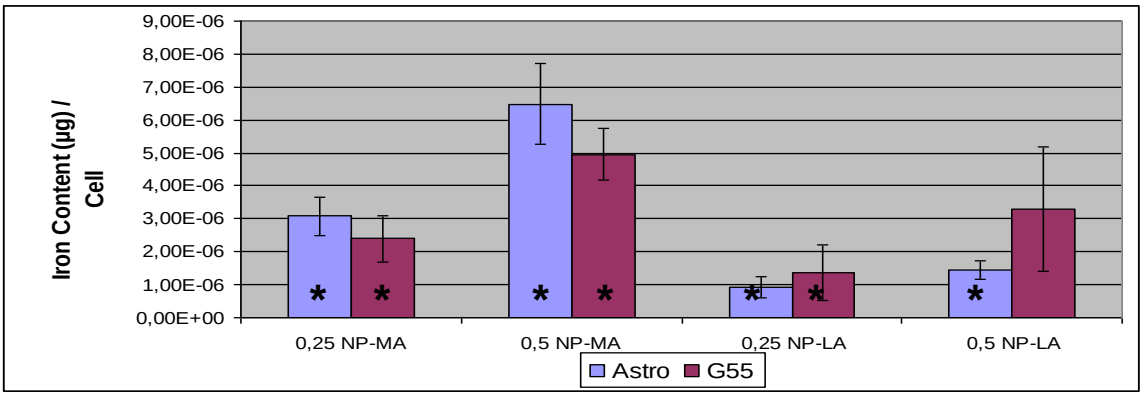

Figure 7: Iron content per cell after a 2d incubation period measured using ICP-MS The results have been normalized to control (non treated cells, natural iron content). Both particles (NP-MA and NP-LA) are incorporated significant by concentration for astrocytes. For G55 it was not possible to achieve a significant concentration dependent nanoparticles uptake for NP-LA. Tested with One way ANOVA and the Holm – Sidak method pair wise against each other n= 6 -19. p=0.01

Figure 7 shows the measured iron content normalized with respect to the control (natural iron content of the cells). The natural iron content of astrocytes is $1.51*10^{-7}$ µg/cell and is $1.33*10^{-7}$µg/cell for G55.

Astrocytes and glioblastoma cells G55 exhibit an uptake dependent on nanoparticles concentration for NP-MA. For NP-LA the uptake is only for astrocytes concentration dependent, the significance test for G55 failed.

The astrocytes have an increased net-content of iron per cell for NP-MA compared with G55. Incorporation of NP-MA in the cell (astrocytes and G55) is proportional to the nanoparticle concentration. The iron content for astrocytes is $3.1*10^{-6}$µg/cell (0.25 NP-MA) and $6.5*10^{-6}$µg/cell (0.5 NP.MA).

For glioblastoma G55 the iron level per cell (NP-MA) is approximately 20% lower than for astrocytes.

Astrocytes incorporate 20% less nanoparticles NP-LA ($0.9*10^{-6}$µg/cell for 0.25 and $1.4*10^{-6}$µg/cell for 0.5) in comparison to the values of G55.

NP-LA uptake within the cells was characterized by large variations even though preparations for incubation were undertaken with the greatest of care to avoid measurement error. Hence the bars as seen in Figure 7 exhibit a high standard error therefore the uptake of NP-LA in G55 cells is not concentration dependent.

Additionally, NP-LA uptake was 40-50% lower compared to NP-MA incorporation for both types of cell.

III.1.3 Measurement of cell sizes

The astrocytes and the glioblastoma cells are very different in their phenotypes, especially in the size of their cells. As it was not known what effect cell size would have on the experimental results, this was investigated. This simplified the comparisons made between the cells and may affect the nanoparticles uptake and the interpretation of following attempts.

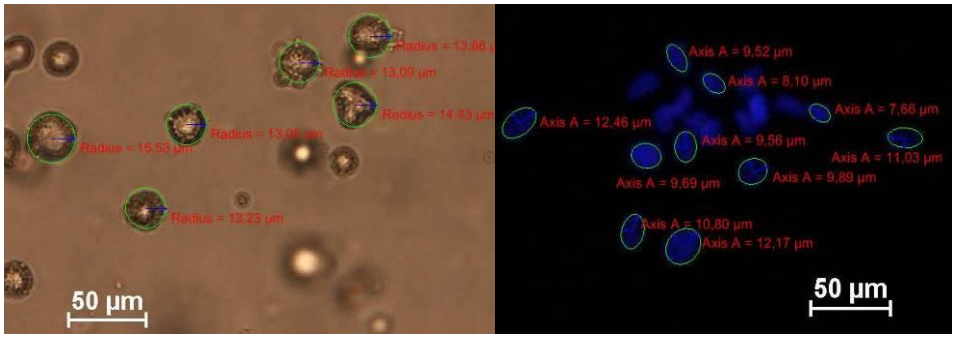

Figure 8: Astrocytes cell size and nucleus measurement.

Spherical cells are observed in the left hand micrograph from which measurements attempts were made to determine the total cell volume. The right hand micrograph is after DAPI staining, this enables the size of the nuclei to be evaluated.

For measurement purposes the cells were trypsinized and the cell suspension was measured (figure 8 and 9 left). This was performed in order to improve the accuracy of the measurements; in the adherent state the cells have many small growths of varying thickness which makes accurate measurement of the cells very difficult.

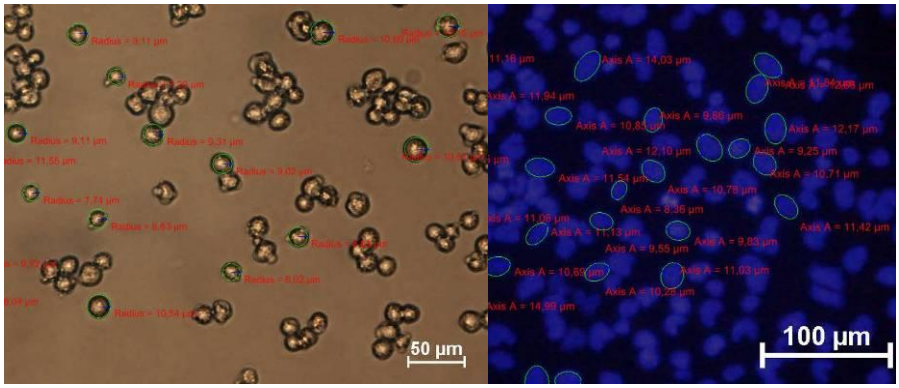

Figure 9: Glioblastoma G55 cell size and nucleus measurements

The left hand micrograph shows spherical cells, cell measurements were made in order to determine the total cell volume. The right hand micrograph is after DAPI staining, and enables the size of the cell nuclei to be evaluated.

After detachment from the substrate the cells formed a spherical shape. This made it easier to analyze the cells when using the NIS-elements software (NIKON).
Minimum sample sizes of 60 cells were measured for each condition in order to improve the size distribution statistics. The total volume of cells and the volume of the nuclei (figures 8 and 9, DAPI staining) were determined enabling the cytoplasm volume to be calculated (figure 13). In the case of ferrofluids the iron content of a particle and the magnetic volume were calculated. With the calculated iron content per cell, the total number of particles per cell was determined as well as the magnetic volume. The ratios (average of the cytoplasm volumes: average of magnetic particle volumes) are presented in figure 10.

$V_{Cell} = 4 \pi / 3 r^3$

$V_{Nucleus} = 4 \pi / 3 ab^2$

$V_{Cytoplasma} = V_{Cell} - V_{Core}$

	V_{cell}	$V_{Nucleus}$	$V_{Cytoplasma}$
Astro	12,90 *10^{-9} cm^3	1,67 *10^{-9} cm^3	11,22 *10^{-9} cm^3
G55	3,45*10^{-9} cm^3	2,39 *10^{-9} cm^3	1,01*10^{-9} cm^3

	magnetic $V_{Particle}$	m_{Fe}/ Particle
NP-MA	4,77*10^{-20} cm^3	1,74*10^{-13} µg
NP-LA	10,7*10^{-20} cm^3	3,93*10^{-13} µg

Figure 10: Results of Cell measurements

The figure indicates the calculated cells and nanoparticle volumes along with the formulas used in the calculations.

The figure shows that the astrocyte cell volume is five times larger than the glioblastoma cell volume. However, they have significantly smaller nuclei, the glioblastoma cells having nuclei twice as large.

For the case of the cytoplasm, the calculations indicate an 11 times larger volume of astrocytes compared to G55. Figure 11 indicates that the uptake of nanoparticles in G55 in comparison to astrocytes is 8-9 times as high when treated with NP-MA, while this difference is even greater; 15 times at the low concentration and 24 times at the higher concentration, for NP-LA.

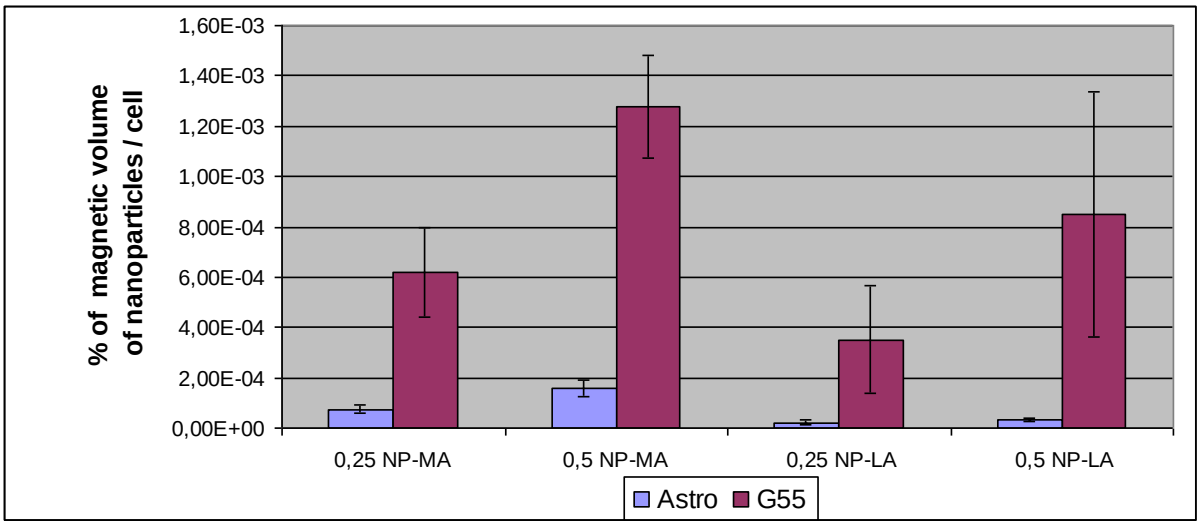

Figure 11: Iron content normalized to cell volume

Ratio of the available cytoplasm volume to magnetic volume normalized against the control.

III.1.4 Summary

The results of the nanoparticle uptake investigations demonstrate that the incorporation of NP-LA into astrocytes is less pronounced than for NP-MA. This is preferable from the point of view of therapeutic treatment because it would be less stress for the brain cells. However, the uptake of NP-LA into glioblastoma cells is very heterogeneous and not significant concentration dependent.

With reference to the nanoparticle volume to cytoplasm volume ratio, the G55 cells contain 900-2400% more nanoparticles than astrocytes.

III.2 Evaluation of Toxicity

In the first above described results it was shown that both ferrofluids were incorporated into the cells, albeit to different extents.

Here it should be stated that only a combination of both - good cell assimilation of the ferrofluids (concentration-dependant) AND very low toxicity meet the requirements for future human brain neoplasm therapy. Hence nanoparticle biocompatibility has been assessed with proliferation assays. Human primary astrocytes were used as the control in all following experiments. Additionally, similar assays were performed on brain tumour cells (glioblastoma cells).

III.2.1 Proliferation assay

III.2.1.1 Proliferation assays of astrocytes incubated with NP-MA or NP-LA supplemented media.

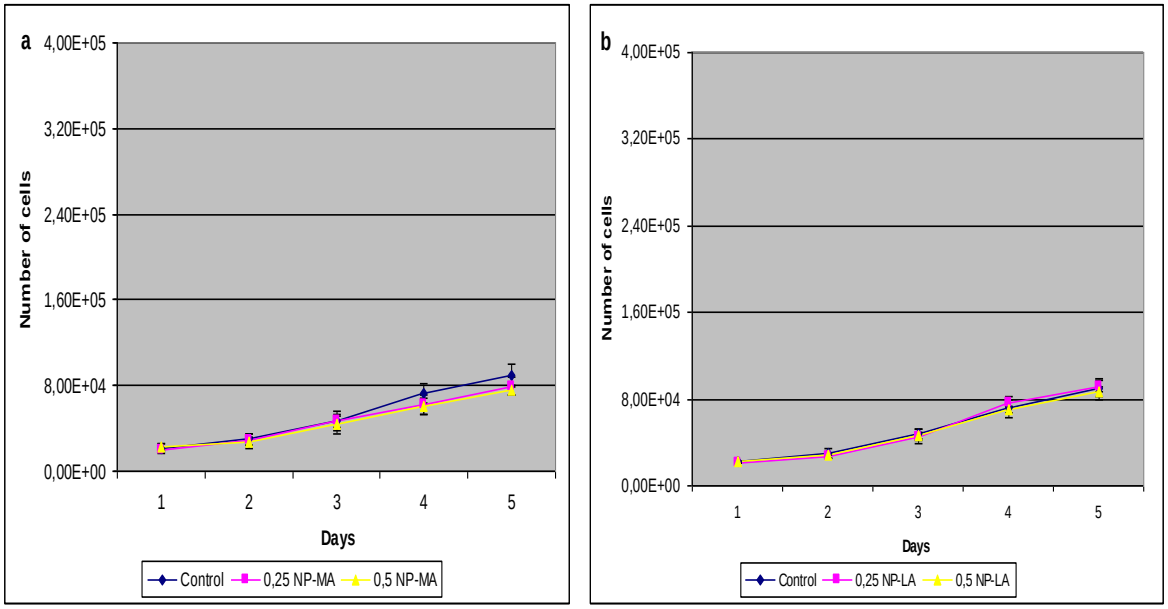

Figure 12: Proliferation of astrocytes incubated with (a) NP-MA or (b) NP-LA supplemented media. The Astrocytes were incubated with 0.25µL/mL or 0.5µL/mL of nanoparticles and the cell number was measured over a 5 day period. Astrocytes without nanoparticles were used as a control. The mean and standard deviation for n=4 were calculated.

Only small deviations between the control and the treated-groups (0.25 NP-MA and 0.5 NP-MA) were detected, although the differences were not statistically significant. This means that neither NP-MA nor NP-LA (figure 12) have a negative effect on cell proliferation. Accordingly, these two varieties of nanoparticles exhibited no toxicity in astrocytes.

III.2.1.2 Proliferation assays of glioblastoma cells incubated with NP-MA or NP-LA supplemented media.

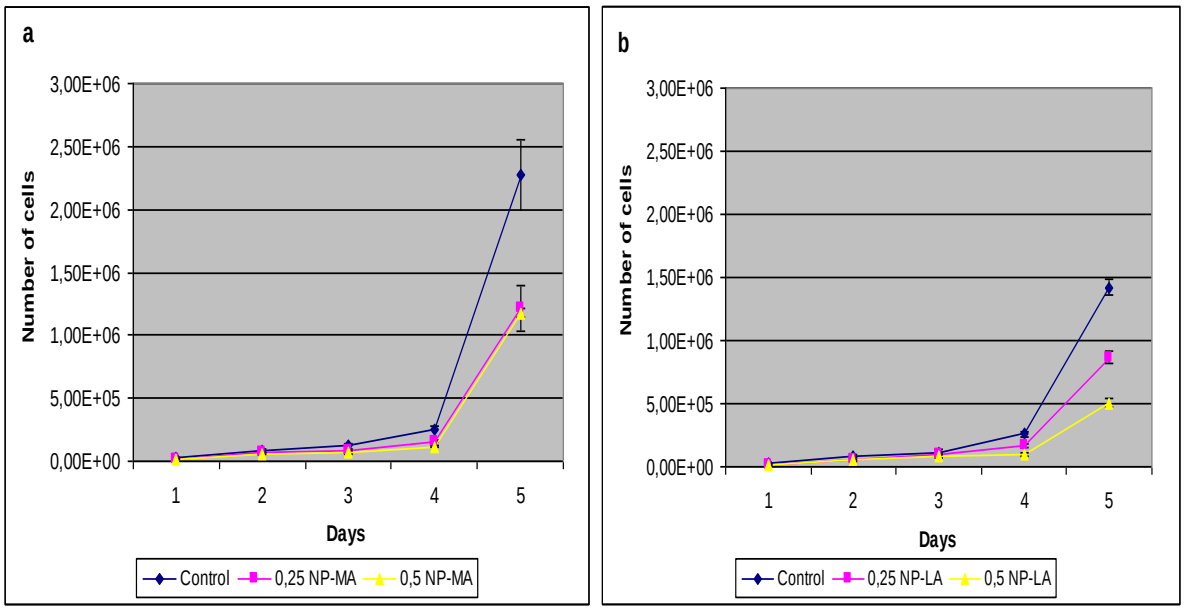

Figure 13: Proliferation of glioblastoma cells G55 incubated with (a) NP-MA or (b) NP-LA supplemented media. G55 cells without nanoparticles were used as control. The number of G55 cells during incubation with 0.25 µL/mL and 0.5 µL/mL of nanoparticles, as well as for the control, was measured over a 5 day period.

The toxicity of NP-MA and NP-LA nanoparticles was assessed in two glioblastoma cell lines, G44 and G55.

The G55 cells in the control and treated cells groups showed only very small differences for up to 3 days incubation, figure 13a. However after day 4, the control group showed a significantly higher proliferation rate than either the 0.25 or the 0.5 NP-MA treated groups. The groups treated with nanoparticles exhibit to day 4 slightly different from each other, then both concentrations reached a similar endpoint. At day 5 the groups treated with nanoparticles show deviations from an average of 1.25 million cells from the control group, or approximately 50%.

Between days 4 and 5 the number of NP-LA treated cells depends on the concentration, unlike for NP-MA treated cells (figure 13b). This implies that the toxic effect of the nanoparticles depends on concentration, with the higher concentration showing greater toxicity. This results in only 500,000 cells remaining in the 0.5 NP-LA treated cells compared to 850,000 for the 0.25 NP-LA treated group and over 1.4 million cells in the control group. Compared to the control group these values correspond to 61% for 0.25 NP-LA - and 35% for 0.5 NP-LA.

On comparing different cancer cells (specifically G55 and G44, figures 13 and 14) treated with NP-MA, it can be seen that major differences in not only growth behaviour but also in response to nanoparticle concentration exist. The proliferation and toxicity of the individual cell lines show big differences, based on their inherent phenotypes.

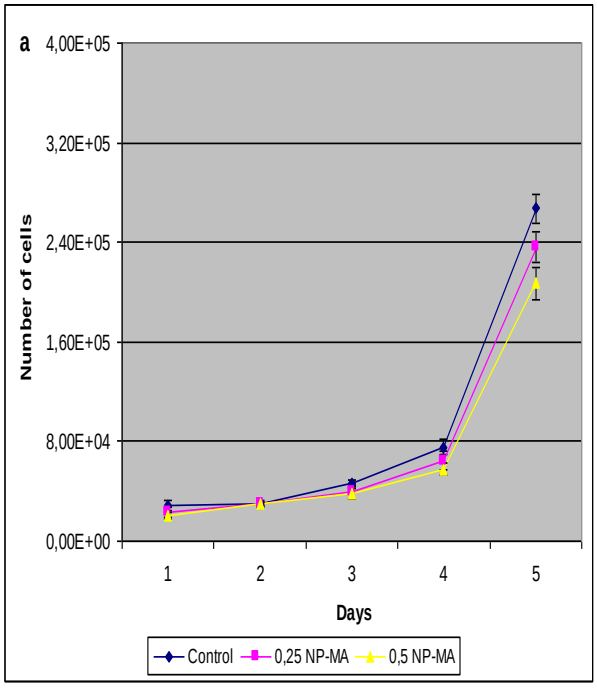

Figure 14: Proliferation of glioblastoma cells G44 incubated with NP-MA-supplemented media. G44 without nanoparticles were used as a control. The number of G44 cells after incubation with 0.25µL/mL and 0.5µL/mL of nanoparticles was measured over a 5-day period.

Comparing Figure 14 for G44 cells and Figure 13a for G55 cells both treated with NP-MA it is clear that not all cancer cells respond with the same sensitivity to the nanoparticle concentration. Although the growth behaviour of the G44 cells up to day 3 is similar to that for G55 cells, differences develop on day 4 and 5. For the G44 cells treated with 0.25 NP-MA the number of cells is 88% of that for the control group and approximately 77% for cells treated with 0.5 NP-MA.

In both figures 13 and 14 it can be seen that cell growth behaviour is very inhomogeneous. The starting point for exponential growth varies between day 2 and 3. The cell proliferation rate varies strongly between the divers cell line. For example on day 5, $2.5*10^6$ cells were measured for the G55 control group whereas only $2.5*10^5$ cells were measured in the G44 control group. Such differences were observed in all experiments. Consequently, in order to create stable and reproducible conditions, the incubation time of further tests was set to two days (figure15).

III.2.1.3 Toxicity after an incubation time of 48h

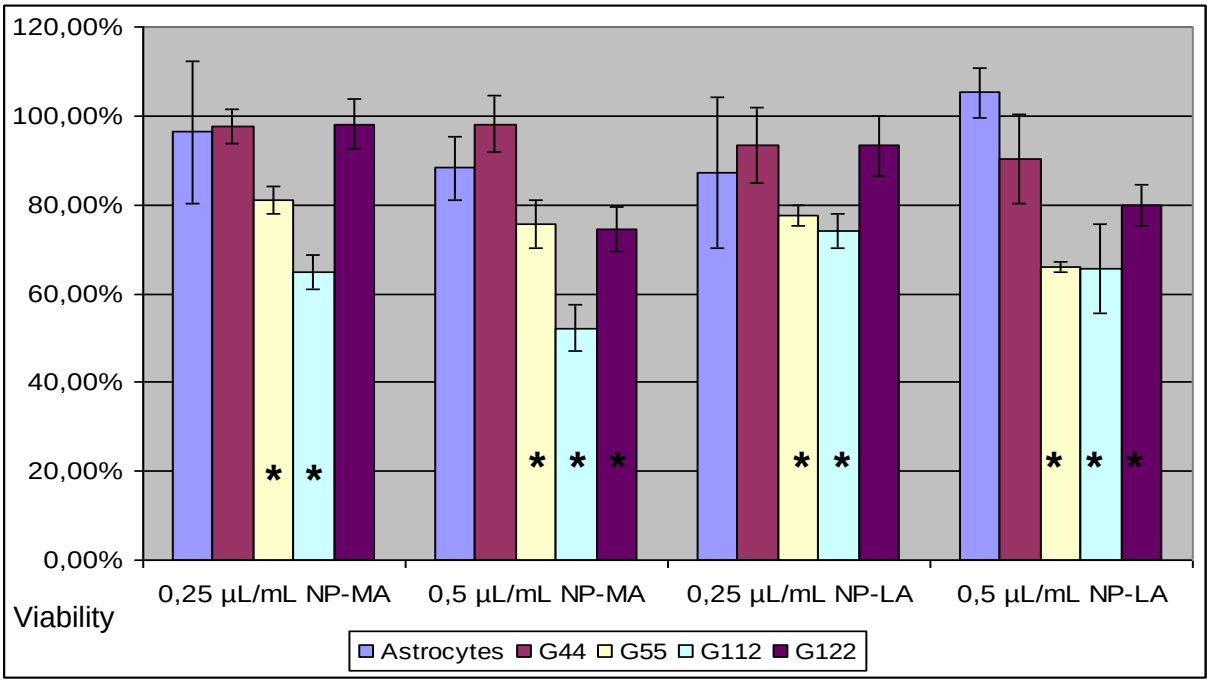

Figure 15: Results of cell viability investigations (determined by cell counting) plotted as a percentage of the control values after a 2-day incubation period for different nanoparticle (NP-LA and NP-MA) concentrations. * Statistically significant using One Way ANOVA with multiple comparisons against the control group (Holm-Sidak-Method). p=0.01

Proliferation measurements using other cell lines with regard to a control were made after 2 days (see figure 15). Recognizable is the heterogeneity of the various cancer cell lines, compared to astrocytes. With regard to the different nanoparticle types, the Astrocytes and G44 cells are not affected in terms of growth pattern after 48h. For the G55 and G112 cell lines lower ferrofluid concentrations give rise to a significant reduction in cell number, which becomes more significant for high concentrations. G55 and G112 cells treated with NP-LA show a cell number reduction to

approximately 70-80% for the lower concentration and to about 65% for the higher concentration of nanoparticles (figure 15). During incubation with NP-MA particles, G55 cells behave like cells treated with NP-LA. G112, however, they demonstrate the highest sensitivity for incubation with NP-MA ferrofluid. For the case of incubation with NP-MA, the reduction in cell number is by about 36% for 0.25 NP-MA and around 50% for 0.5 NP-MA. G122 demonstrate after incubation for 48h with 0.5 NP-MA a reduction of the cell growth by around 20-30%.

Considering the cell viability results as a whole there is no obvious trend that one type of the nanoparticles is more toxic than the other, toxicity depending on cell type and line.

III.3 Summary of Nanoparticle uptake and Toxicity Investigations:

From the outset it was clear that nanoparticle uptake should be limited to a short period in order to exploit the increased metabolism of the cancer cells, and also enabling therapeutic use with a minimal dose to avoid patient side effects. For the establishment of the migration assay and the magnetic field reproducible and stable results are necessary, therefore the results of nanoparticles uptake and toxicity were used for selection of basic parameters and nanoparticles type.

The toxicity tests demonstrate that astrocytes are slightly affected by the nanoparticles while glioblastoma cells (G55), which contain fewer particles, are more sensitive. For toxicity no relevant differences between the nanoparticles types were found. However the proliferation data demonstrated that for all experiments it was only possible to achieve reproducible circumstances (linear growth) during the first two days of incubation.

The results of the nanoparticle uptake investigations showed that the incorporation of NP-LA into astrocytes was less than for NP-MA. This is preferable for therapeutic use because it connoted less stress for the healthy brain tissue. However the uptake of NP-LA into glioblastoma cells is very heterogeneous and independent of concentration. Hence a controlled uptake of this type of nanoparticle is very uncertain. Uncontrollable experimental growth conditions made it difficult to establish reproducible condition for the migration experiments. Consequently, all experiments were limited to a time period of 48h and NP-MA was chosen as favored the nanoparticle type.

III.4 Development of the magnetic field and the migration assay

"The goal is to direct nanoparticle loaded glioblastoma cells, with the help of an external magnetic field to a defined point.''

In order to achieve the goal of directed magnetic migration of glioblastoma cells a new methodology had to be developed. Commercially available migration assays were unsuitable because these are normally based on diffusion of biological or chemical concentration-gradients, e.g. cytokines or proteins. Additionally the migrations of the cells are measured about very short distances circular or vertical.
The challenge here was two fold, (i) to produce cells with super paramagnetic behaviour through insertion of supermagnetic nanoparticles and (ii) to direct the migration of these cells using an external magnetic field. Hence a horizontal migration assay was required in order to observe the migration of the loaded cells under the influence of the magnetic field. Furthermore, various methods such as LIVE DEAD staining, cell organelle staining, goal directed migration and immune histochemical analyses should be observable under the same magnetic conditions. Consequently these considerations were incorporated into the planning and development of the magnetic field.

III.4.1 Cell culture material

Cell culture consumables consisted of chamber slides and/or chambered cover glasses. The reason for this was due to their similar sizes and practical reasons during analytical as well as microscopic analyses under magnetic field conditions. Typically invasive glioblastoma cells are found at a distance of 1-3 cm away from the main tumour (pathology results, Demuth 2004, Kleihues 1995). By correctly choosing the size of the chamber slides this distance could be simulated.

III.4.2 Form of the magnetic field

To achieve a directed force on the super paramagnetic nanoparticles (and so on the cells) a gradient magnetic field is required.

Preliminary test runs made with a 300 mTesla magnet on one side of the chamber slides showed that this natural magnetic field form was insufficient.

The strength of the magnetic field fell off exponentially on moving from magnet to start area of the cells. The desired magnetic field gradient was geometrically too short. Especially due to the external form of the chamber slides, the inner test room is several millimetres away from the magnet. Additionally the area where the cells should be placed at the beginning of the test should be a minimum of 1cm away from the chamber slide wall. Consequently these tests demonstrated that a magnetic field with a relatively strong gradient (155mTesla; for a distance of 7.6cm air gap (length of a chamber slide)) was required.

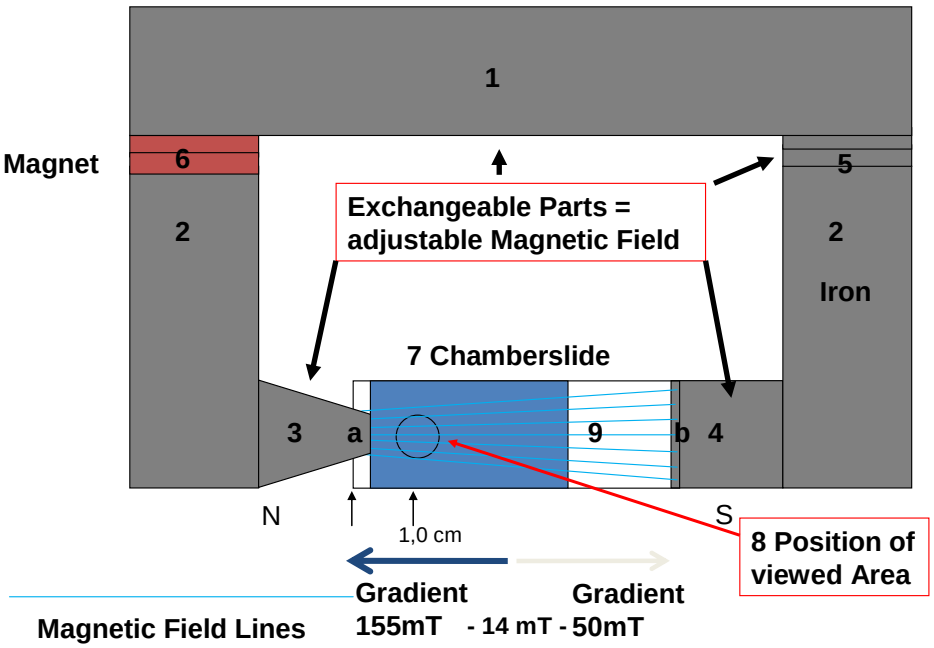

Figure 16: Design of the magnetic field; two magnet type

Top view; all grey parts = iron (h*w*l); **1)** vertical main bar 3*3*18cm; **2)** side bars 3*3*7,5cm; **3)** magnetic pole shoe 1 = 3*2,6*2,5cm; **4)** magnetic pole shoe 2 = 3*2,6*2,5cm; **5)** left side plate 3*3*0,5cm, **6)** magnet D3*3*0,5cm, 1,48 Tesla, **7)** chamberslide ca. 7,6cm; **8)** diameter of viewed area position 8mm, **9)** magnetic field lines; shown gradient was measured with two magnet in these construction.

To solve this problem, a U-magnetic field form was chosen (Figure 16), this structure enlarged the gradient by several centimetres, thus extending the test area of the experiment.

III.4.2.1 The following governing criteria should be fulfilled.

a) The size of the construction has to fit in an incubator fan, so that 6 magnetic fields could be used in parallel for experiments.

b) It should be possible to put the construction on the microscope table without changing the experimental conditions or disturbing the camera and the computer.

As a consequence a permanent magnetic field consisting of ferro neodymium magnets was employed.

III.4.3 Orientation of magnetic lines of flux

Since the investigated cells grow adhering to their underground and then actively migrate it became evident that a prime requirement of the magnetic field was that it operates on the plane of the cells. Furthermore, migrating cells should consolidate in the direction of the magnetic gradient in order to concentrate themselves in the smallest possible area. Hence the magnetic poles or so called shoes (figure 16: 3+4) when designing a magnetic field needed to fulfill the following specific requirements.

In order to strengthen the magnetic flow density B on the one side, it was necessary that magnetic pole shoe 1 (item 3 in figure 16) have a reducing surface in both the horizontal and vertical planes as compared to pole shoe 2 (item 5 in figure 16). The larger surface area of magnetic pole shoe 2 ensured that the magnetic flow field would be weaker on this side of the magnet.

These specifications were then incorporated into the magnet field as depicted in figure 17.

a

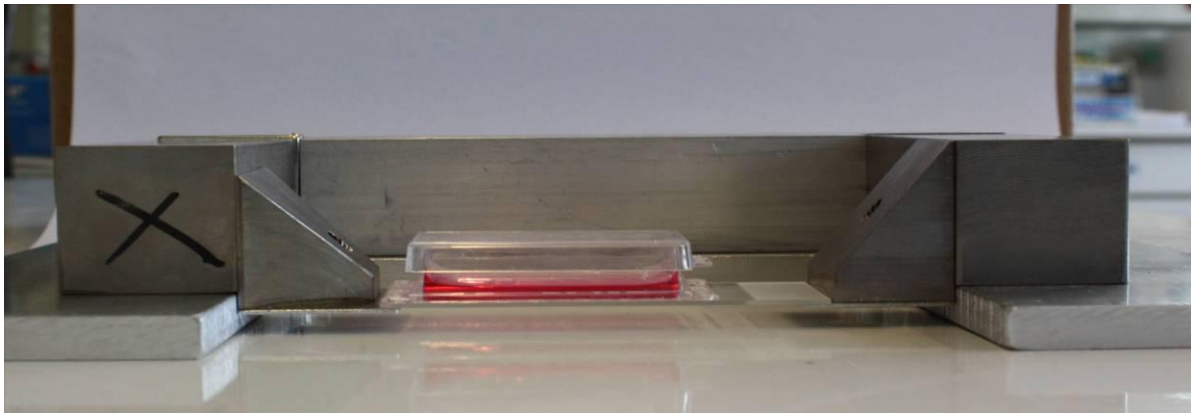

b

Figure 17: Magnet, two magnet type

a) topview **b)** lateral view: The experimental area with the chamber slides is a little lower than the rest allowing for work on the microscope image plane.

The laterally laying form of the magnetic field (17+18) produces a slight one-sided distortion of the magnetic field. With a vertically oriented variant standing over the sample this would not be a problem but:

The lying variant was however necessary for microscopy in that this form did not impede or block the optical light path. Further this form ensured the same conditions applied for all experiments, because it has not been changed for life cell imaging.

In the case of design of the magnetic field between the front surfaces of the magnet pole shoes 1+2, this nevertheless results in a symmetrical form of the chamber slide area, whose influence is depicted in figure 18. This is due mainly to the conical form of magnet pole shoe 1.

The magnets were placed each in one pan with more than 20cm distance to each other, so that no disturbance of the magnetic field test room could be detected (figure 18). And the cells in the different samples have the same incubator conditions (opening frequencies and other external influences).

In order to ensure good reproducibility if was found that cell experiments required a maximum distance of 1-2cm to the magnetic pole shoe 1, since there is the greatest influence of the magnetic field. This is in line with the start of the strongly rising exponential gradient depicted in (figur 19).

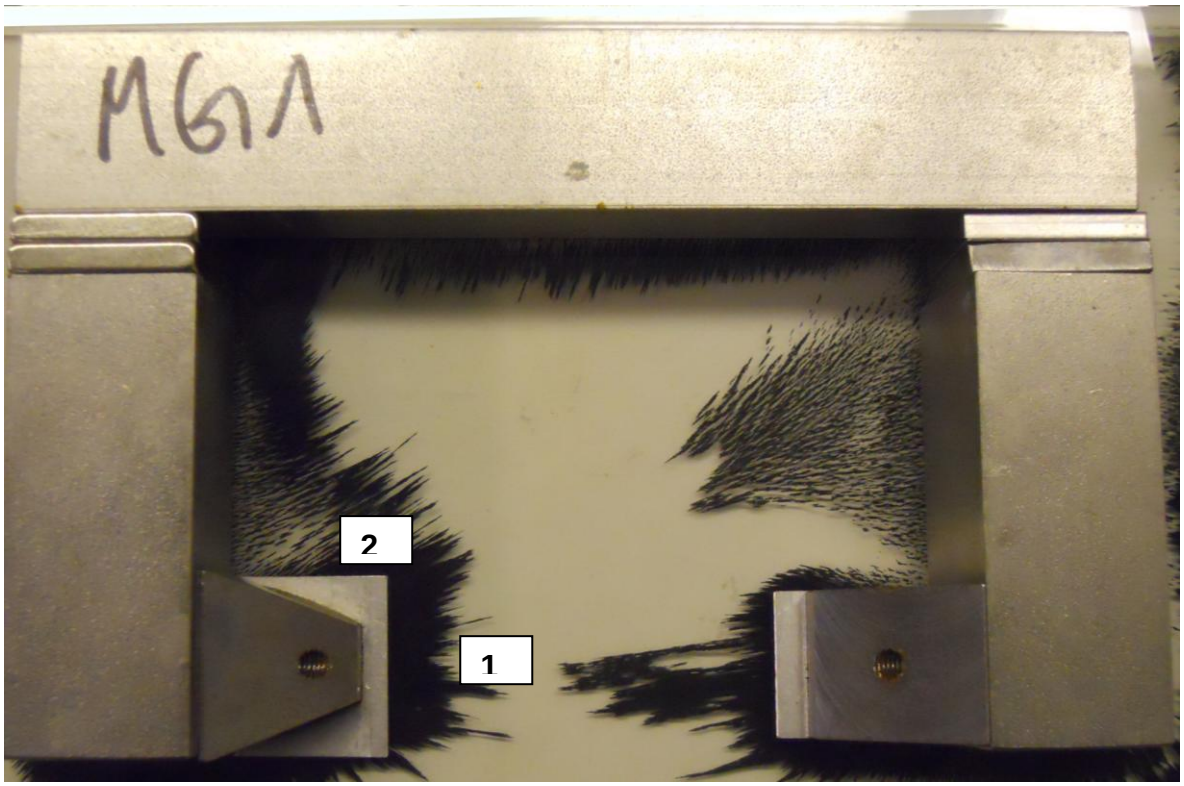

Figure 18: Magnetic field lines; two magnet type

The air gap (test area) shows a symmetrical form of the magnetic field, with nearly parallel magnetic field lines at the cells starting area (1). The magnetic field has a small distortion to the inner field (2), without measurable disturbance of the test area.

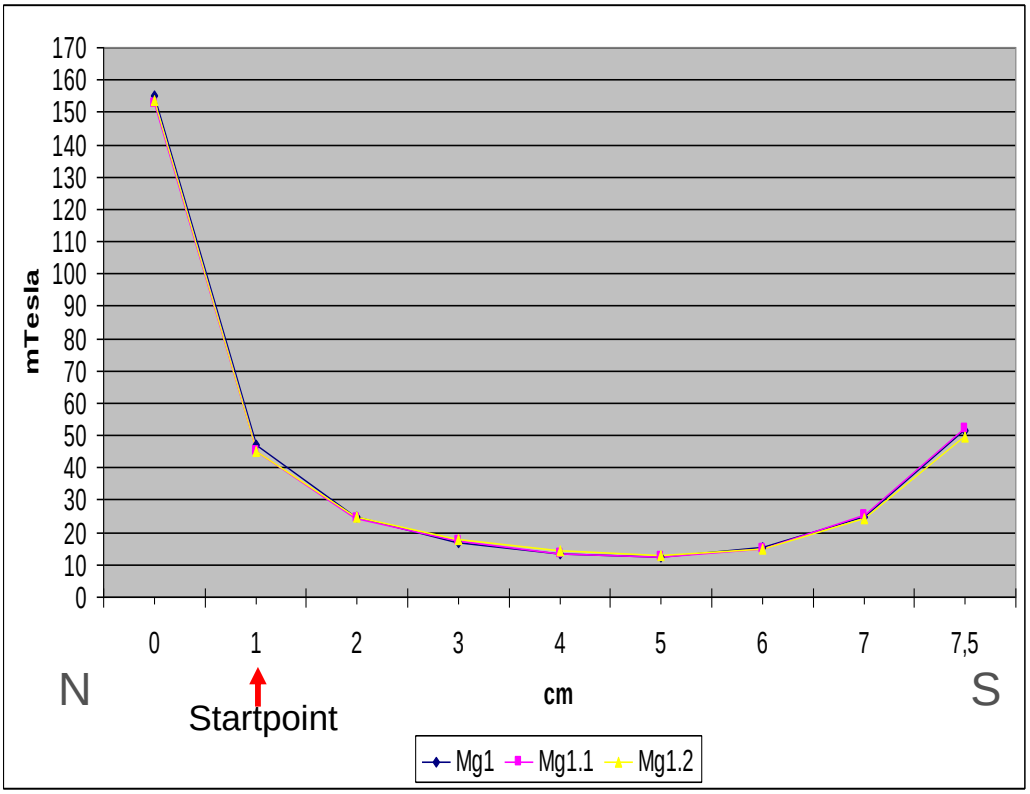

Figure 19: Gradient of the magnetic field, two magnet type.

The gradients of the magnetic field as measured over the distance of the air gap (length of the Chamber slides) are presented here. The exponential path in the center (4cm distance) is contributed to magnetic leakage fluxes.

The developed magnetic field leads to following questions:

Will the magnetic field potentiate the toxic effects on the cells especially on astrocytes?

Is the cell structure of nanoparticles containing cells modified by the magnetic force?

And if astrocytes are only less influenced, is it possible to induce directed cell migration of the glioblastoma cells?

III.5 Live Dead Staining

In the work it was important to establish if the magnetic field employed somehow modified the survival of nanoparticles containing cells. Therefore the Live Dead Staining was performed to help address this concern. The advantage of this method is that the direct influence of the magnetic field (to see for example if increasing the magnetic field strength resulted in more dead cells) can be investigated. Additionally, the vitality of the cells can be recognized by their phenotype.

The Live Dead Staining technique is a microscopic analysis based on hydrolysis of calcein acetoxymethyl ester (calcein-AM) in live cells by intracellular esterase to fluorescent calcein. The fluorescence intensity is proportional to the amount of live cells. A second dye, ethidium homodimer, penetrates dead cell membrane and stains the cell nuclei red.

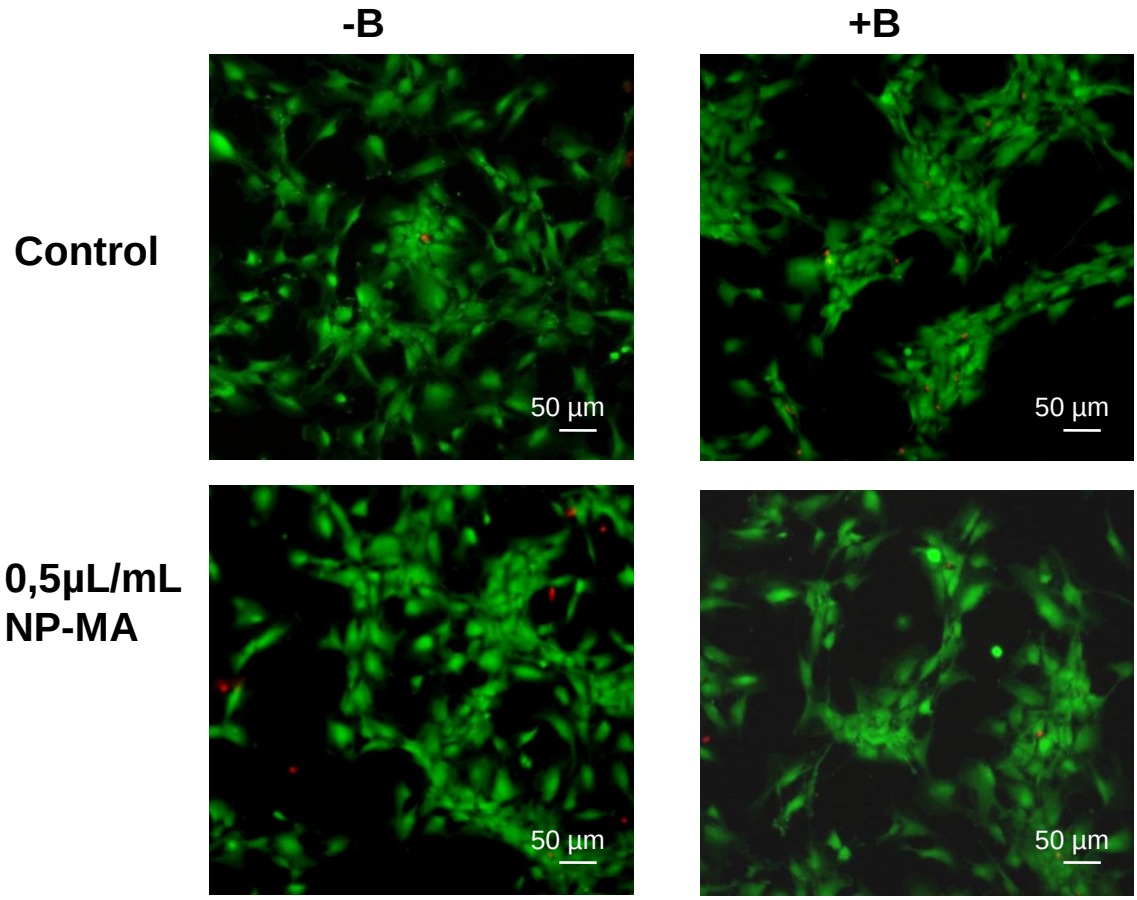

Figure 20: Dual-fluorescence cell viability assay of Astrocytes using ethidium homodimer and calcein AM. Astrocytes incubated with NP-MA for 48h (0.5 µL/mL NP-MA) or astrocytes cells without treatment (control) were either exposed to a magnetic field for 24h (+B) or cultivated without magnetic field (-B).

In this set of experiments, astrocytes and glioblastoma cells G55 were incubated for 48h with either normal media (the control) or media supplemented with 0.5µL/mL nanoparticles. After incubation the media employed was replaced by nanoparticle free media and the cells either exposed to the magnetic field (with incubation) or incubated without magnetic exposure under standard conditions. The aim was to see if the combination of nanoparticles and magnetic field had an influence on the cells.
Both cell types were mostly unaffected after the 2-day incubation period and subsequent exposure to a magnetic field for 24h. The astrocytes (figure 20) show no phenotypic signs of stress. There were very few dead cells found, and when compared to the control cells, their number can be considered as normal. This result correlates well with the observations during the cell proliferation tests.

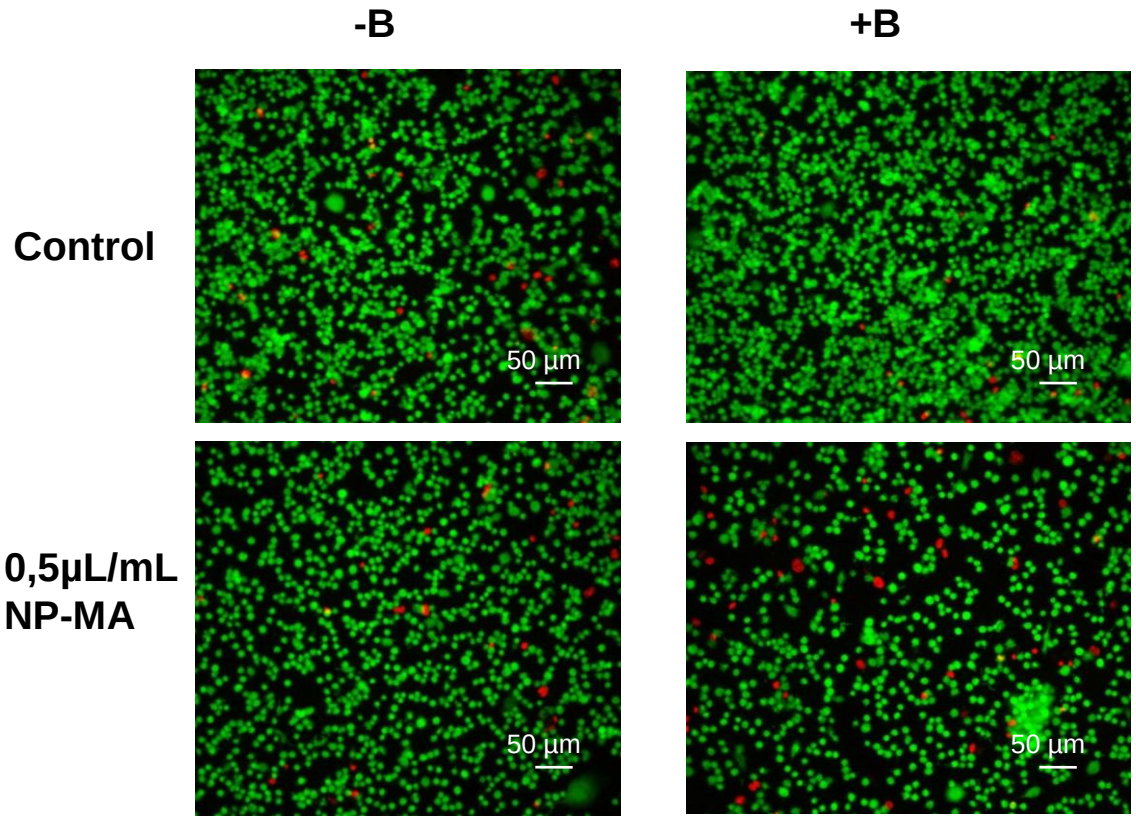

Figure 21: Dual-fluorescence cell viability assay of G55 using ethidium homodimer and calcein AM. Control cells were incubated without ferrofluids with normal media. The pictures on the left hand side demonstrate the results without a magnetic field (-B), while the right hand side micrographs show Glioblastoma cells G55 after an incubation time of 48h with NP-MA and subsequent exposure to a magnetic field for 24h (+B).

The G55 control cells incubated in the magnetic field show no changes in cell number and viability. In contrast the cells treated with 0.5µL/mL NP-MA (figure 21) show a 50 % decrease in the number of cells compared to the control group. Additionally double the number of dead cells was found but no significant influence of the magnetic field could be detected.

Consequently this result does not explain the differences in growth pattern observed in the cell proliferation tests.

If the astrocytes are unaffected by the different circumstances and the glioblastoma cells showing a distinct growth pattern, this leads to some more questions:

Where in the cells are the nanoparticles?

How, do the nanoparticles disturb cell growth?

Is the cell structure of nanoparticles containing cells modified by the magnetic force?

III.5.1 Where are the nanoparticles?

Magnetite quenches fluorescence was used to localize nanoparticles (agglomerates or large accumulations) within the cell. The blue fluorescence light emitted by excessive irradiation at specific-DAPI excitation wavelength (about 341 nm) was identified as a more than capable technique of visualizing the nanoparticles within the cells. Under green and red light (approximate wavelengths of 510 nm and 650 nm, respectively) the particles however, were difficult to identify.
To mark the outer borders of the cells DAPI staining was combined with actin staining. This was realized by phalloidin Alexa 488 (a toxin from the death cap (*Amanita phalloides*), which binds F-actin and is labeled with a fluorescent analog for light microscopy).
Individual particles and small agglomerates are not visible by light microscopy. When employing light microscopy, only the high concentrated nanoparticle supplemented media was used. In order to show that the ferrofluids were inside the cells the samples were analyzed as 3D captions, at 100x magnification using a Nikon Ti-S microscope. The cross on the captions identifies the origin of the slices in reference to the x and y axis. *The original pictures can be found on the data CD at the back cover of this work.*

When exposed to visible light, it is possible to detect dark shadows in cells treated with nanoparticles. These accumulations of the magnetic beads (agglomerates or storage forms) were localized within the cell body.
For both cell types it was found that these accumulations have a circular shape (figure 22 and 23). However, significant differences were also observed:

In astrocytes (figure 22) fewer shadows are detectable, some next to the nucleus, others several micrometers away.

In the glioblastoma cells (figure 23) large accumulations (sometimes more than one micrometer) were found in the immediate vicinity of the nucleus, but also distributed on the center of the cell body. In the “cell feed” region light shadows could also be observed.

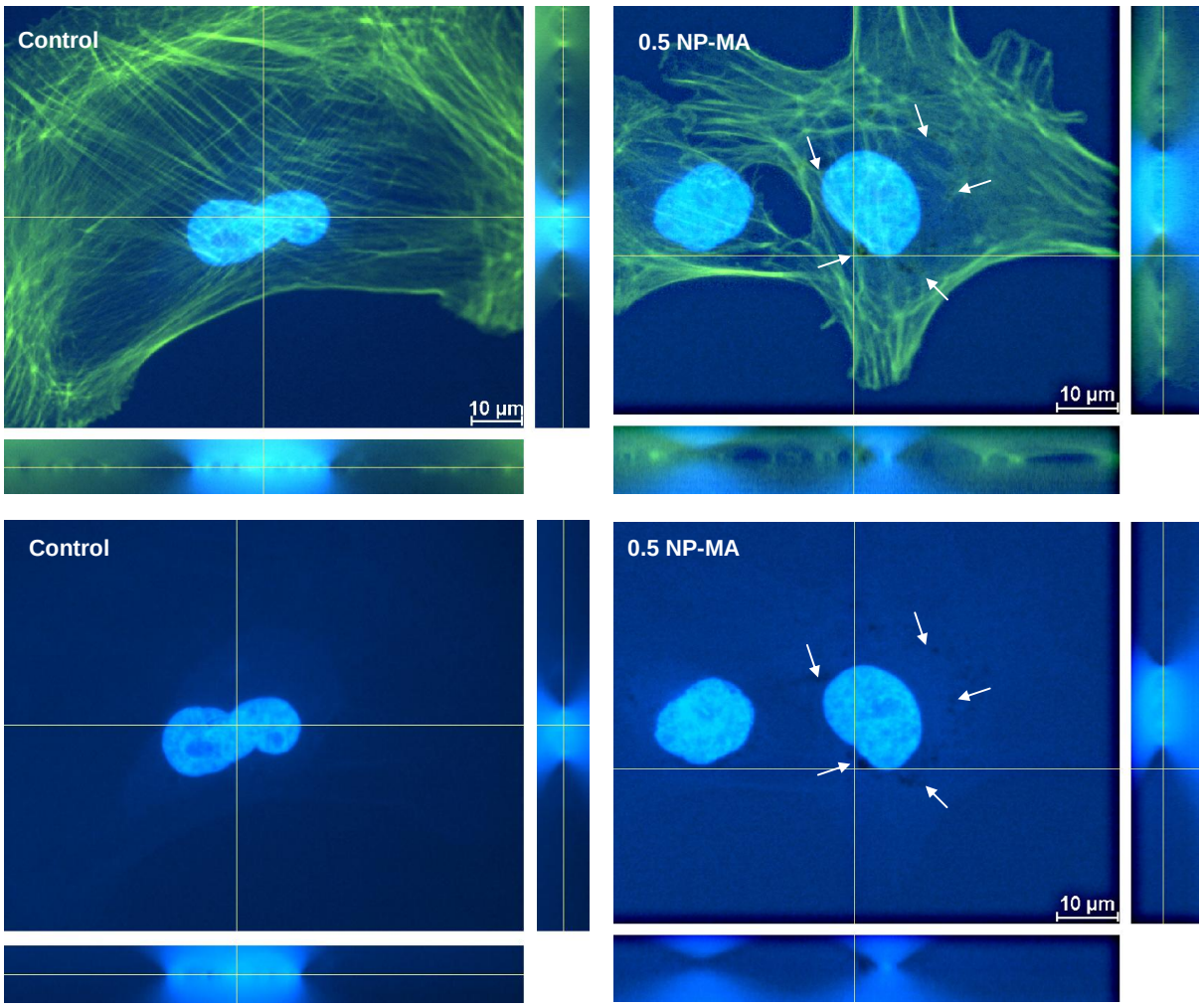

Figure 22: Visualization of the nanoparticles in astrocytes

Presented are 3D captions of astrocytes cells stained with DAPI and actin phalloidin, analyzed at 100x magnification (Nikon Ti-S). The cross through the original caption depicts the origin of the slices. Actin was used to mark the cell borders. In astrocytes treated with the high nanoparticle concentration small agglomerations of ferrofluids could be detected (white arrows).

Bearing in mind the results of ICP-MS (iron measurement) this result here is irritating, because for astrocytes higher concentrations of iron were measured than compared to glioblastoma cells. Glioblastoma cells however always demonstrate more visible agglomerates of ferrofluids. This is very interesting because the glioblastoma cells, especially G55 and G112 show the highest reduction in cell growth (chapter III.2), a possible reason perhaps for the measured cytotoxicity.

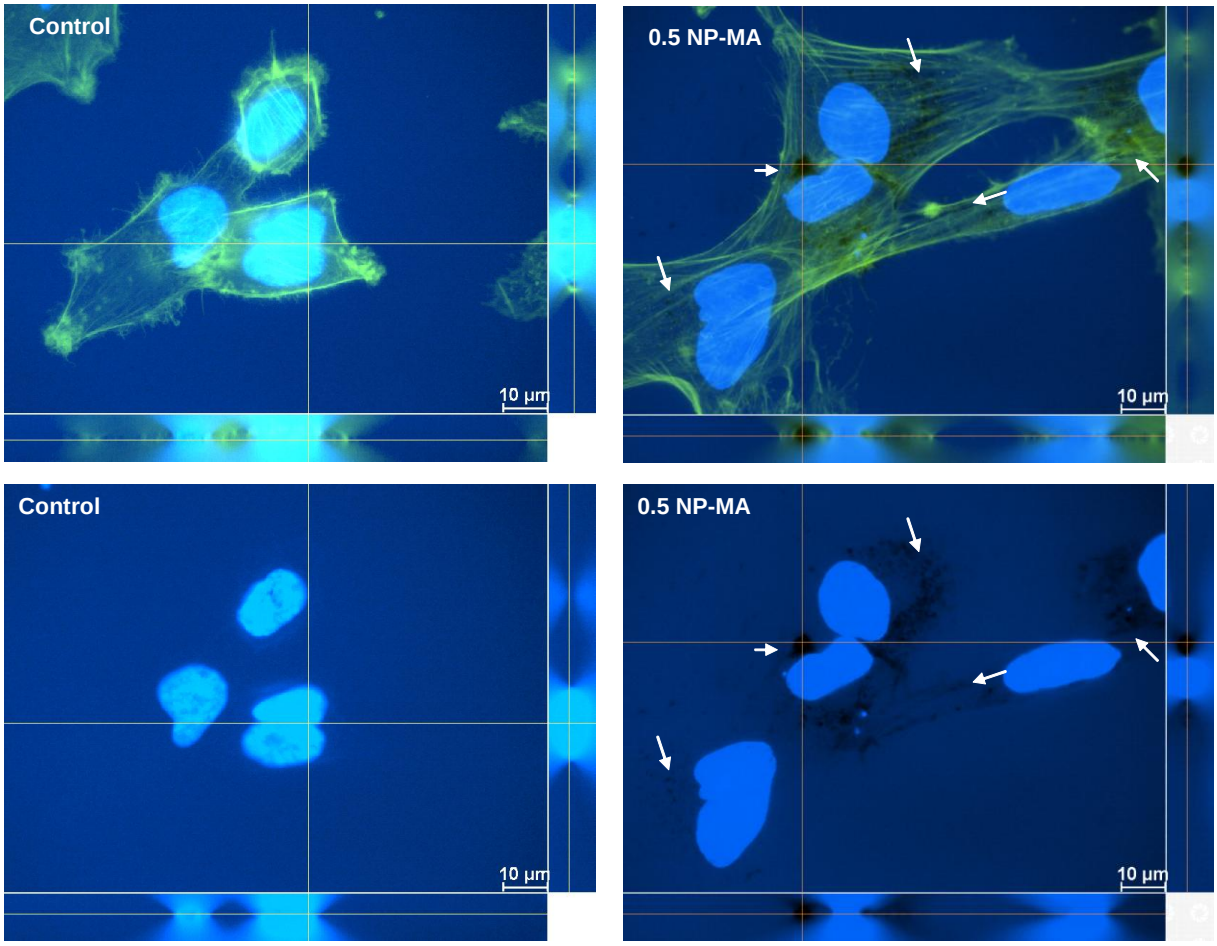

Figure 23: Visualization of the nanoparticles in glioblastoma cells

Presented are 3D captions of gioblastoma cells stained with DAPI and actin phalloidin. Actin was used to mark the cell borders. The cross through the original caption depicts the origin of the slices. Cells treated with ferrofluids show large agglomerates of ferrofluids.

Due to the circular form of the agglomerates this lead to the question as to whether the nanoparticles were stored in some kind of cell organelle?

To find answers to these question lysosomes (known for the waste management of the cells) as well as the endoplasmic reticulum, being the transport system of the cell were investigated. Consequently cell organelle staining was employed.

III.5.2 Cell organell Staining

A cell organell staining with ER-Tracker™ (green) and LysoTracker™ (red) (both Molecular Probes, Invitrogen) was performed to observe where exactly the nanoparticles were within the cells. The nucleus was counterstained with DAPI (blue).

ER-Tracker dyes are cell-permeant live cell stains that are highly selective for the endoplasmic reticulum (ER). ER-Tracker green is the drug conjugate glibenclamide BODIPY® FL respectively. Glibenclamide binds to the suphonylurea receptors of ATP-sensitive K^+ channels, which are prominent on ER (Molecular Probes).

Weak basic amines selectively accumulate in cellular compartments with low internal pH and can be used to investigate the biosynthesis and pathogenesis of lysosomes (Dingle et.al. 1988). The LysoTracker® probes of Invitrogen consist of a flurophore linked to a weak base that is only protonated at neutral pH. This allows LysoTracker® probes to freely permeate cell membranes enabling them to label live cells. LysoTracker® probes are highly selective for acidic organelles (Invitrogen a). Their mechanism of retention has not been firmly established but is likely to involve protonation and retention in the membranes of the organelles.

III.5.2.1 Cell Organelle Staining of Astrocytes

Fluorescence micrographs of the astrocytes were taken and a 3D caption compiled (the layer thickness of the total photographs amounts to 17* 400µm.) so as to be certain that larger accumulations of ferrous fluids or their aggregates had actually accumulated in the cells and cell organelles. As standard method the fluorescence pictures were analyzed by fluorescence-intensity using Nis-Elements software (Nikon). Here the colors red and green were used to improve comparability when presenting the results in terms of light intensity plots. Due to the decomposition of the microscope (0.1µm/px on non biological standards) it is not possible to quantify the lysosomes sizes (uncountable), pursuant to the literature their sizes vary between 0.1µm and 1.2µm (Kuehnel 2003).

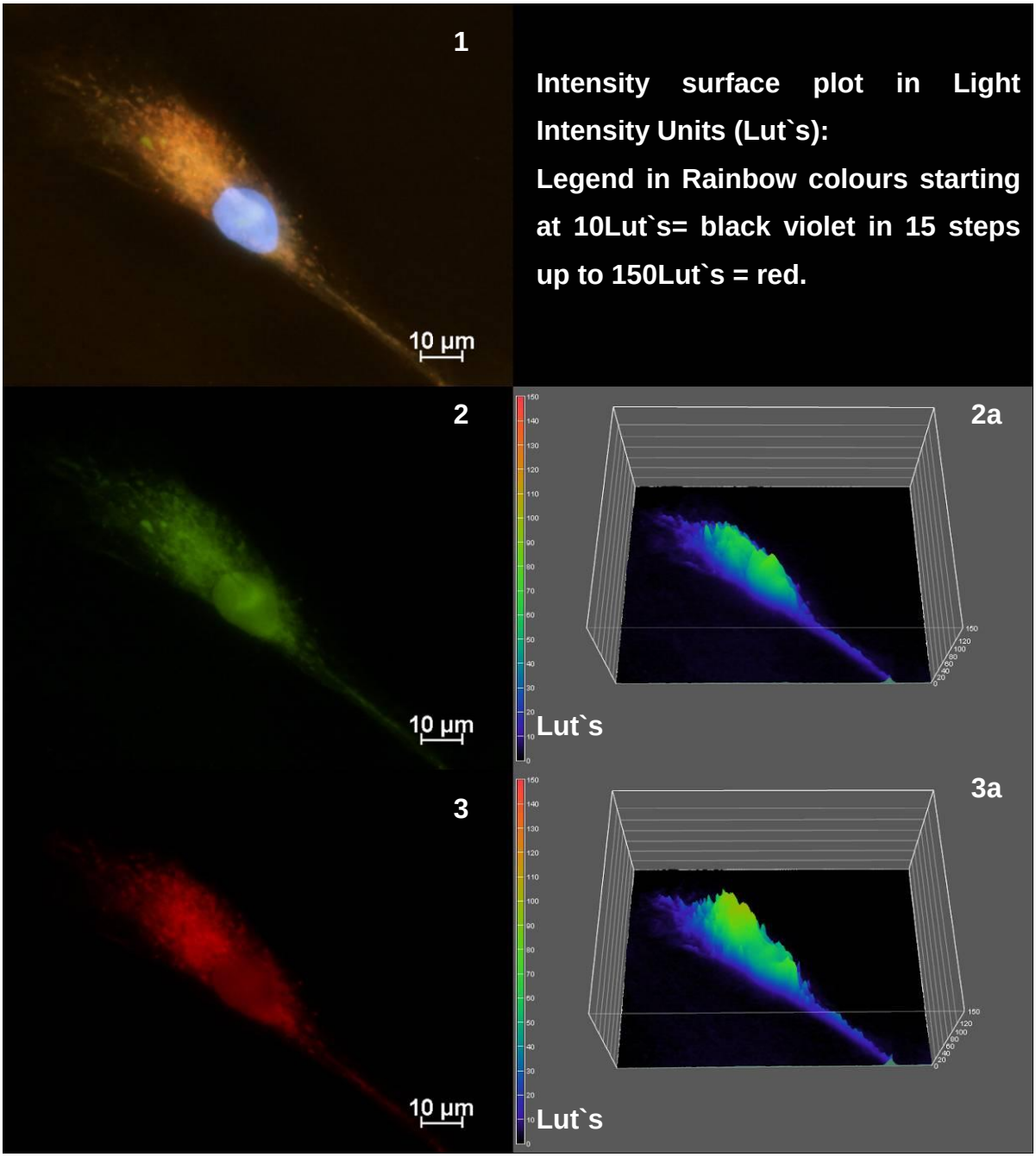

Figure 24: Fluorescence analyzes of Astrocytes control –B

1) Multicolor picture including ER-Tracker, LysoTracker and DAPI stained Nucleus.

2) Green channel: Localisation of Endoplasmic Reticulum

2a) Light Intensity surface plot of green channel

3) Red channel: Localisation of Lysosomes

3a) Light Intensity Surface plot of Red channel

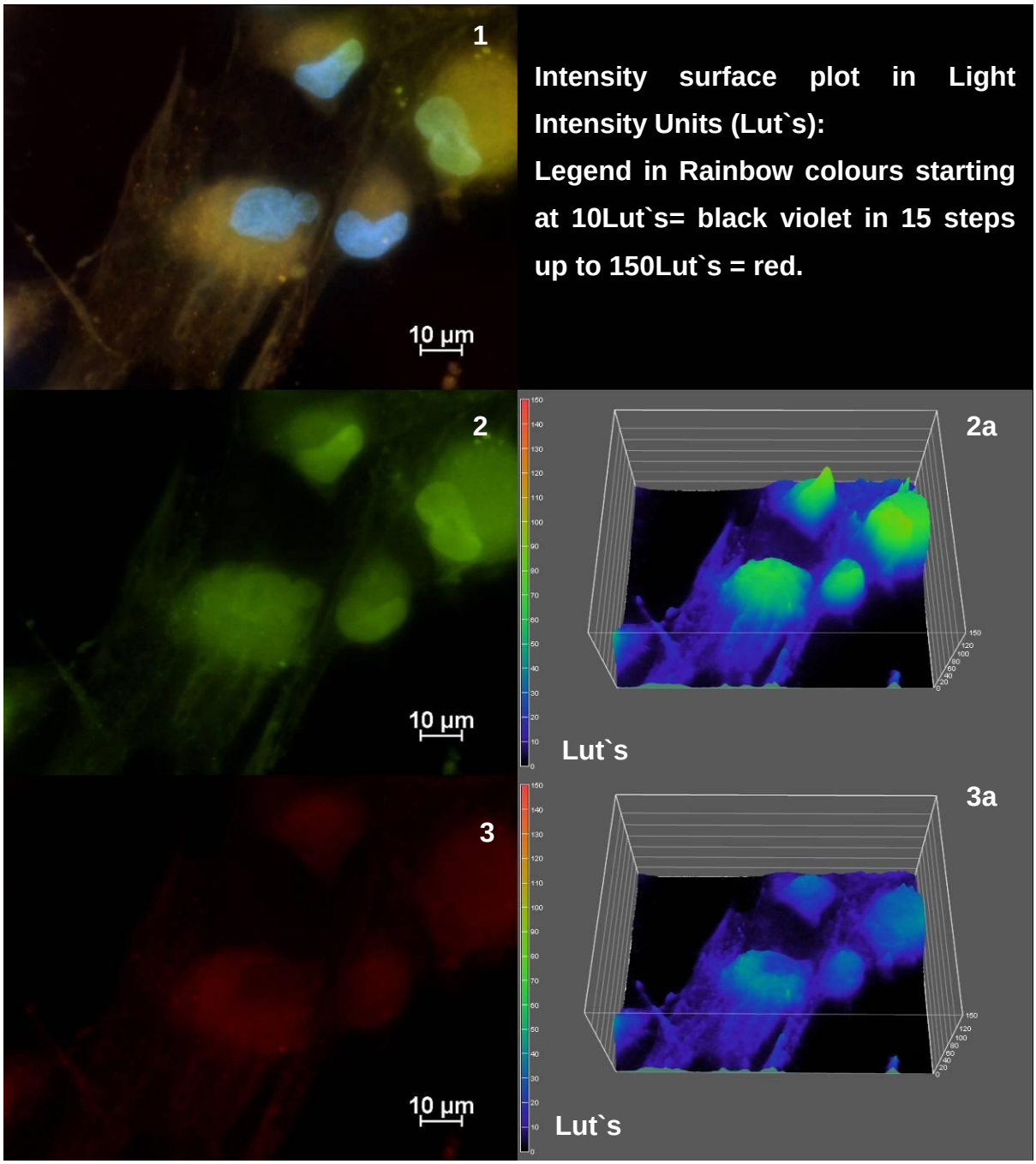

B

Figure 25: Fluorescence analyses of Astrocytes control +B

1) Multicolor picture including ER-Tracker, LysoTracker and DAPI stained Nucleus.

2) Green channel: Localisation of Endoplasmic Reticulum

2a) Light Intensity surface plot of green channel

3) Red channel: Localisation of Lysosomes

3a) Light Intensity Surface plot of Red channel

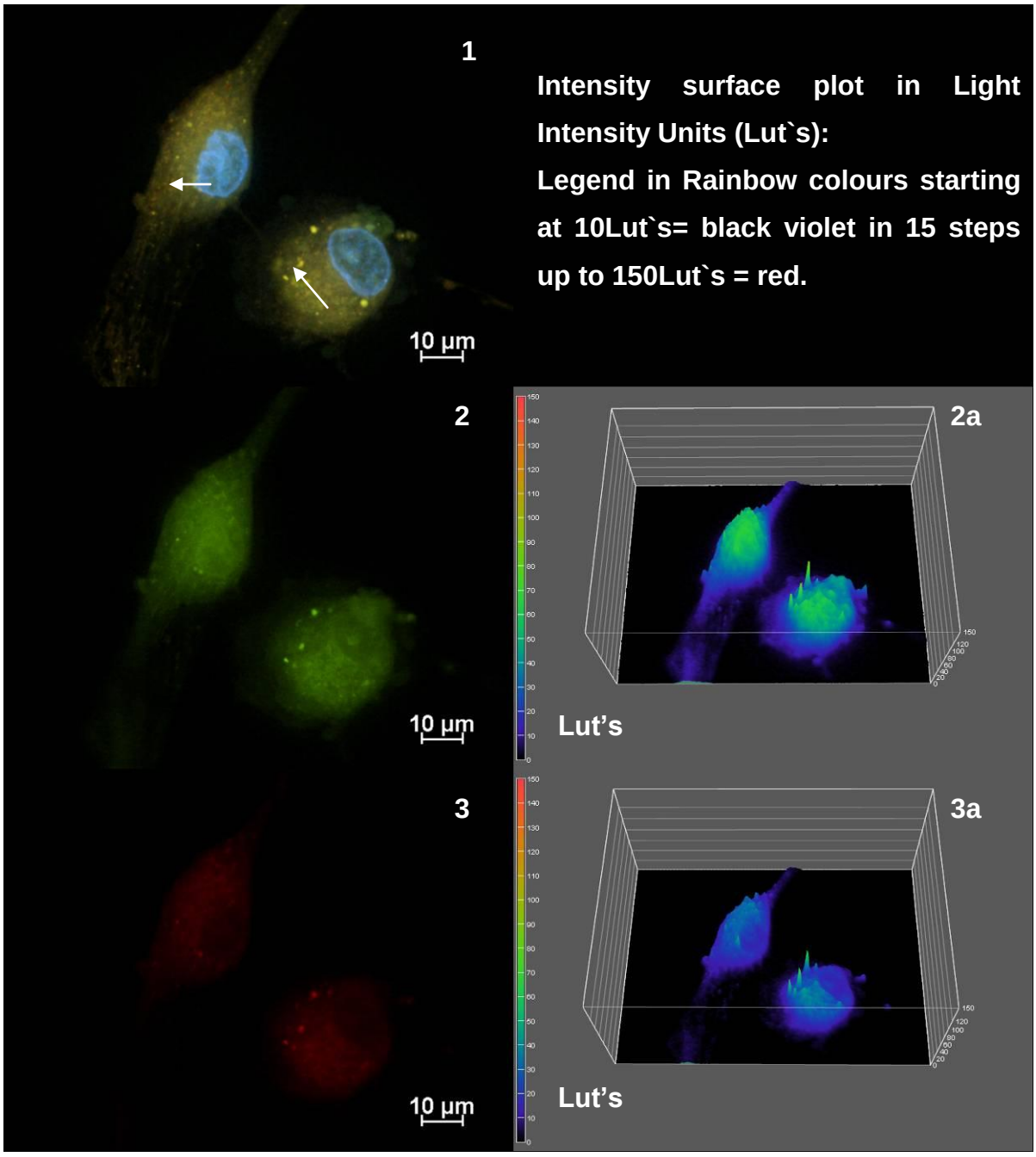

Figure 26: Fluorescence analyzes of Astrocytes 0.25 NP-MA-B

1) Multicolor picture including ER-Tracker, LysoTracker and DAPI stained Nucleus.
   ⟵ Examples for lysosomes with ferrofluids inside
2) Green channel: Localisation of Endoplasmic Reticulum
2a) Light Intensity surface plot of green channel
3) Red channel: Localisation of Lysosomes
3a) Light Intensity Surface plot of Red channel

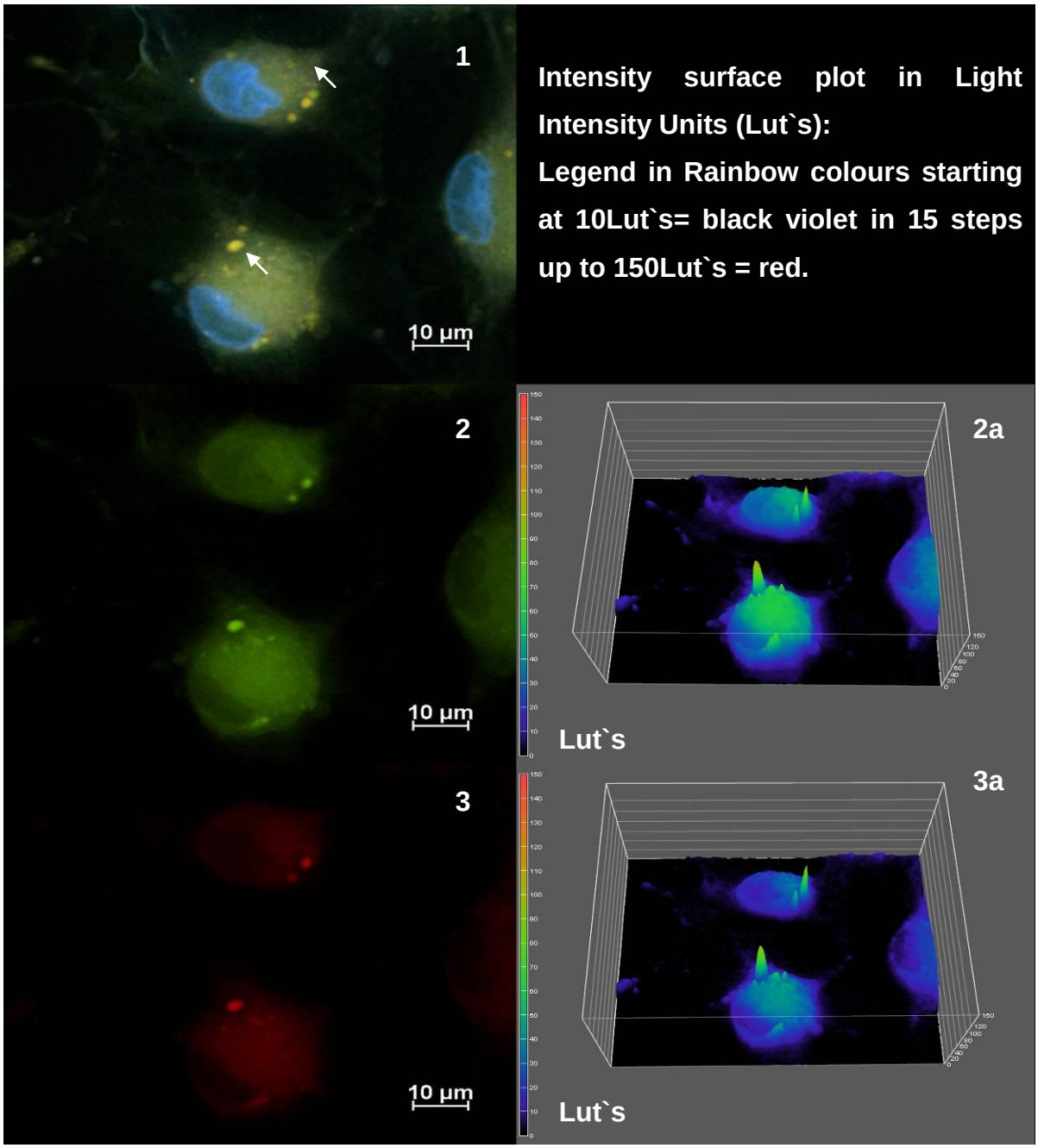

Figure 27: Fluorescence analyzes of Astrocytes 0.25NP-MA+B

1) Multicolor picture including ER-Tracker, LysoTracker and DAPI stained Nucleus.
   ⟵ Examples for lysosomes with ferrofluids inside
2) Green channel: Localisation of Endoplasmic Reticulum
2a) Light Intensity surface plot of green channel
3) Red channel: Localisation of Lysosomes
3a) Light Intensity Surface plot of Red channel

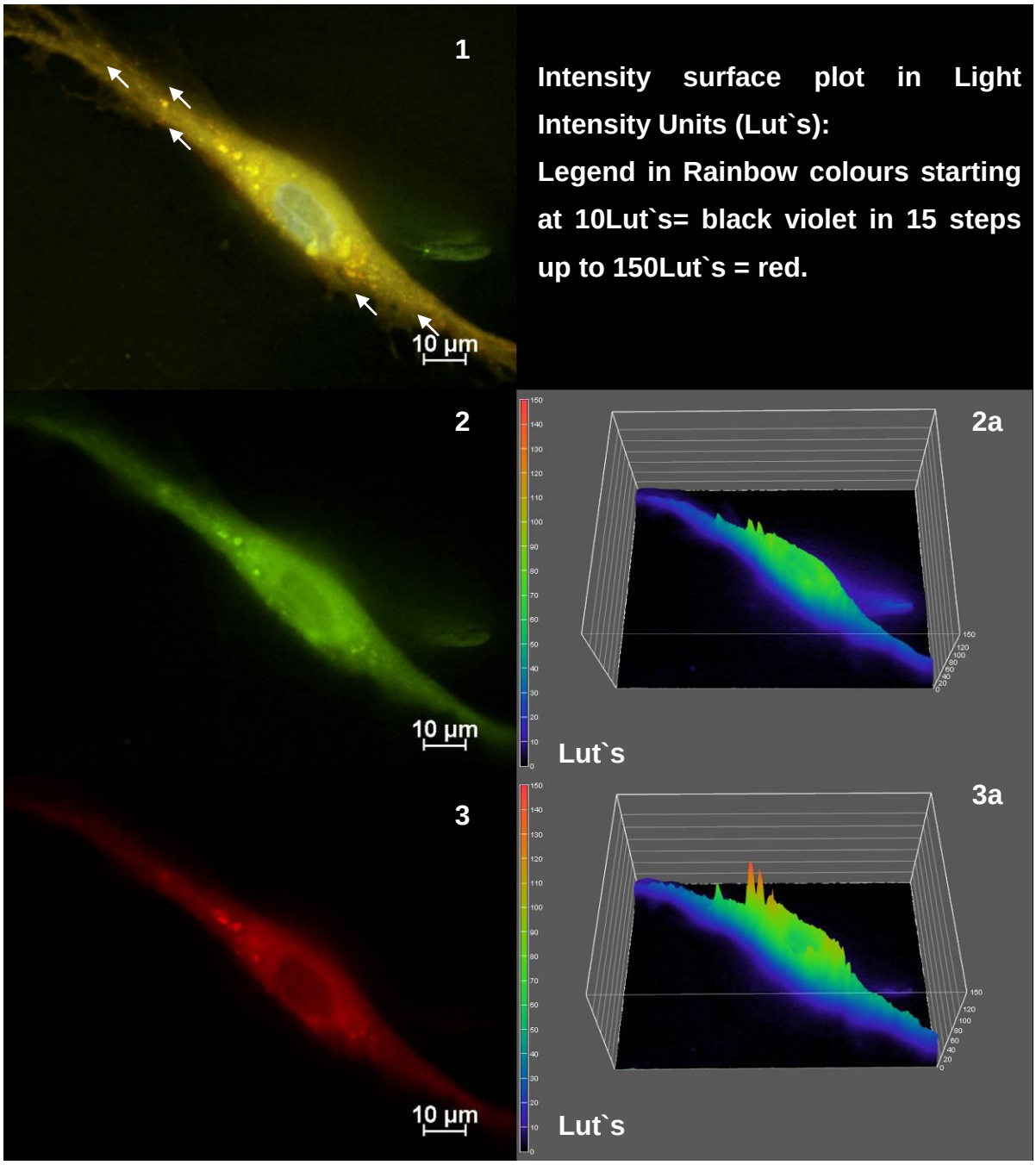

Figure 28: Fluorescence analyzes of Astrocytes 0.5NP-MA –B

1) Multicolor picture including ER-Tracker, LysoTracker and DAPI stained Nucleus.
   ⟵ Examples for lysosomes with ferrofluids inside
2) Green channel: Localisation of Endoplasmic Reticulum

2a) Light Intensity surface plot of green channel

3) Red channel: Localisation of Lysosomes

3a) Light Intensity Surface plot of Red channel

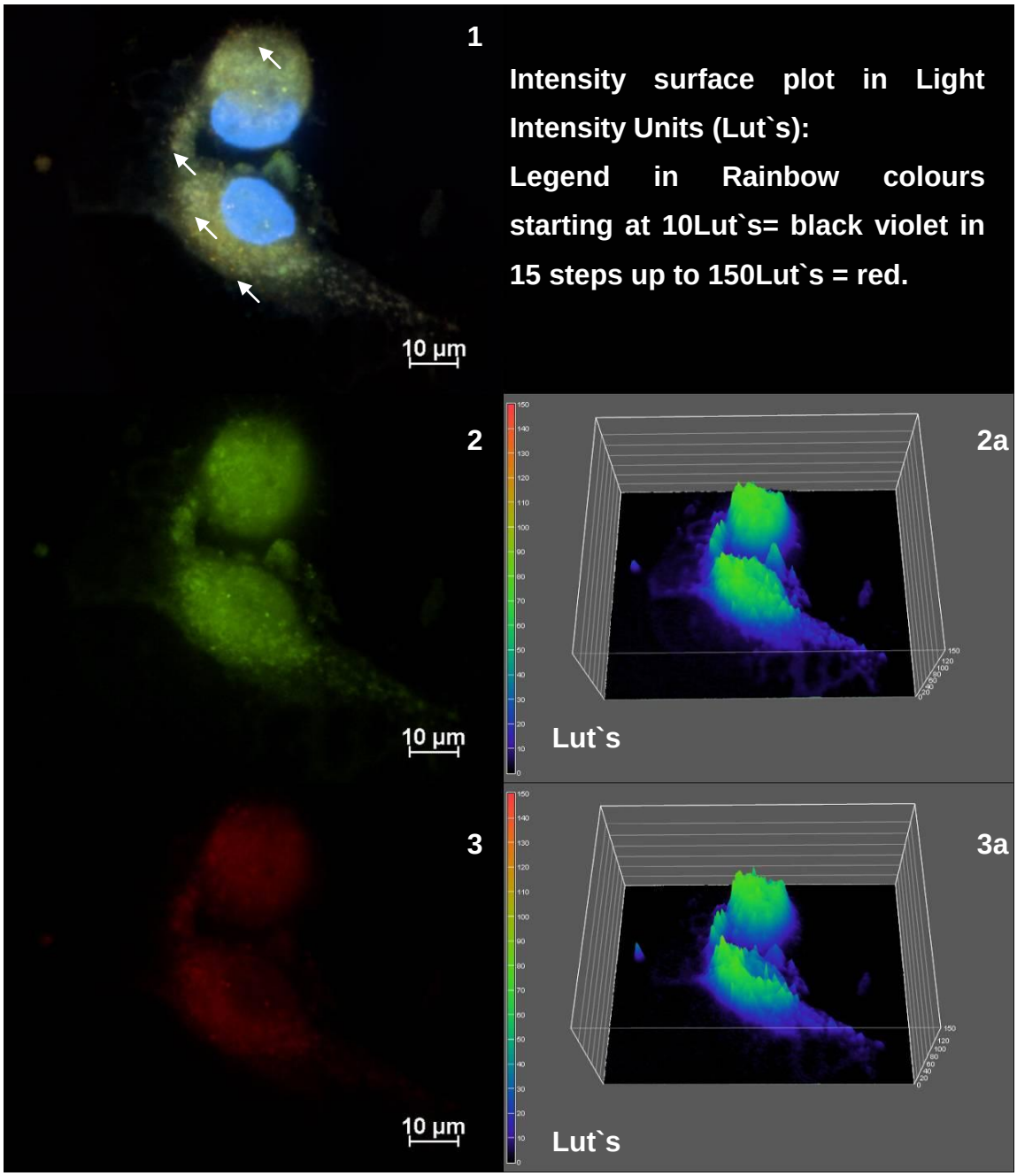

Figure 29: Fluorescence analyzes of Astrocytes 0.5NP-MA +B

1) Multicolor picture including ER-Tracker, LysoTracker and DAPI stained Nucleus.

⟵ Examples for lysosomes with ferrofluids inside

2) Green channel: Localisation of Endoplasmic Reticulum

2a) Light Intensity surface plot of green channel

3) Red channel: Localisation of Lysosomes

3a) Light Intensity Surface plot of Red channel

Figure 24 depicts the ER- network of an astrocyte from the control group with a colocalisation of many small lysosomes (dia. approx. 0.1µm, seen as fluorescence signal). The distribution of the lysosomes is mainly concentrated on the center of the cell. To compare the possible influence of the nanoparticles and the magnetic field, the cells were analyzed using light intensity / area. Therefore all documented cells were used. The averages are presented in the table below.

	Light Intensity of lysosomes		**Light intensity of ER**	
Astrocytes	-B	+B	-B	+B
Control	32.56	24.18	25.96	40.32
0.25 NP-MA	28.76	29.39	34.69	24.44
0.5 NP-MA	35.43	29.87	40.58	35.64

Table 4: Averages of light intensity measurement / area for astrocytes

For both measurements standard deviations between 1 and 13 were found, so that the differences between the groups were not significant. Collectively considered it can be inferred that intensity of lysosomes concentration do not change by the addition of nanoparticles. Furthermore from the intensity measurement of the ER no clear trend could be found. Commonly the astrocytes show no or miniscule intracellular signs of stress. However, as demonstrated in the previous chapter it is very hard to detect agglomerates of ferrofluids in astrocytes. In order to improve the visibility of iron containing regions in astrocytes Berliner Blue Staining was employed, as can be seen figure 36.

For a better visualization the original pictures are found on the data CD at the back cover of this work!

III.5.2.2 Cell Organelle Staining of *Glioblastoma multiforme* (G55)

For analysis of the glioblastoma cells the same conditions as for astrocytes were employed. Here the normal sizes of lysosomes were not able to be measured and or counted. Consequently the micrographs were quantified by measurement of the light intensity using the software intern calibration.

For a better visualization the original pictures are found on the data CD at the back cover of this work!

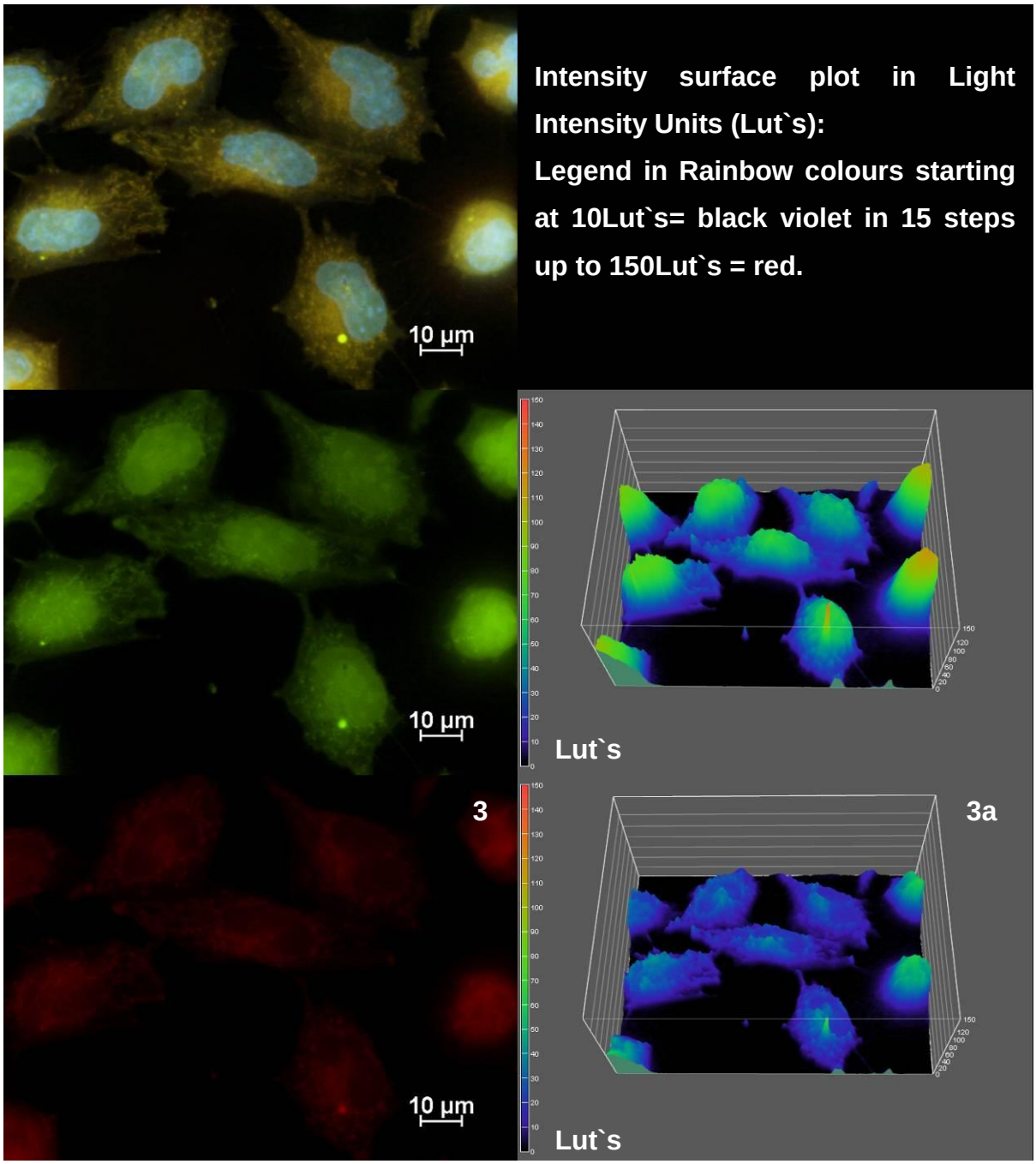

Figure 30: Fluorescence analyzes of G55 control-B

1) Multicolor picture including ER-Tracker, LysoTracker and DAPI stained Nucleus.

2) Green channel: Localisation of Endoplasmic Reticulum

2a) Light Intensity surface plot of green channel

3) Red channel: Localisation of Lysosomes

3a) Light Intensity Surface plot of Red channel

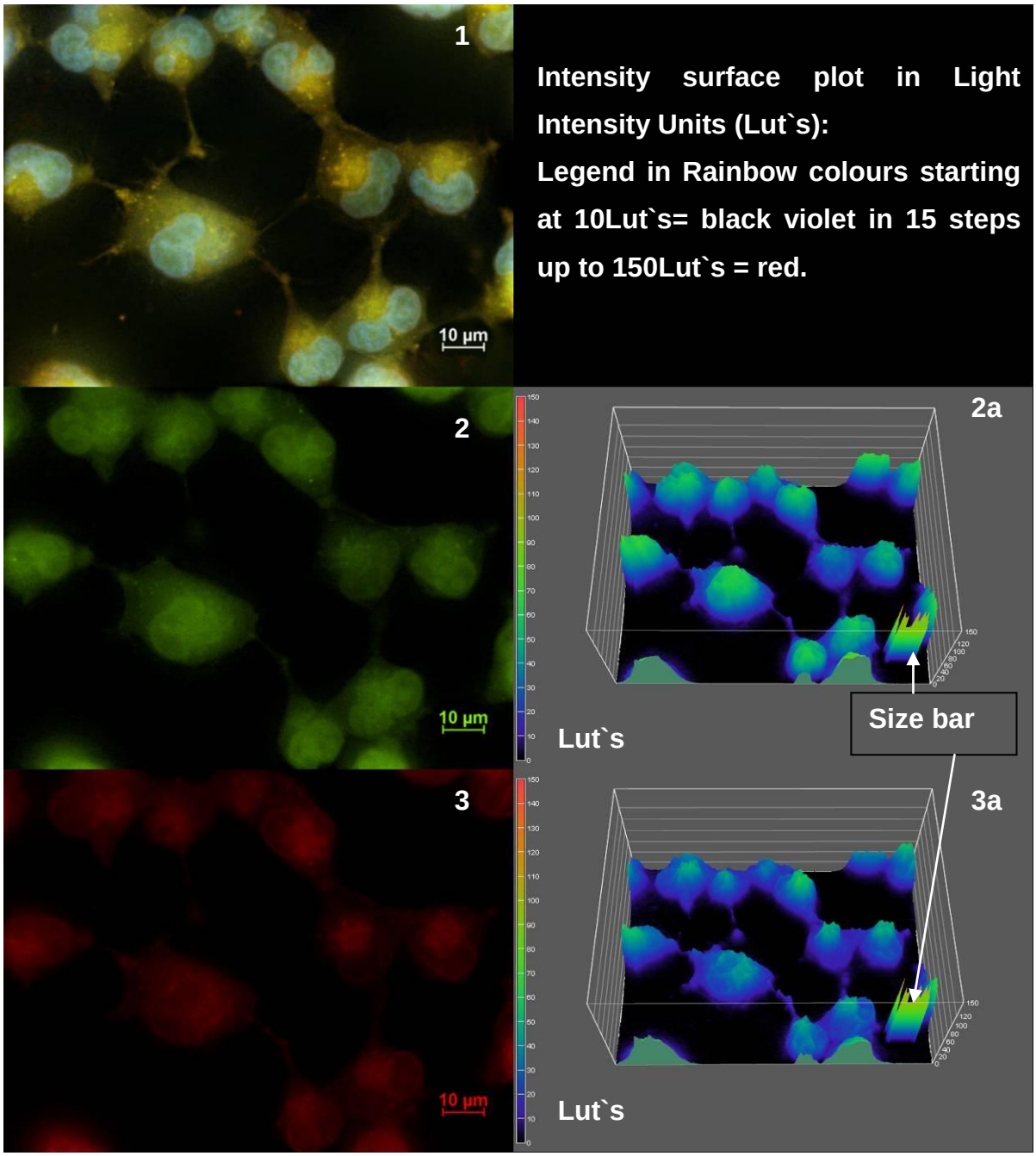

B

Figure 31: Fluorescence analyses of G55 control +B

1) Multicolor picture including ER-Tracker, LysoTracker and DAPI stained Nucleus.

2) Green channel: Localisation of Endoplasmic Reticulum

2a) Light Intensity surface plot of green channel

3) Red channel: Localisation of Lysosomes

3a) Light Intensity Surface plot of Red channel

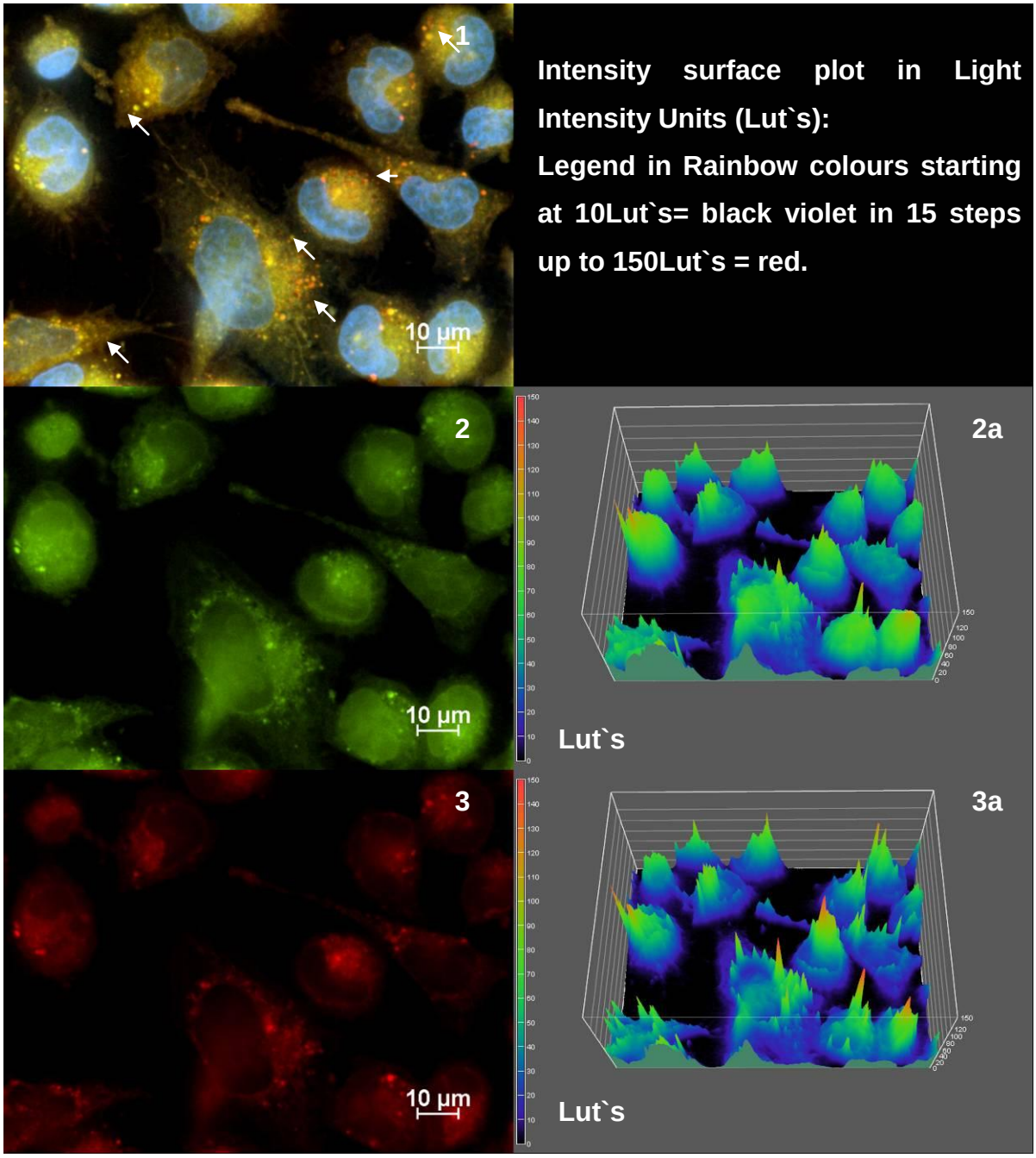

Figure 32: Fluorescence analyzes of G55 0.25NP-MA-B

1) Multicolor picture including ER-Tracker, LysoTracker and DAPI stained Nucleus.
   ⟵ Examples for lysosomes with ferrofluids inside
2) Green channel: Localisation of Endoplasmic Reticulum
2a) Light Intensity surface plot of green channel
3) Red channel: Localisation of Lysosomes
3a) Light Intensity Surface plot of Red channel

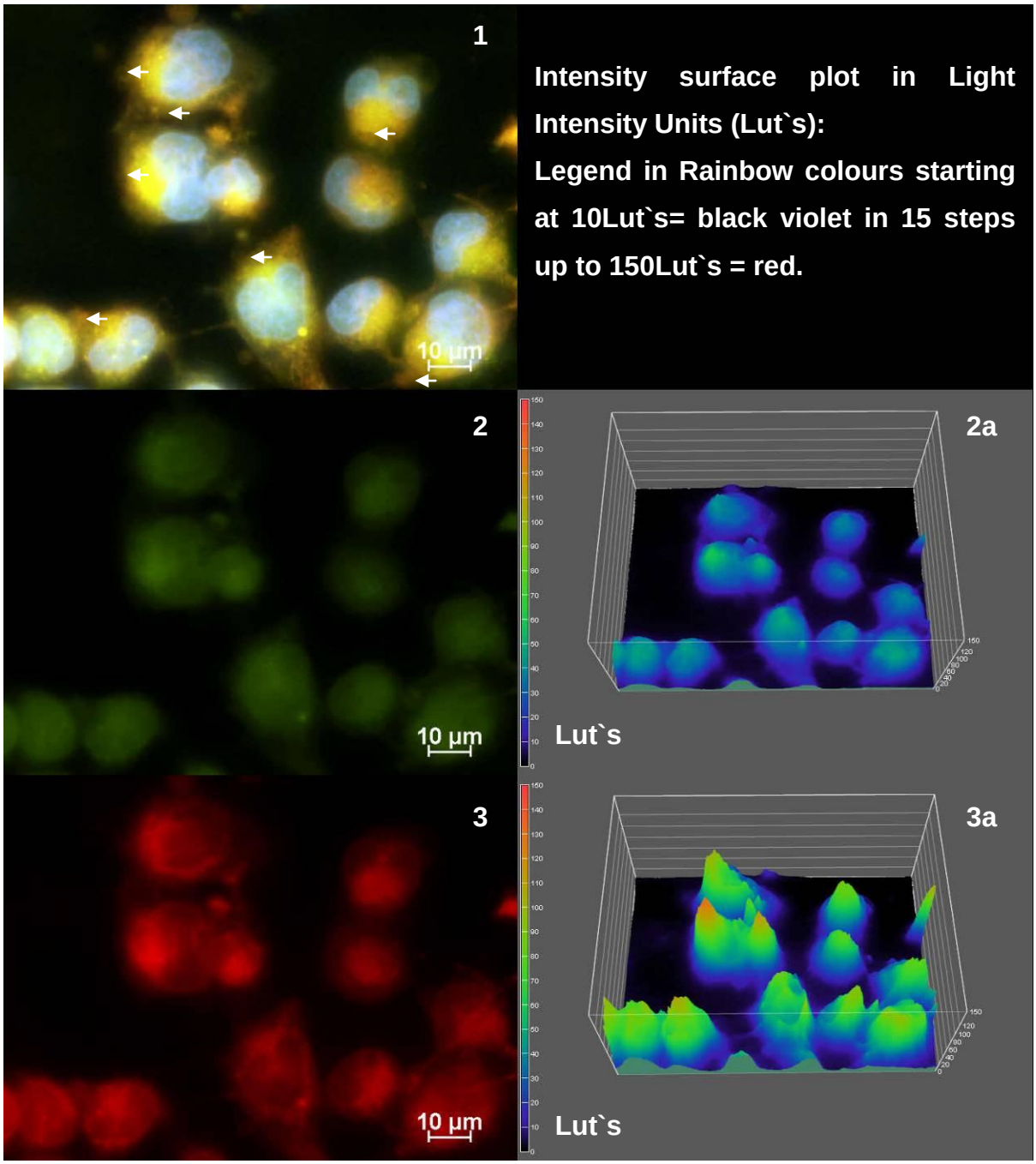

B

Figure 33: Fluorescence analyzes of G55 0.25 NP-MA +B

1) Multicolor picture including ER-Tracker, LysoTracker and DAPI stained Nucleus.
   ⟵ Examples for lysosomes with ferrofluids inside?
2) Green channel: Localisation of Endoplasmic Reticulum
2a) Light Intensity surface plot of green channel
3) Red channel: Localisation of Lysosomes
3a) Light Intensity Surface plot of Red channel

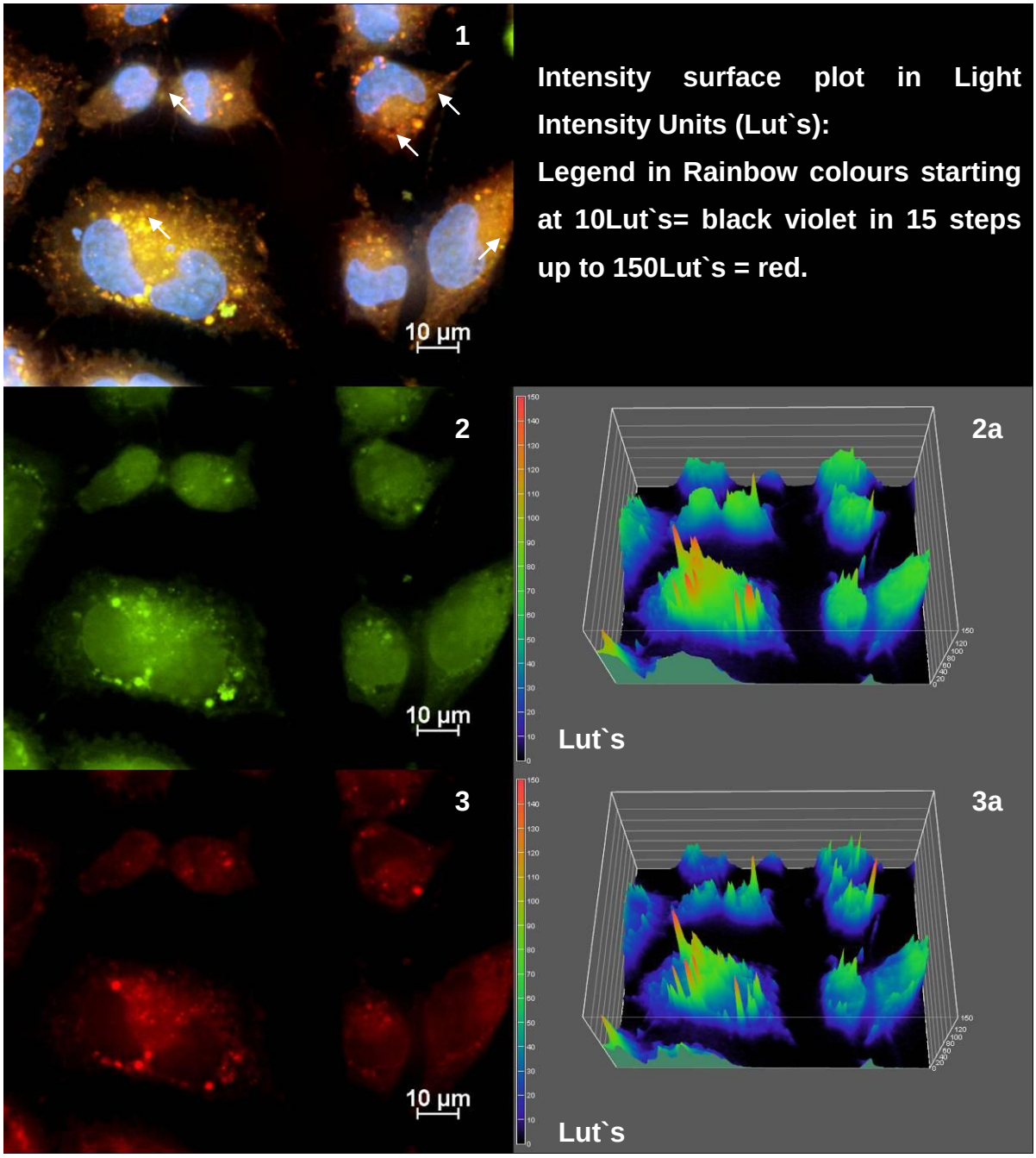

Figure 34: Fluorescence analyzes of G55 0.5NP-MA-B

1) Multicolor picture including ER-Tracker, LysoTracker and DAPI stained Nucleus.
   ⟵ Examples for lysosomes with ferrofluids inside
2) Green channel: Localisation of Endoplasmic Reticulum
2a) Light Intensity surface plot of green channel
3) Red channel: Localisation of Lysosomes
3a) Light Intensity Surface plot of Red channel

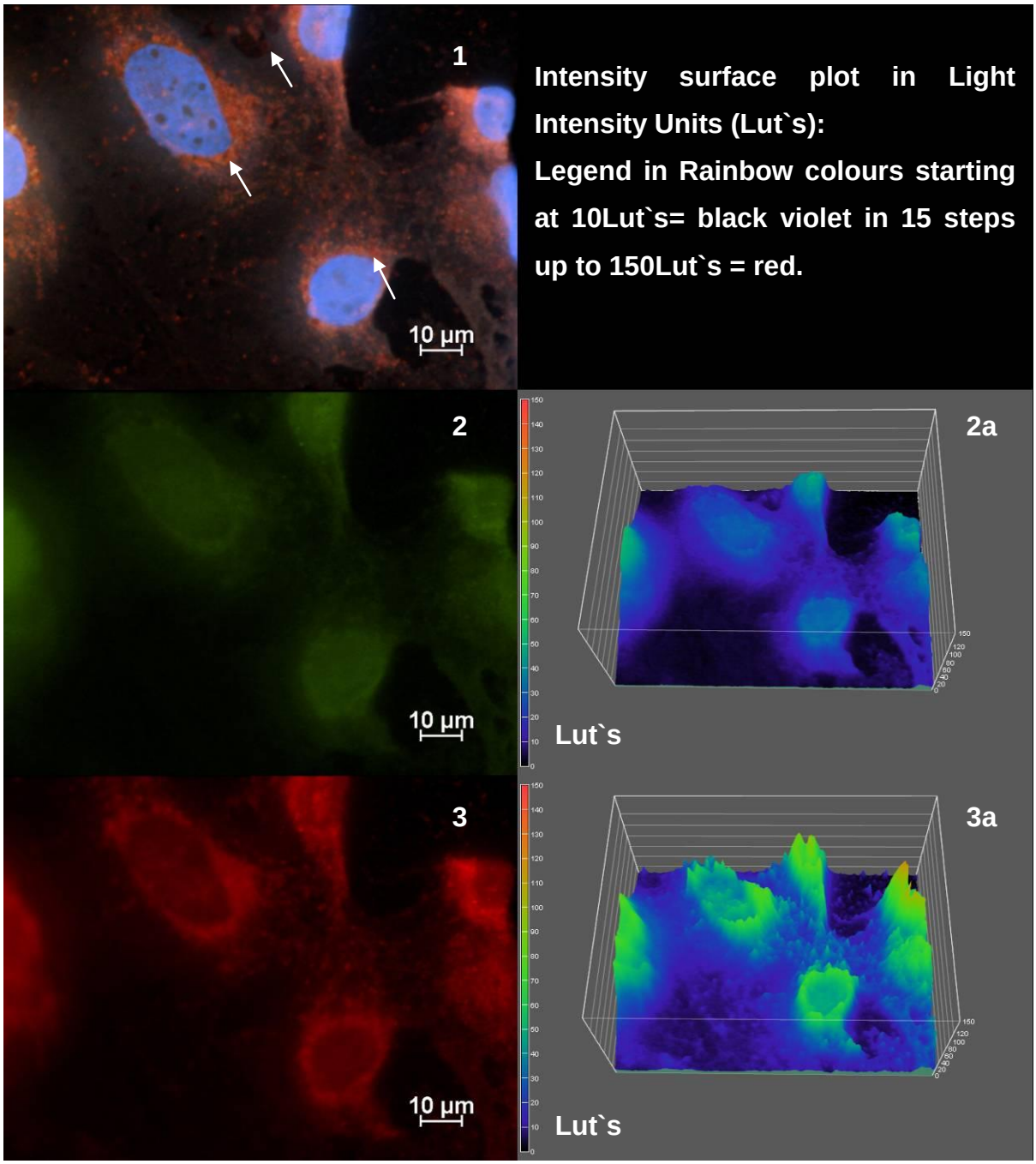

Figure 35: Fluorescence analyzes of G55 0.5NP-MA+B

1) Multicolor picture including ER-Tracker, LysoTracker and DAPI stained Nucleus.

⟵ Examples for lysosomes with ferrofluids inside

2) Green channel: Localisation of Endoplasmic Reticulum

2a) Light Intensity surface plot of green channel

3) Red channel: Localisation of Lysosomes

3a) Light Intensity Surface plot of Red channel

Glioblastoma cells show interesting physical differences compared with control cells and cells fed with nanoparticles, as well as cells incubated with and without the influence of a magnetic field. For example cells incubated without influence of the magnetic field demonstrate a well elongated cell body, whereas cells incubated in the magnetic field are more spherical in appearance and the endoplasmic reticulum and the lysosomes are concentrated more towards the center of the cell (figure 31+35). This is in comparison to control cells figure 30+32 (B-) where the lysosomes show a very even distribution throughout the cell body. In the case of cells incubated containing nanoparticles these demonstrate an amplification of the size and lysosomes intensity dependent on nanoparticles concentration. Results are as presented in the table below. The standard deviation for each is between 2 and 6 Lut´s.

	Light Intensity of lysosomes		**Light intensity of ER**	
G55	-B	+B	-B	+B
Control	20.09	25.05	34.38	29.01
0.25 NP-MA	31.89	39.14	39.51	27.96
0.5 NP-MA	30.49	50.25	41.91	18.63

Table 5: Results of intensity measurement / area for G55 cells

Nanoparticles containing cells not exposed to the magnetic field, Figure 32 (0.25NP-MA) and Figure 34 (0.5NP-MA) demonstrate at equivalent fluorescence strength a less clear structure and reduction of the ER's (see table 5), while strong spherical structures are seen to form in the vicinity of the lysosomes. Within these cells a clear deposit of opaque ferrous fluids (agglomerates) is observed in the lysosomes. These results are correlating with the findings in figure 23, where large spherical agglomerates of nanoparticles could be detected in cells treated with NP-MA.

When observed under the optical light microscope these structures (figure 32+33 (0.25NP-MA) and figure 34+35 (0.5NP-MA)) appear very different.

In Figure 32 (in magnetic field) for example, the majority of lysosomes and the ER are no longer recognizable as individual cell compartments, rather as a large mass essentially concentrated at one point within the cell. These agglomerations show a preference towards the bottom left of the cell in accordance with the magnetic field.

Here most of the cell bodies align their self to the magnetic gradient (figure 32) and that the nucleus at least is also pulled in this direction.
Ferrous fluids however are difficult to visualize but in general are to be found as agglomerates in the lysosomes (Levy 2010). In the case of cells with the highest concentration of nanoparticles and where these cells were incubated in the magnetic field, Figure 35, they demonstrate a decrease in the ER's (fluorescence decreases to 18.63 Luts), while simultaneously there is much less demarcation of the cells visible. Aggregates of ferrous fluids in the lysosomes are also clearly recognizable. As too is the structure of the cell which is clearly different from all other cells. Furthermore these cells are injured and maybe dying.

III.5.2.3 Astrocytes versus G55

When comparing Astrocytes and G55, the G55 cells show a larger quantity and magnification of lysosomes as a result of the incorporated magnetite ferrofluids. Astrocytes show no or miniscule differentiation of the investigated cell organelles. However, the changes of the normal cell-structure are much more pronounced in the glioblastoma cells.
Furthermore, when the results of cells exposed to a magnetic field were compared, Astrocytes showed no reaction, while G55 appeared more rounded and less stretched. When focusing on cells containing nanoparticles, here large differences were observed. G55 demonstrated an interesting reaction after treatment with the low ferrofluid concentration and application of the magnetic field, this being that most of the cells gathered in the direction to the magnetic gradient (figure 33). Astrocytes with the high concentration when exposed to the magnetic field showed no reaction, while glioblastoma cells looks really stressed and injured.

Looking at the distribution of particles in the cell, large differences could be observed between astrocytes and glioblastoma multiforme cells.
When employing cell organelle staining in astrocytes it is very difficult to see hot spots (accumulations) of ferrofluids (figure 26-29) correlating to figure 22, hence a Berliner blue staining was used for a closer view. The result of astrocytes iron incorporation reveals a completely different picture (figure 36). The distribution is

decentralized and focused on several small, well-defined areas spread over the whole cell. Hot spots of iron were found in cells appendages. The area around the cell nuclei can be seen to be largely free.

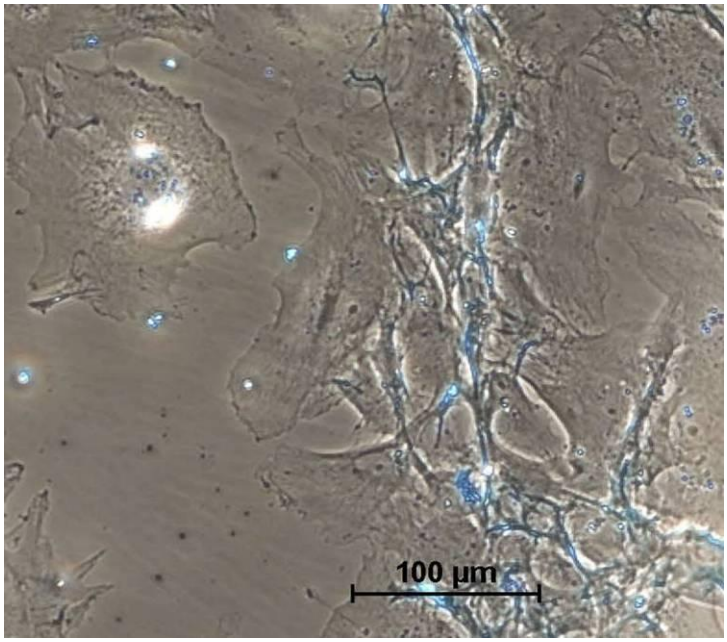

Figure 36: Berliner blue staining of astrocytes treated with media containing nano-particles 0.5 µL/mL NP-MA for 48h.

In the glioblastoma cells, the nanoparticles are concentrated around the nuclei (see chapter III.1. figure 5, III.6 figure 23 and III.7). In these areas are located the endoplasmic reticulum with ribosome's, liposome's, and the Golgi apparatus. From the figures 32, 34 and 35 it is clear that large amounts of nanoparticles are detectable in the lysosomes.

All things considered it is evident that due to the nanoparticles, the astrocytes only have marginal influence on cell compartmental formation, while the influence of the magnetic field is difficult to determine. In comparison with the glioblastoma cells however, a very strong change in internal cell structure can be observed and differences in organizational structure in the magnetic field are considerable. This is a plausible reason for the reduced cell proliferation of G55.
The cell migration experiments clearly demonstrate differences in cell behavior.

III.6 Magnetically directed Migration

The previous chapters have shown that no negative effect on astrocytes could be observed when using nanoparticles in combination with the developed magnetic field. Glioblastoma cells showed varied forms of reactions after incorporation of the ferrofluid, especially in combination with the magnetic field. Of interest now is whether this difference could be observed under conditions of cell migration. To establish the migration assay the samples were placed one centimeter away from the highest gradient (magnets left arm; as depicted on figure 16; page 66). This was the best place for the starting area, because here the highest density of the parallel magnetic field lines is located, having a relatively good magnetic value of 30mT.

III.6.1 Migration of Astrocytes

Unloaded astrocytes (as control) and cells loaded with magnetic particles (incubated for 2 days with 0.25 mL/mL or 0.5 mL/mL NP-MA (nanoparticles / medium)), were tested with and without magnetic field for 24h.

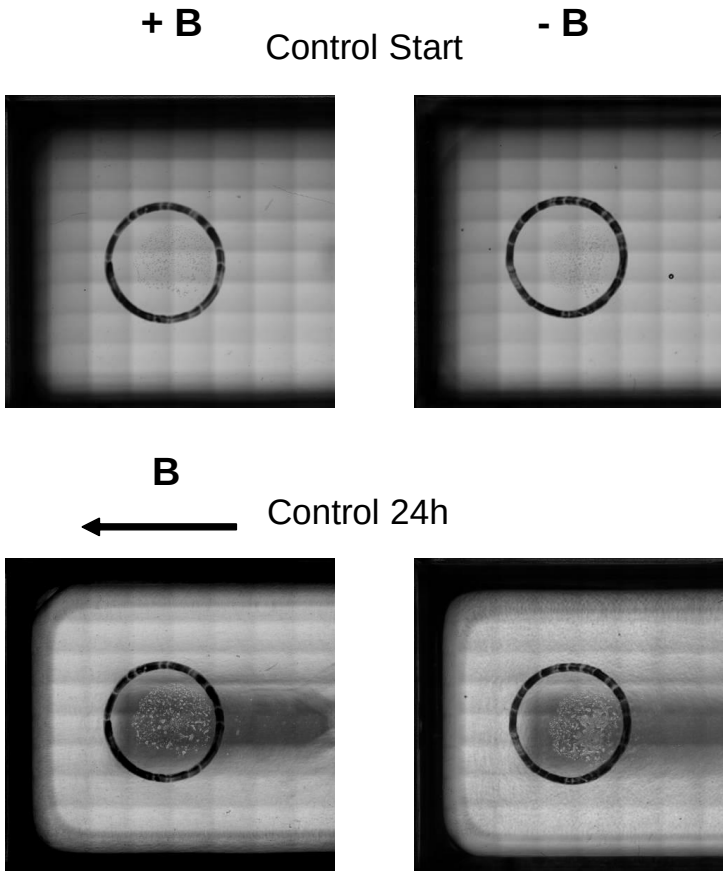

Figure 37: Start and result of migration for Astrocytes control cells.

At the beginning of the experiment the cells are located in the black circle; the cells have at this point not reached their fully adhered form. After 24h the cells are now fully adhered but no migration could be observed. *Because the start cells are barely visible the data are saved as Power Point Astro- Migration on the CD at the end of this work!*

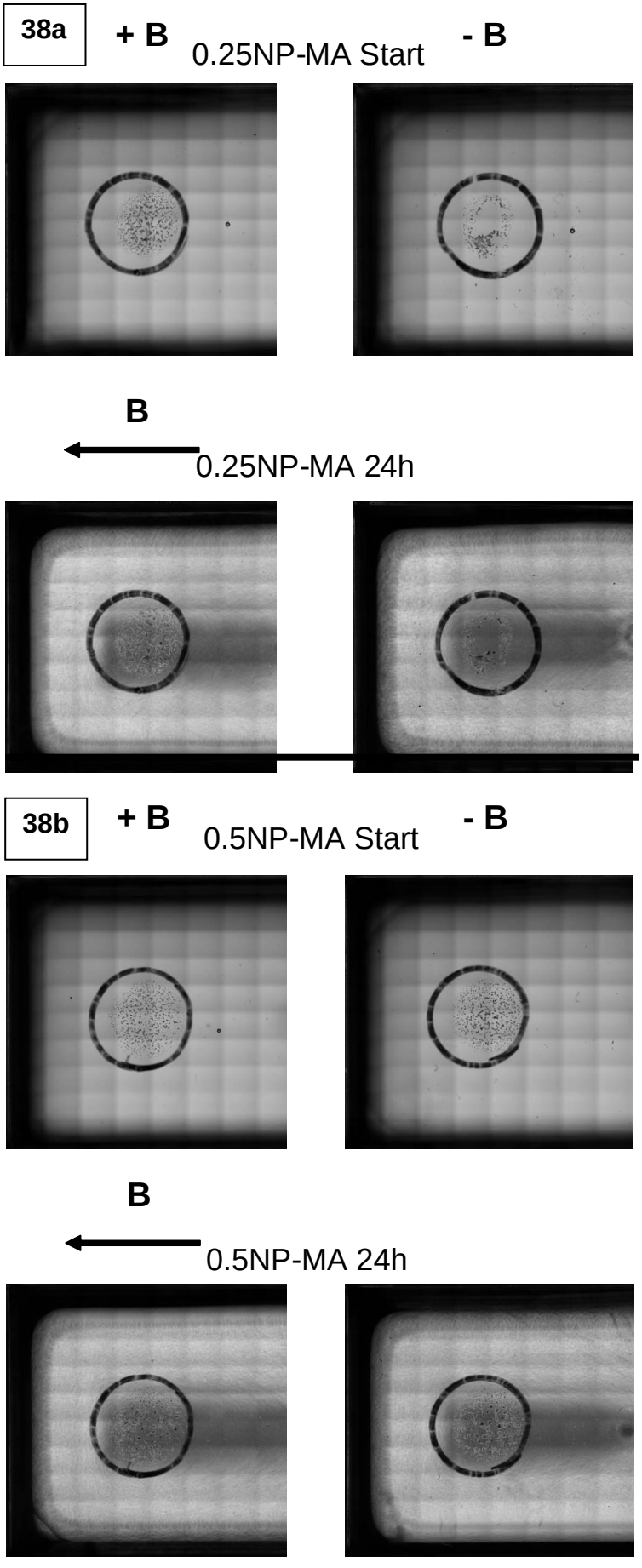

Figure 38:
Start and result of Astrocytes pre-incubated with 0.25NP-MA (38a) and 0.5NP-MA (38b)
It was found that the cells behave like the control cells. No differences between cells incubated with or without exposure magnetic field could be observed.

In this study natural independent movement of cells is classified as 0 since no points of reference are present. This is due to the type of documentation, start and result are presented as scan pictures so only the individual momentary state was able to capture.
For Astrocytes figure 37+ 38 no differences between cells incubated for 24h in the magnetic field or without magnetic field (both cell culture incubator 37ºC, 90% relative humidity). The cells always show normal behaves for adhesion and are fully stretched after 24h. The cells do not migrate.

III.6.2 Migration of Glioblastoma G55

Unloaded glioblastoma cells (as control) and cells loaded with magnetic particles (incubated for 2 days with 0.25 mL/mL or 0.5 mL/mL NP-MA (nanoparticles / medium)), were tested with and without magnetic field for 24h. Comparisons of the pictures taken at the start and after 24h demonstrate that more cells occupy the marked regions than were initially present, but also that cells occupy and close the holes deliberately produced by the tip of a pipette. In this study natural independent movement of cells is classified as 0 since no points of reference are present. However, using the current form of visualization (scan-picture made up of 150 single images) differentiation of small cell movements as described for Glioblastoma cells (De Hauwer, 1997) were not able to be captured. Cells that were not exposed to an external magnetic field showed only a minor natural mobility. It could be observe that cells without nanoparticles (control) move more than loaded cells and mainly to one side. In contrast, cells loaded with minimal nanoparticle- (0.25 NP-MA, figure 41) when exposed to the magnetic field moved the most. During exposure to the magnetic field, heavily loaded cells (0.5 NP-MA, figure 43) however did not and uncharged cells (control) only moved a little.

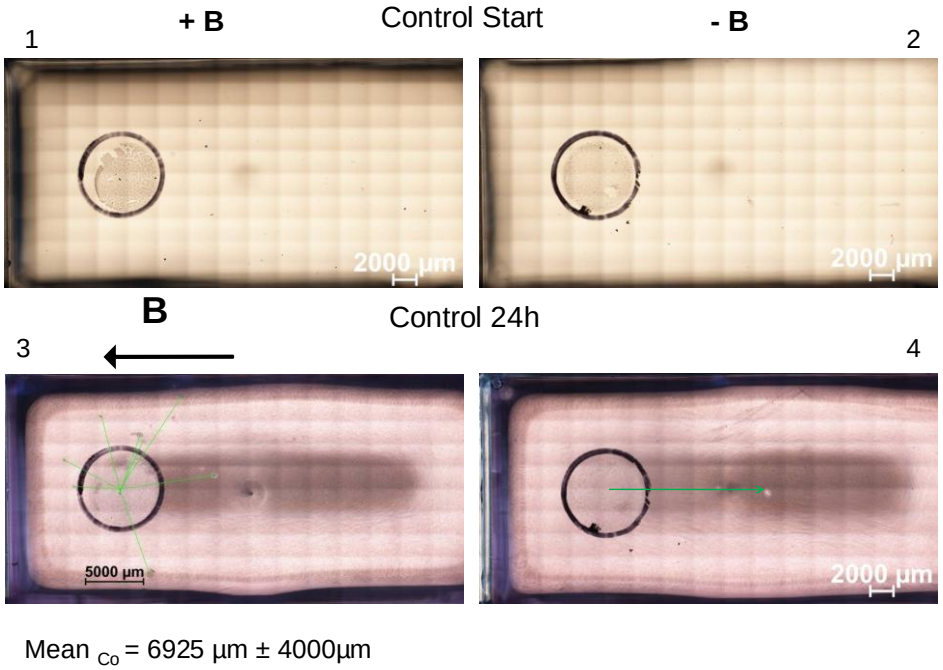

Mean $_{Co}$ = 6925 µm ± 4000µm

Figure 39: Start and result of migration for G55 control cells.

The cells were pre-incubated using nanoparticles free media (control), and then incubated with and without exposure to the developed magnetic field for 24h.

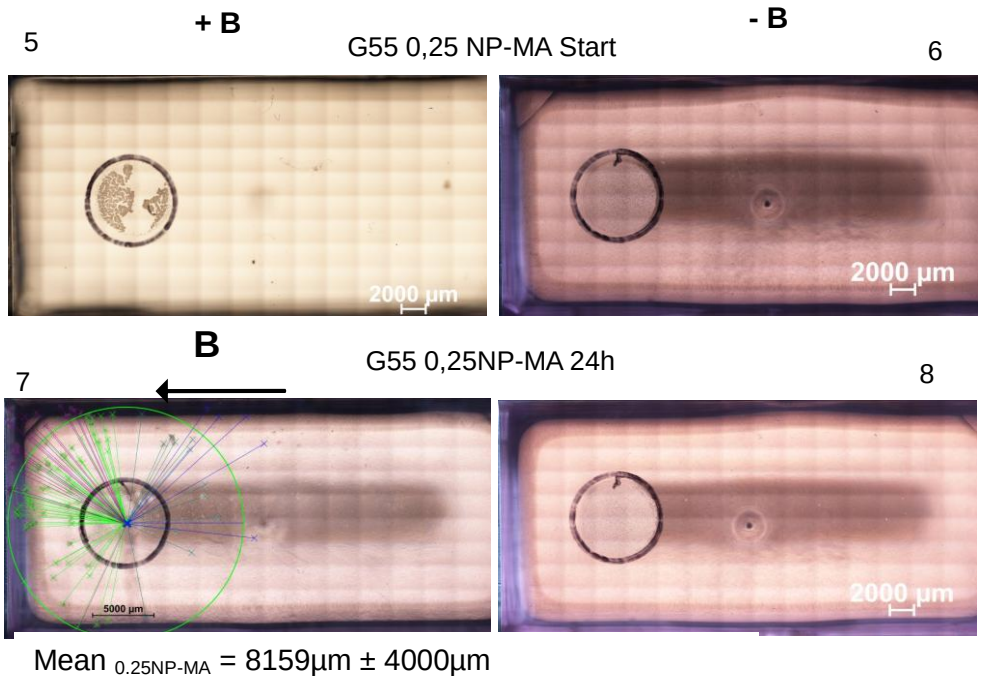

Figure 40: Start and result of migration for G55 0.25NP-MA cells

The cells were pre-incubated with media supplemented with 0.25µL/mL NP-MA, and then incubated with and without exposure to the developed magnetic field for 24h.

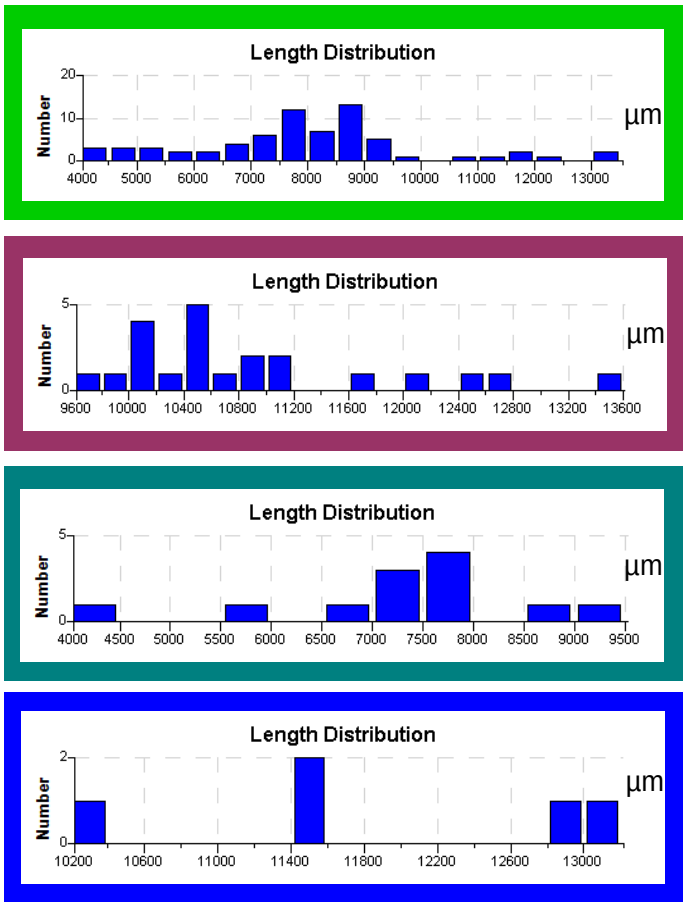

Figure 41: Length distribution of migration

green) measurements to left side inside the green circle mean= 7913.31 ± 1861µm , n=67, **red)** measurements to left side outside the green circle, mean= 10903.22 ± 968,37µm, n=22; **turquoise)** measurements to right side inside the green circle, mean= 7287.58 ± 1312.08µm, n=12, **blue)** measurements to right side outside the green circle, mean= 11879.51 ± 1000µm n=5

Strong divergences in the migration distribution patterns were observable. For control cells (figure 39), no definite movements were detectable (when placed in the magnetic field), while 84% of the low-loaded cancer cells shift to the magnetic wall. A small part is ascribed to any particular direction and a few cell spheres move in an opposite direction to the gradient. Because cells moving to the left side are stopped automatically by the end of the chamber wall, whereas cells moving in the opposite direction are not hindered, a two part analysis is required for better comparison:

The green circle (figure 40) shown at 0.25 NPMA 24h represents the limit of the track when the cells move unhindered straight forward. The measurement of migration is divided into two parts: with the magnetic field and against the major gradient (figure 40+41), as well as within and outside of the circle.

The result is that many more cells 84% move to the larger magnetic gradient. In contrast, 16% move laterally to the chamber and against the major gradients. Some of the cells are still at the marked starting area. These are not included in the measurement, since no movement could be measured (with these assay and type of documentation only measurements over long distance migration is possible).

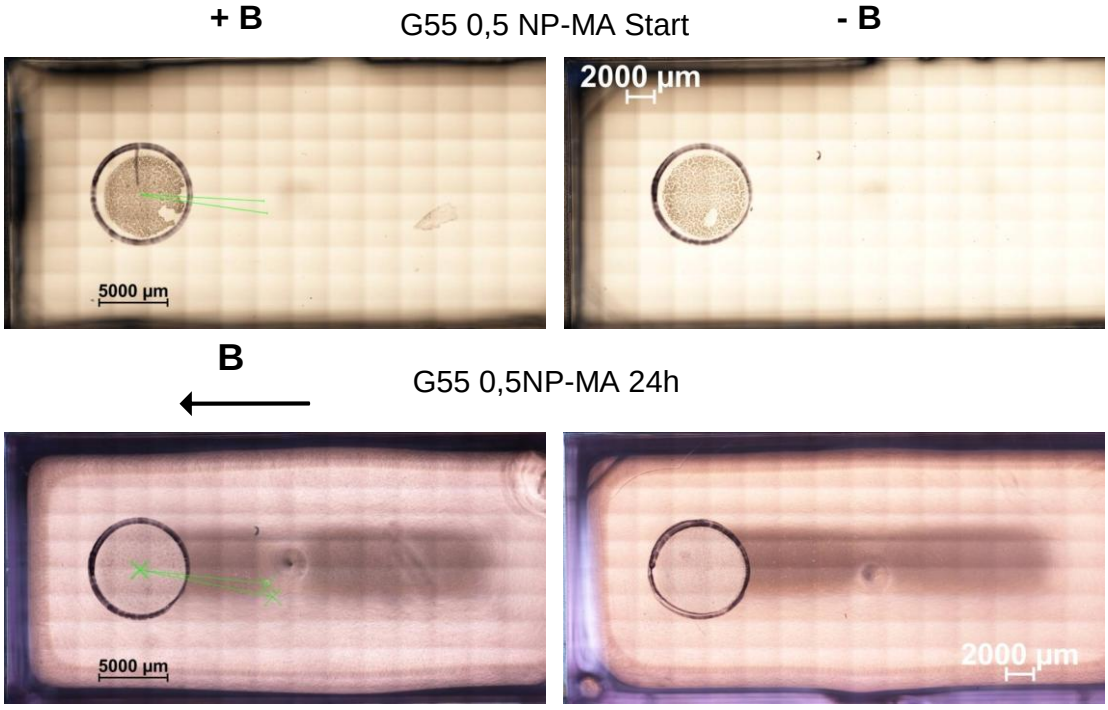

Figure 42: Results of migration experiment with G55 0,5 NP-MA cells

Start and result of migration for glioblastoma cells G55 pre-incubated with 0.5 NP-MA, without and with magnetic field.

III.7 Biochemical Effects

Following the promising results of magnetically migration it was questioned whether this was a result of active migration or only magnetic force. For an active migration the cell must up regulate the nucleation process of actin filaments. This is mediated by the Arp2/3 complex and regulated by WASP (Wiskott Aldrich Syndrom Protein) family members (Wu 2004).

N-WASP was here of greatest interest because Rohatgi et.al. (1999) demonstrated that binding of N-WASP with an active form of Cdc42 enhances the ability of the protein to activate Arp2/3. So for the first time a signalling pathway for actin nucleation was identified.

For a magnetically induced active migration of cells it can be expected that the cells demonstrate an up regulation of active N-WASP (phosphorised form). An inactive form of the protein however is also present in the cell, and hence the investigated method must be able to differ between both forms of this protein. The best chance of observing this was found to be using immunhistochemical staining in combination with a marker for actin filaments.

Therefore in this experiment, the cell cytoskeletons (actin-based) were stained with phospho - specific anti N-WASP (a protein involved in actin nucleation) antibody (second antibody, labeled with Texas red) and phalloidin Alexa 488 (a toxin from the death cap (*Amanita phalloides*), it binds F-actin and is labeled with a fluorescent analog for lightmicroscopy) and the cell nuclei with DAPI.

III.7.1 Immunhistochemical analyzes of Astrocytes

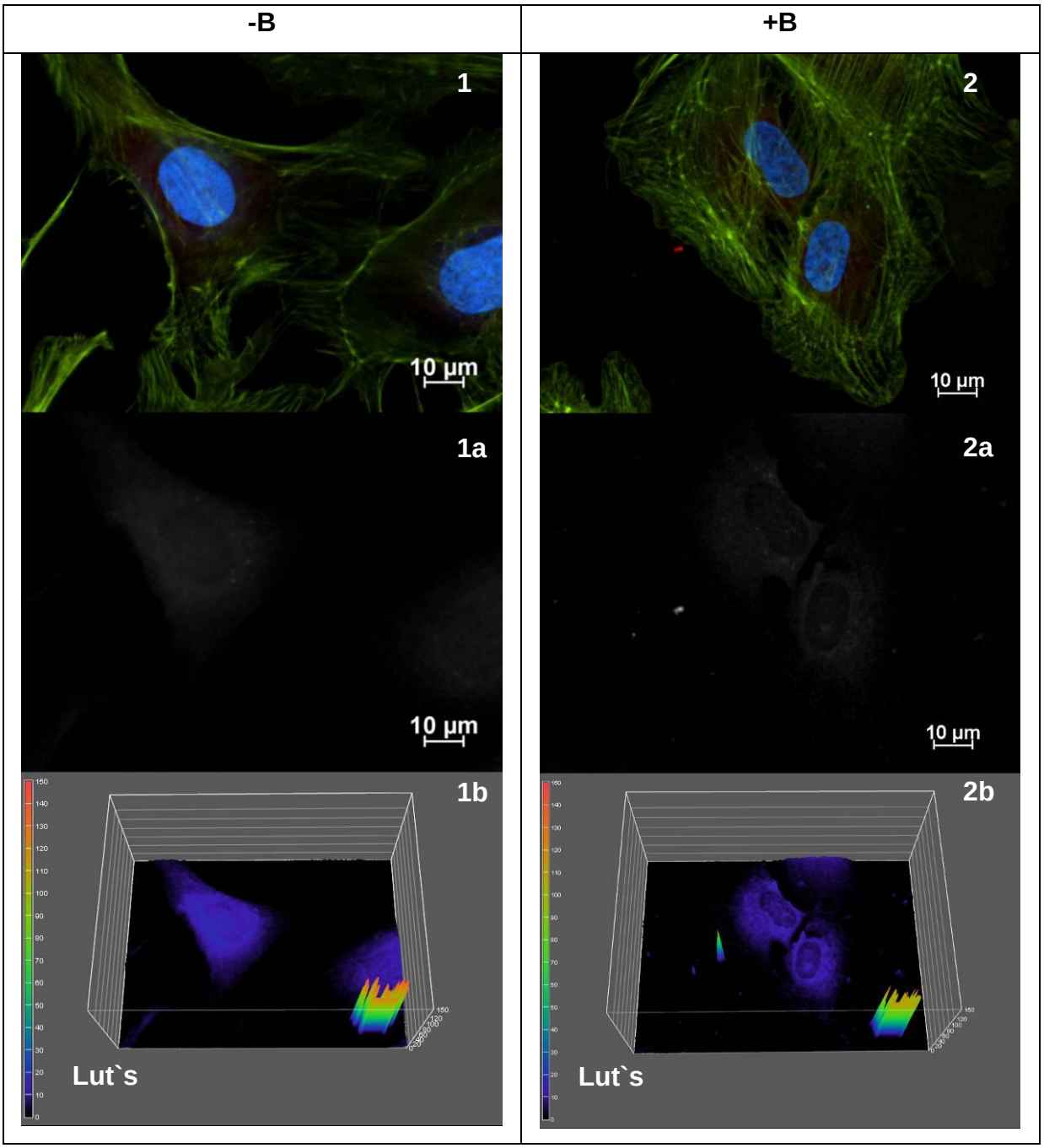

Figure 43: Visualisation of Actin and N-WASP in Astrocytes control

1+2) Results of Actin (green) and N-WASP (red) Staining, Counterstaining of Nucleus with DAPI (blue)

1a+2a) Fluorescence channel of N-WASP in white

1b+2b) Light Intensity Surface plot of N-WASP channel

B

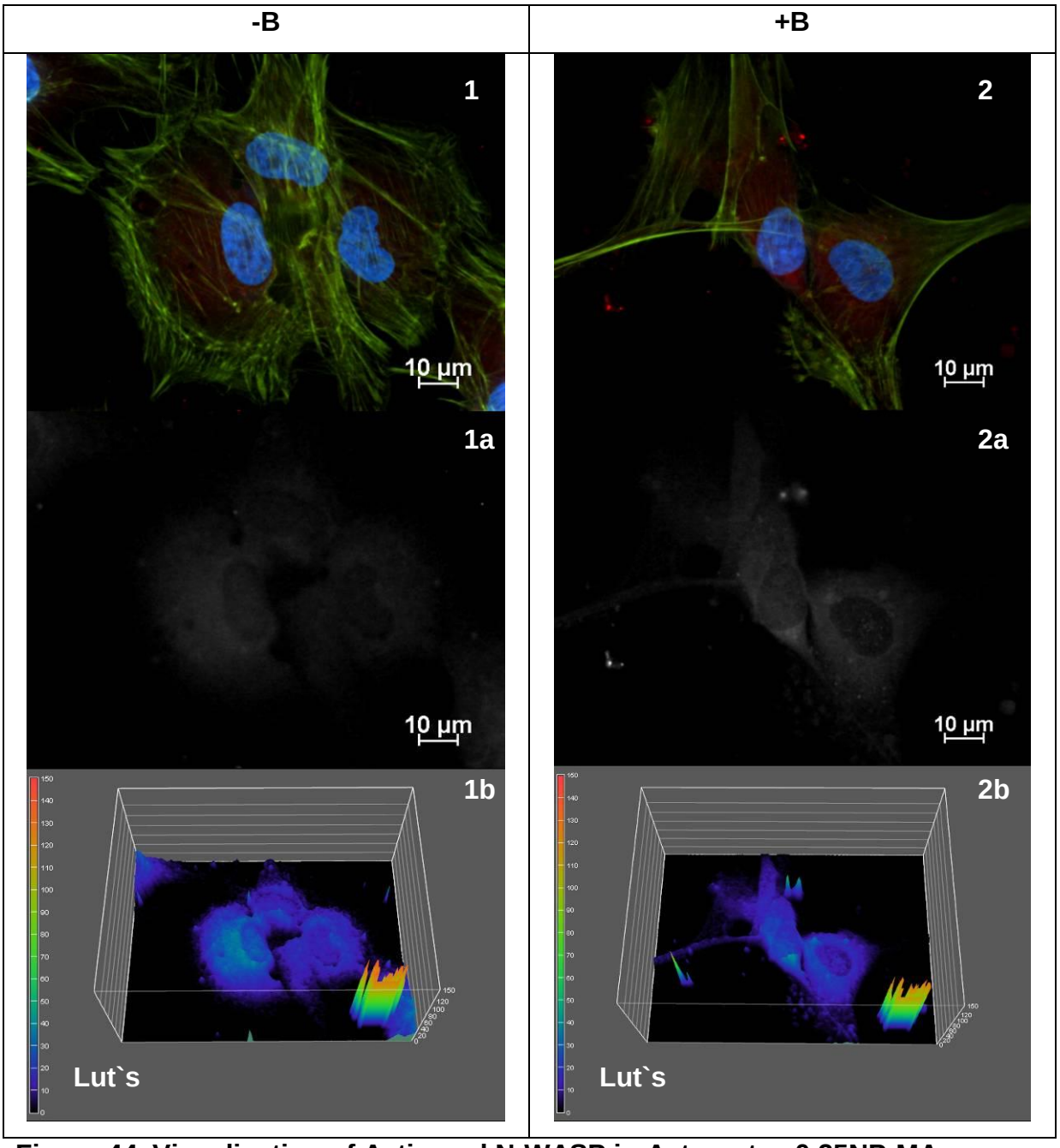

Figure 44: Visualisation of Actin and N-WASP in Astrocytes 0.25NP-MA

1+2) Results of Actin (green) and N-WASP (red) Staining, Counterstaining of Nucleus with DAPI (blue)

1a+2a) Fluorescence channel of N-WASP in white

1b+2b) Light Intensity Surface plot of N-WASP channel

B ←

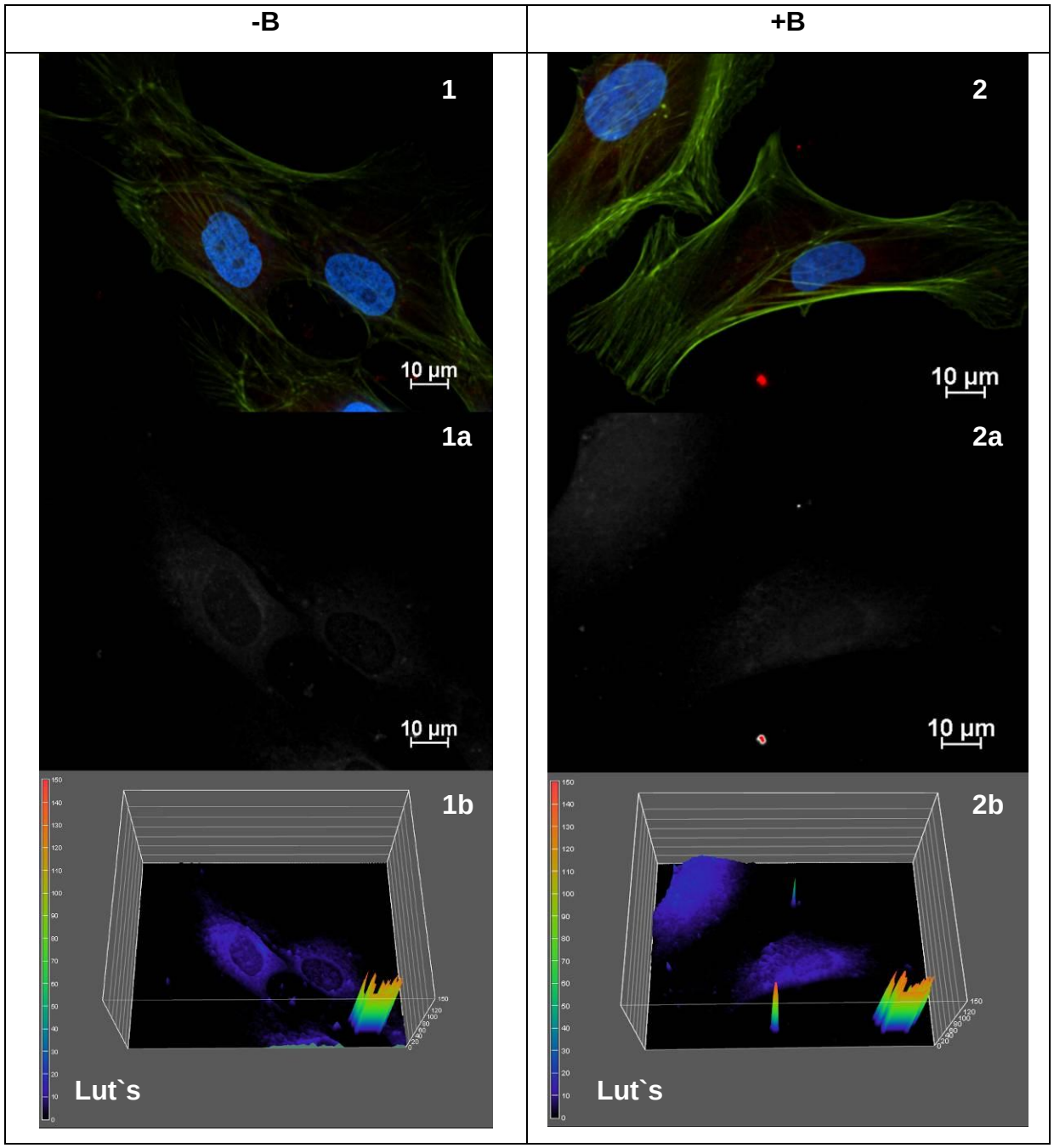

Figure 45: Visualisation of Actin and N-WASP in Astrocytes 0.5NP-MA

1+2) Results of Actin (green) and N-WASP (red) Staining, Counterstaining of Nucleus with DAPI (blue)

1a+2a) Fluorescence channel of N-WASP in white

1b+2b) Light Intensity Surface plot of N-WASP channel

B ←

Between the different groups of Astrocytes no differences were found for the expression of N-WASP. The values detected by fluorescence measurement all show a 10 to maximal 30Lut's mainly located in the corpse of the cells.

III.7.2 Immunhistochemical analyzes of *Glioblastoma multiforme* G55

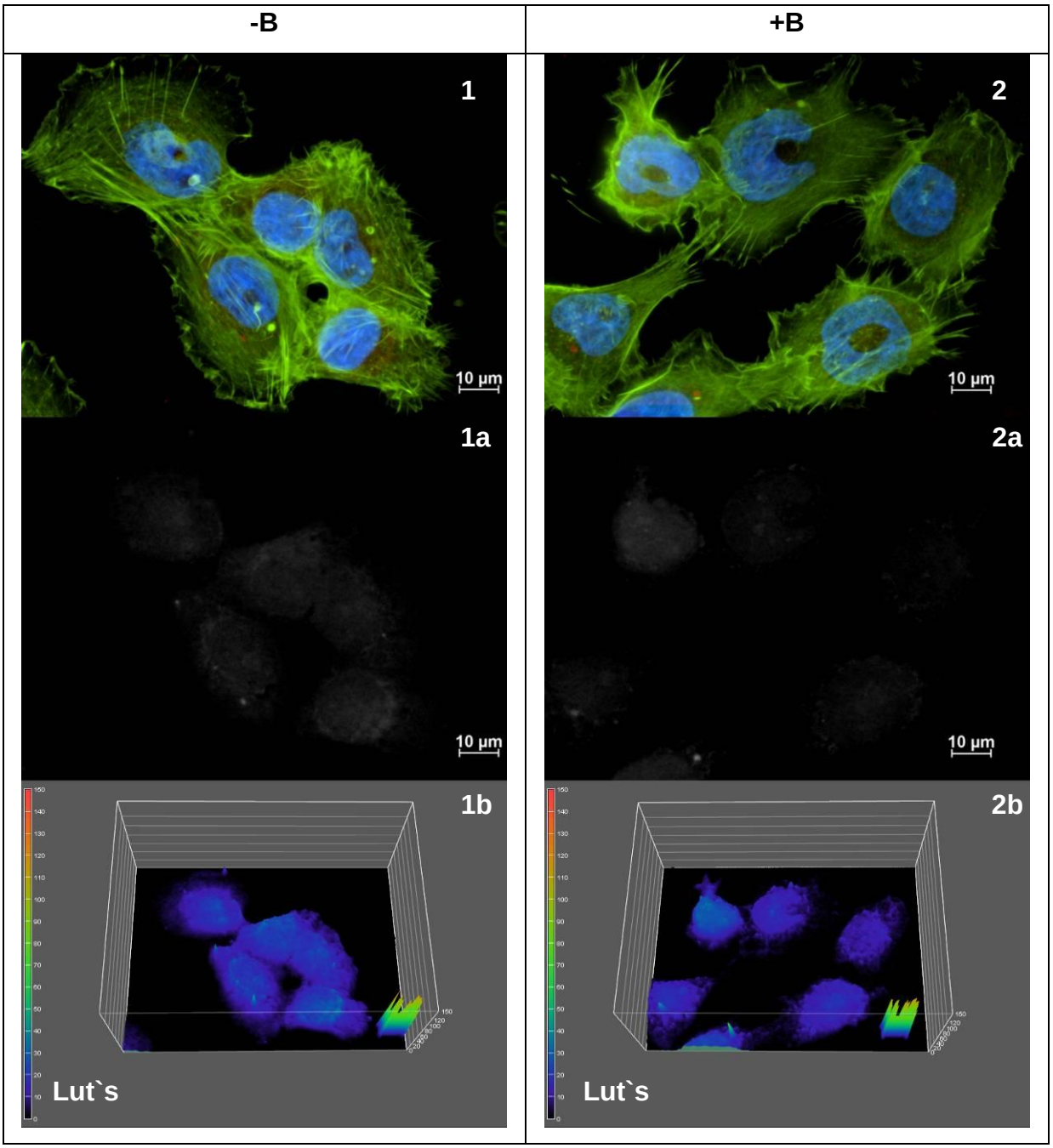

Figure 46: Visualisation of Actin and N-WASP in G55 control

1+2) Results of Actin (green) and N-WASP (red) Staining, Counterstaining of Nucleus with DAPI (blue)

1a+2a) Fluorescence channel of N-WASP in white

1b+2b) Light Intensity Surface plot of N-WASP channel

B ←

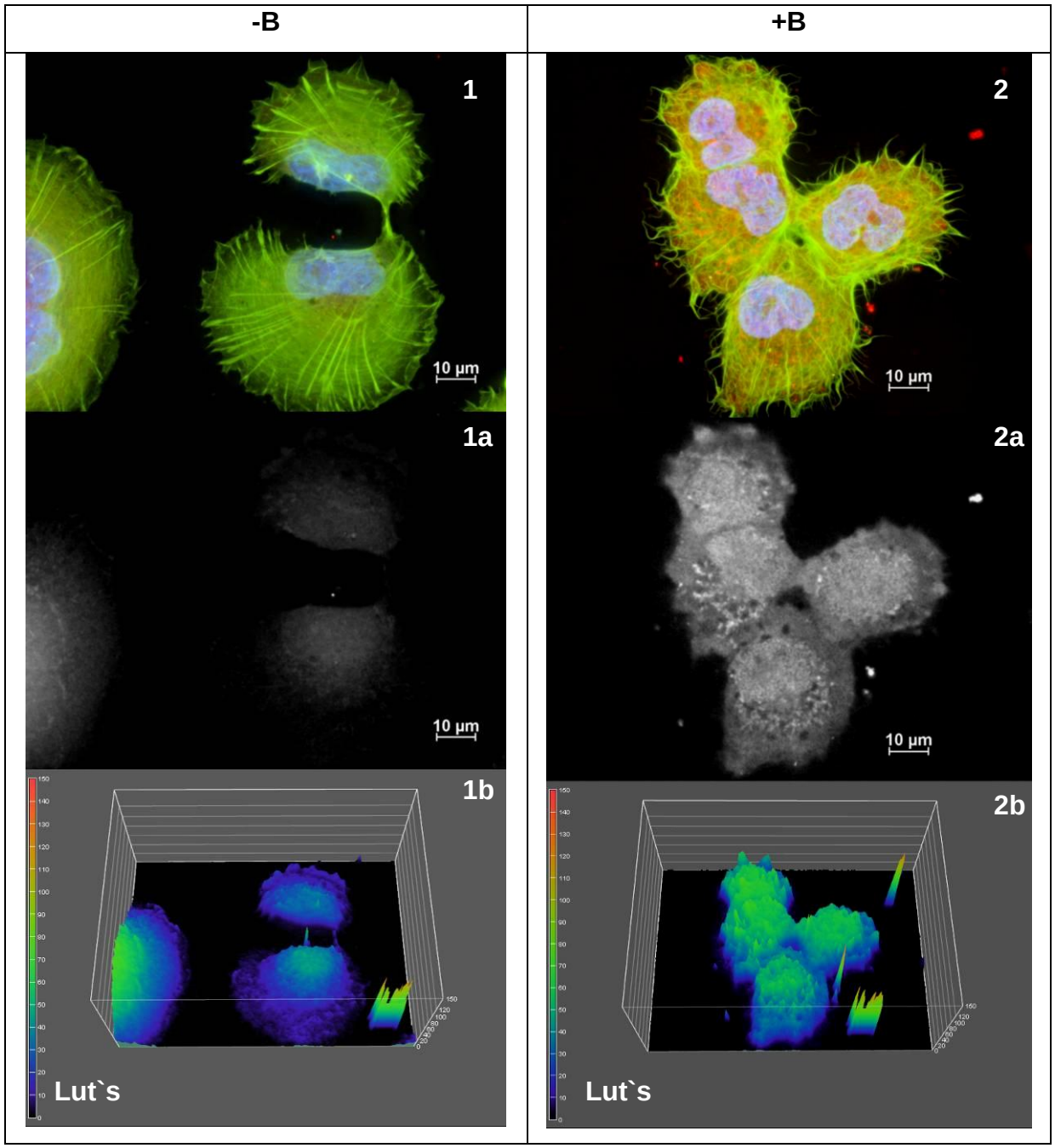

Figure 47: Visualisation of Actin and N-WASP in G55 0.25NP-MA

1+2) Results of Actin (green) and N-WASP (red) Staining, Counterstaining of Nucleus with DAPI (blue)

1a+2a) Fluorescence channel of N-WASP in white

1b+2b) Light Intensity Surface plot of N-WASP channel

B ←

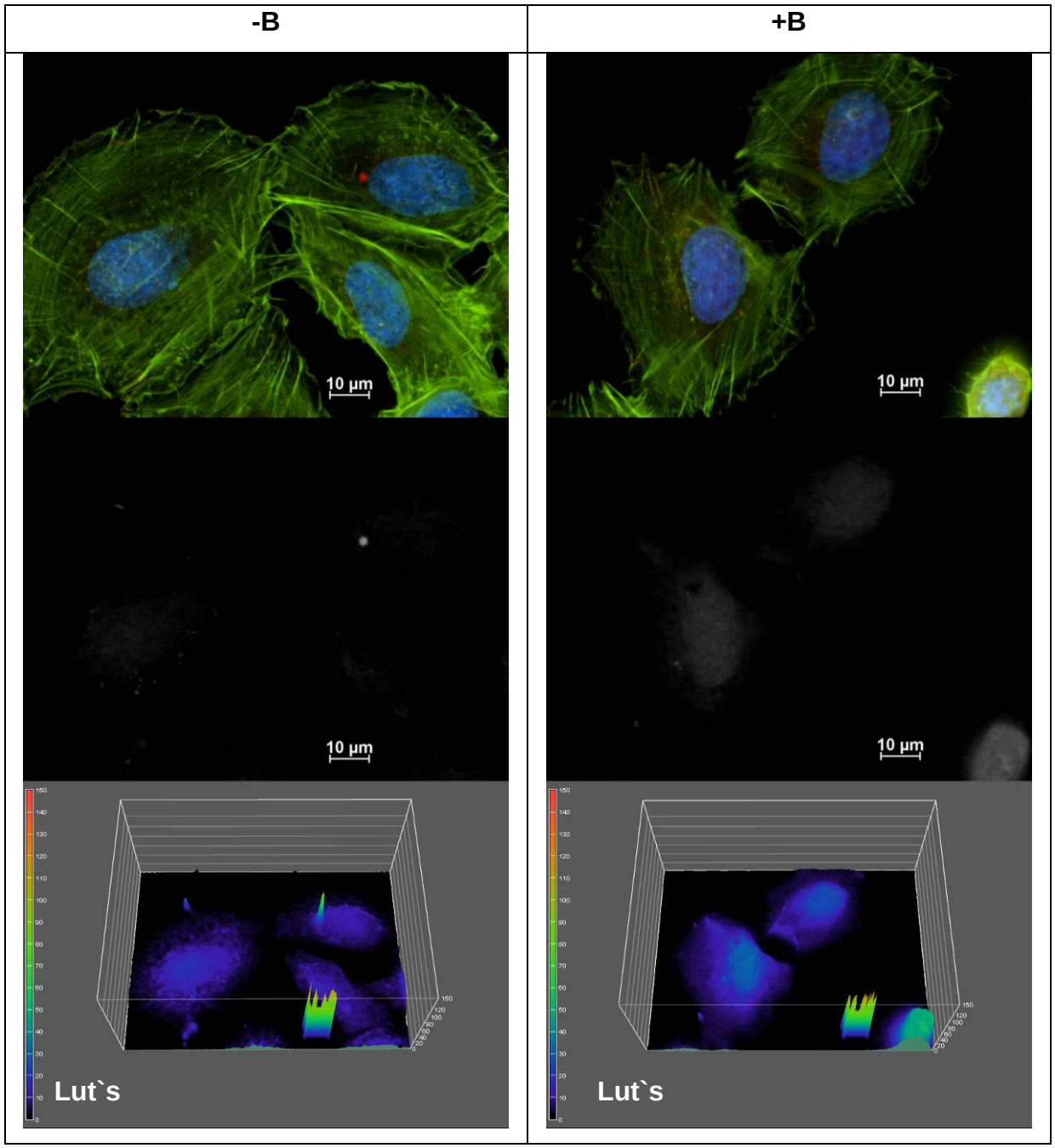

Figure 48: Visualisation of Actin and N-WASP in G55 0.5NP-MA

1+2) Results of Actin (green) and N-WASP (red) Staining,
Counterstaining of Nucleus with DAPI (blue)

1a+2a) Fluorescence channel of N-WASP in white

1b+2b) Light Intensity Surface plot of N-WASP channel

B

The results of N-WASP studies demonstrate that the cancer cells have a Lut's value of 40 around the nucleus, whereas fort the cell boundary this ranges between 10 to 20 Lut's. Differences between normally incubated cells and those exposed to the magnetic field cannot be differentiated. Furthermore the cytoskeletons all have a similar appearance with boundaries lightly frayed and stronger actin fibers with a fine transverse network orientated towards the cell nucleus (figure 46-48).

An exception to this is found for the cells incubated with a concentration of 0.25µL/mL NP-MA and then exposed to the magnetic field (figure 47). These cells show a strong increase in the N-WASP content and the entire cell appears red, corresponding to a Lut's value of up to 90 in the region of the cell nucleus and between 50 and 60 Lut's for the cell boundary. In addition the cells appear morphologically very different from other types investigated in this study. For example in the region of the cell boundary the actin fibers are much longer building filipodia, which gives the cell a strong frayed appearance. Furthermore the boundary region is not so strongly flattened.

This coincides with observations documented in the migration experiments where pre-incubated cells having 0.25µL/mL NP-MA (figure 40+ 47) could be observed to move more actively in the magnetic field as opposed to cells treated with higher concentrations (figure 42 + 48) hardly moving at all.

IV Discussion

IV.1 Nanoparticle uptake and Toxicity

When introducing nanoparticles into brain cells it's particularly important that nanoparticle uptake within the cells is dependent on particle concentration. This ensures accuracy of dosage but also good reproducibility of results coming from experimental investigation. Furthermore, it is essential that the employed nanoparticles be compatible with cells found within the brain, especially normal healthy cells required by the brain to function properly. This also applies in terms of toxicity, with the exception that any negative toxic effects only occur for cancerous cells, since the ultimate goal is their eradication without harm to these normal cells.

With regard to the criterion of nanoparticle uptake in cancer cells, having to be dependent on both tested particle concentration, this was only achieved for NP-MA. NP-LA demonstrated far too inconsistent admission under the investigated experimental conditions. Were it the goal however to restrict particle uptake into the astrocytes, since this constitutes reduced levels of stress placed on the cell; this criterion could be fulfilled employing NP-LA. To this end it would be worthwhile developing nanoparticles with shell material out of a mixture of NP-MA and NP-LA. The mix-coat particles should then ideally demonstrate concentration dependent uptake into the cells just as was the case for NP-MA, but with a much reduced uptake in the astrocytes (see results for NP-LA). Ideal shell-mixture ratios of NP-MA and NP-LA are however to be determined, including possible side effects (e.g. toxicity) to the cells.

A material's toxicity has repercussions in the development of any therapeutic application wishing to make use of this material. As such astrocytes (control group) were also tested in this study. Astrocytes constitute 20-50% of brain cells and play a central role in iron metabolism within the brain (refer Introduction).
The results of proliferation experiments demonstrate clear differences in the growth behavior between astrocytes and cancer cells, due to the presence of magnetic nano-particles. Whereas astrocytes exhibit no change in growth behavior,

glioblastoma cell lines (G55, G112, G122) demonstrate a statistically significant reduction in cell number after two days of incubation, and when compared with the control cells.

This result has been confirmed via Live-Dead Staining. Here the number of astrocytes and G55 correlates well with the results of proliferation experiments. The astrocytes demonstrate no toxicity in relation to the nanoparticles and exhibit a normal stretched cell structure, where as glioblastoma cells demonstrate a strong reduction in the number of living cells. This result for astrocytes and G55 is very much unexpected and in contrast to what was observed during the daily work with astrocytes. Here they react very sensitively to any changes of medium. While glioblastoma like G55 are known to be resistant to chemotherapy (see chapter I.3.5 page 7) and other such therapies, these demonstrated hindered growth in the presence of ferrofluids.

So what happens to the nanoparticles in different cells?

Levy et.al (2010) postulated that the magnetic and crystallographic properties of iron oxide particles are conserved throughout degradation, while the concentration of soluble iron species decreases. The group headed by Prof. Weller (2011) demonstrated that iron oxide nanoparticles like magnetite are degraded to iron ions; this reaction is cell type specific and time dependent. The mechanism and involved proteins are still unknown. This means that the cells have to deal with iron overload and this can lead to oxidative stress (Nel 2006, Naqvi 2010). A second possibility is that due to the large amounts of nanoparticles in the cells, some cell organelles may be blocked by strong accumulations of the magnetite particles (Levy 2010).
Key elements here are the lysosomes with their acidic PH value. These act as detoxification centers for metallic compounds, as well as waste regulators within the cell. Cases of lysosomal disorders are known as Lysosomal Storage Diseases (LSDs), here the accumulation of macromolecules leads to the dysfunction of these cell organelles (Seregin 2011). McLeland (2011) postulate that nanoparticles may cause lysosomal pathologies, since they are likely to accumulate in lysosomes.
Micrographs have shown that it was possible to visualize plentiful circular opaque structures (agglomerates of nanoparticles) in cells treated with nanoparticles.

Interestingly in astrocytes only few agglomerates were found, whereas in glioblastoma cells high concentrations could be observed. Additionally the sizes of these agglomerates were often up to 2 micrometers and placed in the vicinity of the nuclei. Here the structure and distribution in the cells were cell organelle like.

So where are the nanoparticles localized?

It was important to determine which structural changes and associated reactions resulted as a consequence of introducing a foreign material (nanoparticles) into the cell.

IV.2 Cell-organelle Staining and Localisation of Ferrofluids in Cells

Several studies have shown that metallic nanoparticles always accumulate in the lysosomes (Levy 2010, Tan 2010, Islam 2009), whereas they are rarely found in the endoplasmic reticulum (Singh 2010).

The results of cell organelle staining clearly show a nanoparticle concentration-dependent increase of lysosomes size and intensity for G55 cells.
Astrocytes on the other hand demonstrate significantly less reaction compared to cancer cells. This can be contributed to, on the one hand by the smaller number of nanoparticles / cytoplasm volume, but on the other hand these don't demonstrate any change in the magnetic field, although the total iron content per cell is higher than for G55.
In comparison the cancer cell line G55 exhibit serious differences in cell structure. This speaks volumes for the fact that the cells deal differently with an introduction of biological materials (both type and dosage).

Studies by (Behrendt 2009) demonstrate that the make-up of shell material (oleic acid) used for nanoparticles can influence their accumulation in the lysosomes. It is conceivable that this has also been the case in this study, since particle coating material consisted of myristic acid ($C_{14}H_{28}O_2$), which only differs from oleic acid

($C_{18}H_{34}O_2$) in terms of length of the carbon chain. This pre-supposes however that the nanoparticle shells are themselves not affected during transport into the lysosomes, a point, which to date has not been clarified. Another possibility is that the organic shell components are degraded before the nanoparticles are included into the lysosomes. Many different nanoparticles (for example: magnetite, silver; Konczol 2011, Greulich 2010) are found in lysosomes. The figure below shows the intracellular transport paths.

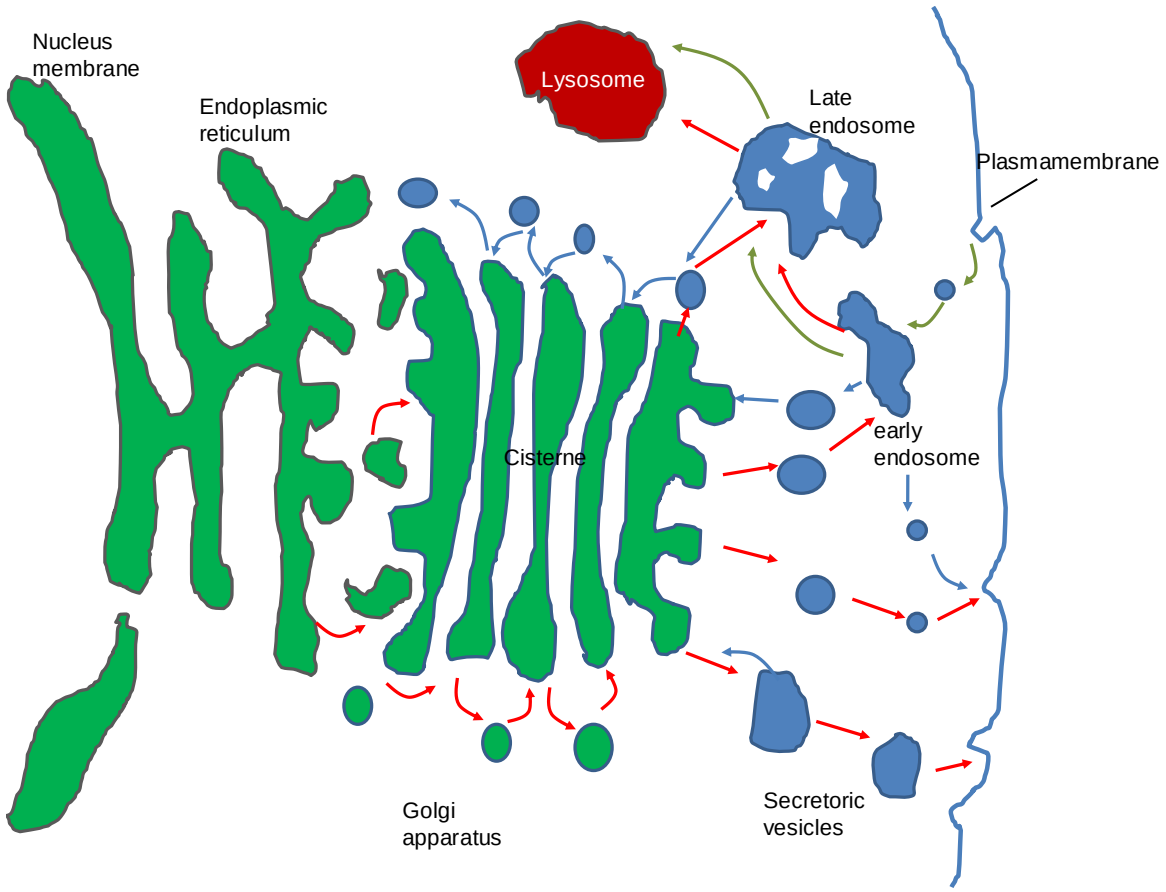

Figure 49: Vesicle transport in cells

Shown are the transport ways of endocytosis (green), exocytose (red) and re-transport between the different cell compartments (blue). All cell compartments communicate with one other and with the extracellular periphery. The biosynthetic – secretoric way (red arrows) transport protein molecules from the ER to the plasma membrane by (passing late endosomes) to the lysosomes. For the endocytose pathway molecules are incorporated in vesicles and then transported to early endosomes (passing the late endosomes), which then end in the lysosomes. The blue arrows indicate that many endocytic molecules are re-transported from the early endosomes to the plasma membrane. Similarly some molecules

are back transported from endosomes and Golgi apparatus to Golgi apparatus or ER. (Picture and text adapted from Alberts 2011.)

For G55, a strong reduction in cell numbers (proliferation data) would imply an increase in the number of dead cells. This however was demonstrated not to be the case. The most likely cause here is being disruption of intracellular mechanisms within the cell. A possible explanation is that large quantities of nanoparticles within the cells and the lysosomes result in active blocking of certain cell organelle functions, without killing the cells. Hence this may explain why so few dead cells were observed. Parts of the cells die, and due to large amounts of iron accumulation in the lysosomes, both cell metabolism (like autophagy pathway, McLeland 2011) proliferation is massively inhibited. As observed, the ER in nanoparticle containing cancer cells shows a modified structure similar to the lysosomes. Such results imply that part of the ferrofluids is transported into the ER, and may be mediated by the myristic acid shell. Secondly the possibility exist that a re-transport to the lysosomes takes place.
Blocking of the lysosomes and ER via large quantities of nanoparticles is likely to cause a restructuring of the cell, which obstructs cell division and hence inhibits cell growth (like for the different forms of Lysosomal Storage Diseases). Bear in mind that iron oxide particles induce oxidative stress (Nel 2006, Naqvi 2010) leading to cell injury and death (Naqvi 2010), which can explain the found toxicity of NP-MA for glioblastoma cells.

G55 exhibits clear deposition of opaque magnetite in the lysosomes (see chapter III.5.2.2. page 65-71). The deposit locations correspond with the results produced via BBS (III.1.1. page 34), the exception being localization for G55 0.25NP-MA after exposure to the magnetic field. In this instance nanoparticles are barely visible.
The displacement of lysosomes leads one to suspect however that these contain an even larger accumulation of nanoparticles, since they align themselves with the magnetic field gradient. However, visual evidence of this localization is difficult to determine and BBS is unable to help any further. This is due to the complexity of the colouring which forms, and hence no exact picture of particle location is possible, because during staining the magnetite is dissolved by the hydrochloric acid (Weller 2011).

In the case of the astrocytes, even with their high concentration of ferrous fluids, it was difficult to gauge because single particles were too small to detect employing optical light microscopy. The difficulty here was that only well lit up regions throw shadows making boundary regions indiscernible (when the fluorescence of the nucleus stained with DAPI was used). Hence Berlin-Blue staining was employed to try to overcome this problem. Via this technique it was possible to visualize for the case of the astrocytes a decentralized distribution of iron within the cell. However, this only partially corresponded to the localization within the lysosomes (or ER) (see chapter III.5.2 page 58). These differences in comparison to the iron content of the cells led to the thought that astrocytes were able to degrade the nanoparticles in lysosomes by combined effect of acidic pH, lysosomal hydrolases and eventually iron chelators involved in iron regulation (Levy 2010). Stormer (2008) assumed that astrocytes play a role in the magnetite based memory in the brain, implying that they have the necessary equipment for destruction of such crystals. Levy (2010) described that the kinetics of iron oxide dissolution strongly depends on the nanoparticles surface coating. Organic materials like myristic acid (shell component of NP-MA) as natural element within cells represents therefore no obstruction for destruction. The dissolution of the ferrofluids would also explain why it is so difficult to visualize them, even though the measurable iron content is high. However, if one regards the fact that actrocytes play a key role in the metabolism of iron within the brain (see I.2), then it can be assumed that this also help to protect the cell from oxidation damage, particularly when confronted with too much iron.

Astrocytes are known, to be able to store large amounts of iron in Ferritin, converted to a less oxidative and non-toxic form (Dringen 2007). This would explain why astrocytes do not respond to the magnetic field, within the dissolution of the nanoparticles, since they loose their magnetic behavior (Weller 2011).

Microscopic analyses like TEM (transmission electron microscopy) or similar would likely be more useful in a more exact analysis of particle localization, since this methodology has a far higher local resolution. Hence future work on this theme is necessary in order to be able to define what is actually occurring inside of the cells.
The result obtained for migration experiments conducted on 0.25NP-MA cells indicate that direction orientated migration of cancer cells is possible. Results already

show an adjustment of the lysosomes in the direction of the magnetic field, while cells also demonstrate good vitality. In the case of G55 0.5NP-MA cells however, this is not to be expected (only those cells with minor iron content) because of their strongly changing and severely stressed cell structure.

IV.3 Magnetically Activated Migration and Immuno-histochemical Analyses

The methodology developed in context to this work has successfully demonstrated that it is possible to activate glioblastoma cells to purposefully migrate under the influence of a magnetic field. Furthermore, this methodology promises a new therapy for the treatment of aggressive brain cancer (glioblastoma in its associated forms). Important to note here is that cells, which constitute healthy brain tissue, are not able to migrate.

The horizontal form of the magnetic field and the resulting methodology were chosen to study the directional migration of cells independent of the gravity. With this method it is as well possible to visualise the influence of the magnetic field, in terms of the migration behaviour of the cells, making it possible to modify parts (e.g. magnetic shoes) of the magnet for better adjustment. Hence the developed method is well suited to the visualisation and quality of migration (direction, length) of cells. A negative point however is that the quantity analysis is very difficult to conduct. Here cells always build small spheres so that it is almost impossible to say how many cells are exactly there. Video tracking normally used for migration analyses (e.g. Nikon) does not overcome this problem. This method only allows for the tracking of single cells over a relative short period, because the permanent cell division of the cancer cells is not traceable using this software (Nikon, Zeiss 2009).

Therefore future work is required to quantify a second parallel method, consisting of a vertical test system based on Inserts, with 3 micrometer sized holes in the membrane, located in a well plate. The whole experiment looks than like a sandwich. On the membrane pre-incubated cells are added in the space below. Here a medium is added between well and membrane.

Below the well plate a plate with fixed ferro-neodymium magnets reveals as attractant Cells reacting to the magnetic field and pass the membrane by active migration where they are collected by the well below. Consequently it is possible to analyse the number of cells by cell counting or colorimetric assays. Such a test system was developed in this work, but not finished.
If one accepts the migratory behavior of the control cells as natural behavior, no preferential migratory direction is recognizable and cell movement is coincidental. Furthermore, for control groups of both cell types no obvious movement within the samples is recognizable.

With regard to the astrocytes, these exhibited no reaction to the magnetic field in the migration assay. This corresponds with the other experimental trials, for example toxicity, cell-organelle staining and immune coloring by application of Actin-phalloidin and N-WASP (see chapter III.7. page 84-86).
The reasons for this are postulated as follows:

1. The nanoparticle / cell-volume relationship is much smaller for astrocytes and as such magnetization is considerably reduced.
2. Localization of the nanoparticles is decisive for the attraction, transmission and activation of cell migration. This is differently weighted with regard the astrocytes.
3. Nanoparticles taken up in the iron specializing astrocytes no longer exist in their original form, as discussed in the previous chapter.

Clearly evident from the results of migration experiments for nanoparticle loaded G55 cells (0.25 NP-MA), is that these cells demonstrate distinctly more movement than unloaded cells, when each are placed in the magnetic field. In fact the majority of nanoparticle loaded cells orientates and distribute themselves in the direction of the gradient of the magnetic field (see chapter III.6. page 77). For samples G55 0.5 NP-MA, as examined with and without influence of the magnetic field, it is clear, and based on the definition for migration (given above) that these do not migrate (refer III.6 page 79). This confers with what was expected from the results of toxicity and

cell-organelle staining analyses (Chapter III.6. and III.8). Here the cells show stress reactions and appear injured (Naqvi 2010) after exposition to a magnetic field.
To be sure that the observed migration occurs through active movement of the cell and not as a result of magnetic attraction, histochemical analysis via Actin-Phalloidin and N-Wasp was introduced to the study. The protein N-WASP (activated by Cdc42, see I.6 page 11) is only marked by the used antibody in its phosphorous activated form. Under conditions of strong activation N-WASP starts Actin-polymerization and bundling in the cell, which is mediated by the activiation of the GTPase Cdc42 (Alberts 2011). Hall (1998) demonstrated that when microinjecting Cdc42 into cells this leads to the formation of many long Filopodia. The resulting phenotype of these cells (shown in chapter I) is very similar to the findings of G55 0.25NP-MA cells (incubated for 24h in a magnetic field). These results confirm that the magnetic field induces active cell migration of these G55 cells. Furthermore, this is complemented by the findings coming from cell-organelle staining and migration (see III.7 page 80 and III.6 page 75). Common for all investigating experiments is that the investigated cancer cells demonstrate an orientation in the direction of the magnetic gradient. Additionally, it was found that the cells are more contractile than control cells. Fritsch *et al.* (2010) reported that the contraction of cancer cells can pre-strain and thus stiffen the cytoskeletons, reducing a cells ability to form adhesive contacts with other cells. Moreover, contractile tumor cells migrate significantly better through the extracellular matrix; this could play a key role in metastasis.

How is it then possible that the cells are activated?

In reference to the results what's most conspicuous is the fact that G55 0,25NP-MA entails a misalignment of the lysosomes towards the magnetic gradient when placed in a magnetic field. This demonstrates that the lysosomes are somehow involved in the process. But what is the link between small cell organelles and directed migration processed by active actin-nucleation?
Components of the cytoskeleton are the microtubules, hollow cylinders with a diameter of 25 nm, which consist of the protein Tubulin and intracellular engine proteins Dynein and Kinesin. They are responsible for movement and longer transport pathways, e.g. responsible for intracellular transport of organelles in the cytosol (Alberts 2011). Moeller *et al.* (2000) analyzed the motion of phagosomes and

their connection to cytoskeletal filaments in human cells via incorporation of micrometers sized magnetite particles. Here they employed an external magnetic field to induce a twisting of the magnetic phagosomes; they found that elastically stored energy does not force the phagosome back to their initial orientation. Especially for longer twisting durations (over 1min) they measured that the fraction of recoverable strain decreases and disappears, which originates from a dissipation of the elastic energy due to the stochastic phagosome motion and cytoskeletal rearrangements. Marugg (2010) used similar cytomagnetometric experiments to demonstrate that actin filaments contribute to the movements of lysosomes. This indicates that it is possible to transfer via magnetic attracted lysosomes shear stress and strain to the actin skeleton. Like the findings of Moeller (2000) it is theoretically possible that the cells react with an active rearrangement of the actin. This explains why the cells are directed toward the gradient, i.e. by the permanent strain the activity of process involved proteins being up regulated and demonstrated by the results of this work.

Cancer cells with the appropriate loading of nanoparticles migrate actively in the magnetic field, since they feel the effect of the field.

The nanoparticles employed in this work have super paramagnetic characteristics. They demonstrate that they can be magnetized very strongly in an external magnetic field with no residual magnetism once the field is removed. If larger quantities of nanoparticles accumulate in a cell, it is likely that this obstructs and or brakes natural motion of the cell due to an increase of oxidative stress induced via iron oxide particles.

If one exposes cells loaded with ferrous nanoparticles to a magnetic field, the nanoparticles experience magnetization. Here the cells are draw under the influence of the magnetic field on the particles in the lysosomes so that they align themselves in the direction of the magnetic gradient.

As a consequence cells aligned in the direction of the magnetic field are stimulated to activate the GTPase Cdc42 (see chapter I.7. figure 3) resulting in cell polarization (Tzima 2003) and Actin nucleation (high N-WASP activity; refer Actin N-WASP coloring, chapter III.8. figure 44). Through influence of the magnetic field on the nanoparticles, the otherwise random movement of the cells is translated into an active and visible migration of the cells towards the magnet.

A small portion of the cells (G55 Control and 0.25 NP-MA; figure 40, page 78) migrate in the opposite direction. At the moment there exists no explanation for this phenomenon.
By further improving the magnetic field it should be possible to move cells more strongly to one point or in one direction. The prototype developed in this study has served for the development of a methodology where actual parameters were initially unknown.

The developed methodology presents a promising therapeutic way of treating of *Glioblastoma multiforme*, whereby the invasive migratory cancer cells, which cannot be operatively removed from the brain, are redirected to a more accessible location for treatment and or removal.

To prove the hypothesis, that magnetically induced lysosomal shear stress leads to activation of actin nucleation in glioblastoma cells, further investigations should however be undertaken.
One possibility is to create transgenic cancer cell lines which express a fusion-protein of actin and clip tag (BioLabs). The fusion-protein alone is non fluorescent; this can be achieved by adding special substrates (different colors) to the living cells. By covalent binding of one substrate to the protein this then become fluorescent. If used for live cell imaging together with the Lyso-tracker, this should then allow for the visualization of actin nucleation, since the color of the actin fusion-protein can be exchanged during experimention. Similar investigations can clarify the involvement of other proteins e.g. Cdc42 in this process.

V Summary

Magnetically induced directed Cell Migration as a new Approach for Therapy of *Glioblastoma multiforme*

The predominating problem investigated in this doctoral thesis has been the development of a therapy for dealing with Glioblastoma multiforme (malignant brain tumors of the type class 4). Despite all efforts including surgical removal of the main tumor, chemotherapy and irradiation, the chance of survival after 6 months still lies under 2% (Van Meir *et al.* 2010). This can be attributed to an inability of such therapies to completely eliminate invasive and migratory cancerous cells from in and around the near vicinity of the tumors.

Fundamental to this work has been the idea of employing the so called negative aspects of Glioblastoma behaviour, namely their ability to migrate and use this for positive therapeutic application against brain cancer. Here magnetically activated and biocompatible nanoparticles were transferred into the cells. Thereafter the cells were placed in a magnetic field where it was possible to induce actively migration of these cells in the direction of the magnetic field. For this to occur it was first necessary to investigate and establish parameters (inclusive here is cell culture) and necessary conditions for the magnetic field, whose flow had to be concentrated on the cell level.
The findings have led to a patent being filed (Mucha 2009) for future therapeutic application in removing Glioblastoma cells from the brain.
The thesis discusses findings with regard to the uptake of nano-particles in the cells and their compatibility concerning Glioblastoma cells and primary human astrocytes (as control group for healthy cells) under in vitro conditions, with and without influence of the magnetic field. The results demonstrate that the employed ferrous fluids are taken up concentration-dependent by the cells and are very compatible for use with astrocytes (Avdeev, Mucha *et al.* 2010), whereby it was also observed that several Glioblastoma cell-lines had a significant reduction in cell growth.
Microscopic analyses of the cell-organelle structure demonstrated a concentration-dependent increase and enlargement of the lysosomes, which are substantially more pronounced with the Glioblastoma cell, and further correlated with the reduction in cell growth.
Analyses after 24h exposure time to the magnetic field led nanoparticle rich glioblastoma cells to polarize with adjustment of the lysosomes to magnetic gradients, whereas astrocytes did not show a reaction to the magnetic field. Thus the goal of the study (purposeful migration of Glioblastoma cells) has been achieved and continuously improved throughout the course of this work.
Immunhistochemical analyses of components of the cytoskeleton and their structure involved protein N-WASP confirmed that an active migration of the cells takes place. Here nanoparticle containing cancer cells (0.25NP-MA) demonstrate not only a strong polarization in the direction of the magnetic field but also show very strong activity of N-WASP and the building of many Filopodia necessary for cell migration. This active migration is caused by the stress induced by these nanoparticles within the cells and is steered in all probability via the Cdc42 signal path. Astrocytes however do not show a reaction to the magnetic field.
The results clearly demonstrate that magnetically induced purposeful cell migration and its conversion as therapy for use in living patients is indeed promising, since the penetration depth of the invasive cells amounts to on average 1-3 cm around a main tumor and an active migration of cancer cells is needed a fundamental requirement for their extraction.

Magnetisch induzierte zielgerichtete Zellmigration als neuer Ansatz für die Therapie von *Glioblastoma multiforme*

Diesem Thema lag die vorherrschende Problematik bei der Therapie von Glioblastoma multiforme (maligner Hirntumor Grad IV) zugrunde, dass trotz maximalem Standard-Therapieeinsatzes bestehend aus chirurgischer Entfernung des Haupttumors, Chemotherapie und Bestrahlung nur eine geringe Verbesserung der Überlebenschance von unter 2% nach 6 Monaten erzielt werden kann (Van Meir *et al.* 2010). Das Hauptproblem hierbei sind invasive infiltrierende Tumorzellen, die bei den oben genannten Therapieansätzen nicht erfaßt und entfernt werden können, da sie bereits ins umliegende Gewebe eingewandert sind.

Grundidee dieser Arbeit war es diese negative Eigenschaft der Glioblastomazellen auszunutzen, um diese zu positivem Zweck für die Therapie dieses Gehirnkrebses umzuwandeln. Hierfür wurden biokompatible magnetische Nanopartikel verwendet, die in die Zellen eingeschleust wurden. Nach Aufnahme der magnetischen Nanopartikel wurden die nun magnetisierbaren Zellen in einem externen Magnetfeld zur zielgerichteten Migration angeregt, um bei einer künftigen Anwendung am Patienten die Glioblastoma Zellen aus dem gesunden Gewebe zu separieren (Mucha 2009).
Sämtliche hierfür nötigen Parameter und die benötigte Beschaffenheit des Magnetfeldes mussten zu diesem Zweck etabliert werden. Ein permanentes Magnetfeld wurde entwickelt, dessen Magnetfluss auf die Zellebene konzentriert ist.
Die Aufnahme der Nanopartikel in die Zellen und deren Verträglichkeit, wurde an Glioblastomzellen und primären humanen Astrocyten (als Kontrollgruppe für gesundes Gewebe) unter *in vitro* Bedingungen mit und ohne Magnetfeld getestet. Die Ergebnisse zeigten, dass die verwendeten Ferrofluide von den Zellen konzentrationsabhängig aufgenommen werden und sehr gut verträglich für die Astrocyten sind (Avdeev, Mucha *et al.* 2010) während bei mehreren Glioblastom-Zelllinien eine signifikante Reduktion des Zellwachstums beobachtet werden konnte.
Mikroskopische Analysen der Zellorganell-Struktur demonstrierten eine konzentrationsabhängige Zunahme und Vergrößerung der Lysosomen, die bei den Glioblastomazellen wesentlich ausgeprägter ist und mit der Reduktion des Zellwachstums korrelierte. Analysen nach 24h Expositionszeit im Magnetfeld führten bei nanopartikelhaltigen Glioblastomazellen zu Polarisierung der Zellen mit Ausrichtung der Lysosomen zum magnetischen Gradienten, während Astrocyten keine Reaktion auf das Magnetfeld zeigten.
Mit Glioblastomazellen konnte das angestrebte Ziel einer zielgerichteten Migration erreicht und im Laufe der Arbeit stetig verbessert werden.
Immunhistochemische Analysen von Komponenten des Zytoskeletts und an deren Aufbau beteiligtem Protein N-WASP bestätigten, dass es sich hierbei um eine aktive Migration der Zellen handelt. Nanopartikelhaltige Krebszellen weisen im Magnetfeld nicht nur eine Starke Polarisierung zum Gradienten auf sondern zeigen eine sehr starke Aktivität von N-WASP und die Ausbildung vieler Filopodien. Diese aktive Migration wird durch die in den Zellen enthaltenen Nanopartikel Zugstress abhängig induziert und möglicherweise über den Cdc42 Signalweg gesteuert. Astrocyten hingegen zeigen keine Reaktion auf das Magnetfeld.

Die Ergebnisse zeigen das die magnetisch induzierte zielgerichtete Zellmigration für die Umsetzung als Therapie im Patienten sehr hoffnungsvoll ist, da die Eindringtiefe der invasiven Zellen durchschnittlich 2-3 cm um den Haupttumor beträgt und eine aktive Migration der Krebszellen für deren Separation benötigt wird.

VI References

Alberts Bray, Hopkin J, Lewis R, Roberts W (2011): Molekulare Zellbiologie, Wiley VCH, chapter 13+16

Alexiou C; Jurgons R, Seliger C, Iro H (2006): Medical Applications of Magnetic Nanoparticles. J. of Nanoscience and Nanotechnology Vol. 6: 2762-2768

Avdeev M, Mucha B, Lamszus K, Vekas L, Garamus V, Feoktystov A, Marinica O, Turcu R, Willumeit R (2010): Structure and in Vitro Biological Testing of Water-Based Ferrofluids Stabilized by Monocarboxylic Acids; Langmuir 2010, 26(11):8503-8509

Babincova M, Babinec P. (2009): Magnetic drug delivery and targeting: principles and applications. Biomed Pap Med Fac Univ Palacky Olomouc Czech Repub. 153(4):243-50

Banaclocha MAM, Bókkon I, Banaclocha HM (2009): Long-term memory in brain magnetite Med Hypotheses. 74(2):254-7. Epub 2009 Oct 7.

Bao *et al.* (2006): Glioma stem cells promote radioresistance by preferential activation of the DNA damage response. Nature 444: 756- 760

Bazylinski DA (1999): Synthesis of the bacterial magnetosome: the making of a magnetic personality. Int. Microbiol. 2: 71-80

Beason R and Semm P (1996): Does the avian ophthalmic nerve carry magnetic navigational information? J Exp Biol 199:1241-1244

Benarroch EE (2005): Neuron-astrocyte interactions: partnership for normal function and disease in the central nervous system. Mayo Clin Proc 80: 1326-1338

Behrendt M, Sandros MG, McKinney RA, McDonald K, Przybytkowski E, Tabrizian M and Maysinger D: Imaging and organelle distribution of fluorescent InGaP/ZnS nanoparticles in glial cells; Nanomedicine (2009) 4 (7),747-761

Bica D, Vekas L, Avdeev MV, Marinica O, Socoliuc V, Balasoiu M, Garamus VM (2007): Sterically stabilized water based magnetic fluids: synthesis, structure and properties; Journal of Magnetism and Magnetic Materials 311 17-21.

Black, P. Mc L. (1991) Brain Tumours (second part)
The new England journal of medicine 324, 1555-1564;

Blakemore RP, Frankel RB, and Kalmijn AJ, (1980): South-seeking magneto-tactic bacteria in the southern hemisphere, Nature, 236, 384-385,

Brem H, Piantodosi S, Burger PC, *et al.* (1995): Placebo controlled trial of safety and efficacy of intra operative controlled delivery by biodegradable polymers of chemotherapy for recurrent gliomas.
The Polymer brain Tumor Treatment Group. Lancet 345:1008-1012

Cavenee WK *et al.* (2000): Glioblastoma In: WHO Classification of Tumours. Lyon IARC Press

Clarke *et al.* (2006): Cancer stem cells-perspectives on current status and future directions: AACR workshop on cancer stem cells. Cancer Res. 66: 9339-9344

Coulondre C, Miller JH (1977): Genetic studies of the lac repressor.
Nucleic Acid residues, J.Mol. Biol. 117 525-567

Davila AF, Winklhofer M, Shcherbakov V, Petersen N (2005): Magnetic pulse affects a putative magnetoreceptor mechanism. Biophys J, *89*(1), 56-63

Demuth T and Berens ME (2004): Molecular mechanism of glioma cell migration and invasion. J Neuro Onc 70: 217-228

Demuth T, Rennert JL, Hoelzinger DB *et al.*(2008):
Glioma cells on the run - the migratory transciptome of 10 human glioma cell lines. BMC Genomics 2008, 9:54doi:10.1186/1471-2164-9-54

Dent EW & Gertler FB (2003): Cytoskeletal dynamics and transport in growth cone motility and axon guidance. Neuron 40, 209-207

Dingle JT *et al.*, (1988): Lysosomes in Biology and Pathology, Eds., North Holland Publications Co. (1969), Cell 52, 329

Dobson J and Grassi P (1996): Magnetic Properties of Human Hippocampal Tissue - Evaluation of Artefact and Contamination Sources. Brain Res. Bull., vol. 39: 255-259.

Dringen R, Hirrlinger J (2003): Gluthatione pathways in the brain.
Biol Chem 384:505-516

Dringen R, Liddell JR, Knorpp T *et al.* (2006): Detoxification of hydrogen peroxide by astrocytes. In : Häussinger D, Kircheis G, Scliess F (eds) Hepathic Encephalopathy and Nitrogen Metabolism, Springer, Dordrecht, The Netherlands, pp 50-59

Dringen R, Bishop GM, Koeppe M, Dang T and Robinson SR (2007):
The pivotal role of astrocytes in the metabolism of iron in the brain.
Neurochem. Res. 32, 1884-1890.

Fritsch A, Höckel M, Kiessling T, Nnetu KD,Wetzel F, Zink M and Käs JA (2010):
Are biomechanical changes necessary for tumor Progression?
NATURE PHYSICS Vol 6 October 2010

Feoktystov AV, Avdeev MV, Aksenov VL, Petrenko VI, Bulavin LA, Bica D, Vekas L, Garamus VM, Willumeit R (2009): Contrast Variation in Small-Angle Neutron Scattering from Magnetic Fluids Stabilized by Different Mono-Carboxylic Acids. Solid State Phenomena, 152-153 (2009) 186-189.

Frankel RB, Bazylinski DA, Johnson MS, BL Taylor (1997): Magneto-Aerotaxis in Marine Coccoid Bacteria, Biophys J. Vol.73; 1997:994-1000

Graham CH, Conelly I, MacDougall JR, Kerbel RS,Stetler-Stevenson WG, Lala PK (1994): Resistance of malignant trophoplast cells to both the anti-proliferative and anti-invasive effects of transforming growth factor-beta. Exp Cell Res 214: 93-99,1994

Gorby YA, Beveridge TJ, Blakemore RP (1988): Characterization of the bacterial magnetosome membrane; *J. Bacteriol.,* Vol 170, 834-841.

Grayson RAC., *et al.* (2003): Multi pulse drug delivery from a resorbable polymeric microchip device. Nat Mater 767-72

Greenberg M, Canter K, Mahler I, Tomheim A (2005): Observation of Magnetoreceptive Behaviour in a Multicellular Magnetotactic Prokaryote in Higher Geomagnetic Fields. Biophys. J. Vol. 88:1496-1499

Greulich C, Diendorf J, Simon T, Eggeler G, Epple M, Köller M (Epup. 2010): Uptake and Intracellular distribution of silver nanoparticles in human mesenchymal stem cells. Acta Biomaterialia 2011; 7(1):347-54

Grodzinski P, Silver M, Molnar L (2006): Nanotechnologie for cancer diagnostics: promises and challenges. Expert. Rev. Mol. Diagn. 6(3): 307-318

Groothuis DR (2000): The blood –brain and blood –tumours barriers: a review for strategies for increasing drug delivery. Neuro Oncol 2: 45-59

Hall A (1998): Rho GTPases and the Actin Cytoskeleton; Science 279:509-514

Harris AK, Wild P and Stopak D (1980): Silicone rubber substrata: a new wrinkle in the study of cell locomotion, Science 1980; 208:177-179

de Hauwer C**,** Camby I, Darro F, Decaestecker C, Gras T, Salmon I, Kiss R, Van Ham P (1997): Dynamic characterizations of cell motility *Biochem. and Biophys. Research Communications* 232; 267-272

Held-Feindt J, Bernedo Paredes E, Blömer U, Seidenbecher C, Stark AM, Mehdorn HM and Mentlein R (2006): Matrix-degrading proteases ADAMTS4 and ADAMTS5 (disintegrins and metalloproteinases with thrombospondin motifs 4 and 5) are expressed in human glioblastomas. Int. J. Cancer: 118,55-61 (2006)

Hoepken HH, Korten T, Robinson SR *et al.* (2004): Iron accumulation, iron- mediated toxicity and altered levels of ferritin and transferrin receptor in cultured astrocytes during incubation with ferric ammonium citrate. J Neurochem 88:1194-1202

Hegi ME *et al.* (2005): MGMT gene silencing and benefit from temozolomide in glioblastoma. N Engl J Med 352:997-1003

Hua MY *et al.* (2010): The effectiveness of a magnetic nanoparticles-based delivery system for BCNU in the treatment of gliomas.
Biomaterials Volume 32, Issue 2, January 2011, Pages 516-527

Invitrogen http://probes.invitrogen.com/media/pis/mp03224

Invitrogen a; http:// products.invitrogen.com/ivgn/product/L7528

Islam T, Wolf G (2009): The pharmacokinetics of the lymphotropic nanoparticle MRI contrast agent ferumoxtran-10. Cancer Biomark 2009;5:69-73

Jacinto FV, Esteller M (2007): MGMT hypermethylation: a prognostic foe, a predictive friend; *DNA Repair* **6** (8): 1155–1160

Karlsson HL, Gustafsson J, Cronholm P and Möller L (2009): Size-dependent toxicity of metal oxide particles—A comparison between nano- and micrometer size
Toxicology Letters Volume 188, Issue 2, 24 July 2009, Pages 112-118

Kleihues P, Burger PC and Scheithauer BW (1992): Histological typing of the tumours of the central nervous system, Springer-Verlag Berlin, Cancer Biomark. 2009;5(2):69-73.

Kleihues P, Burger PC, and Scheithauer BW (1993): The new WHO classification of brain tumours. Brain Pathol 1993*; 3:*255-268.

Kleihues P, Soylemezoglu F; Schäuble B, Scheithauer BW,and Burger PC (1995): Histopathology, classification, and grading of gliomas. glia 15, 211-221

Kirschvink JL, and Gould JL (1981) Biogenic magnetite as a basis for magnetic field detection in animals biosystems Volume 13, Issue 3, 1981, Pages 181-201

Kirschvink JL, Kirschvink AK and Woodford B. J (1992a): Magnetite biomineralization in the human brain. Proc. Natl. Acad. Sci. USA.89:7683-7687

Kirschvink JL, Kobayashi-Kirschvink A, Diaz-Ricci JC and Kirschvink SJ (1992b): Ferromagnetic material in human tissue: implications for background levels of ELF exposure. Bioelectromagnetics Suppl. 1:101-113.

Kirschvink JL, Walker MM, Diebel CE (2001): Magnetite-based magnetoreception. Curr Opin Neurobiol. , 11:462-467

Kobayashi A, Yamamoto N and Kirschvink J (1997): Studies of Inorganic Crystals in Biological Tissue: Magnetite in Human Tumor: Kirschvink Reprinted from Journal of the Japan Society of Powder and Powder Metallurgy 44, 294

Kőnczöl M, Ebeling S, Goldenberg E, Treude F, Gminski R, Gieré R, Grobéty B, Rothen-Rutishauser B, Merfort I, Mersch-Sundermann V (2011): Cytotoxicity and Genotoxicity of Size-Fractionated Iron Oxide (Magnetite) in A549 Human Lung Epithelial Cells: Role of ROS, JNK, and NF-κB. Chem Res Toxicol. 2011 Jul 18

Kubo T, Sugita T, Shimose S, Nitta Y, Ikuta Y, Murakami T (2000): Targeted delivery of anticancer drugs with intravenously administered magnetic liposomes in osteosarcoma-bearing hamsters. Int J Oncol. 17(2):309-15.

Kuehnel, W (2003): *Color Atlas of Cytology, Histology, & Microscopic Anatomy* (4th ed.). Thieme. pp. 34. ISBN 1-58890-175-0.

Kückelhaus S, Reis SC, Carneira MF, Tedesco AC, Oliveira DM, Lima ECD,. Morais PC. Azevedo RB and. Lacava ZGM (2004): In vivo investigation of cobalt ferrite-based magnetic fluid and magnetoliposomes using morphological tests. Journal of Magnetism and Magnetic Materials Volumes 272-276, Part 3, May 2402-2403

Lauffenburger DA and Horwitz AF (1996): Cell migration: a physically integrated molecular process. Cell 84, 359-369

Lawson HC, Sampath P, Bohan E *et al.* (2007): Interstitial chemotherapy for malignant gliomas: the John Hopkins experience. J Neurooncol 83:61-70

Lévy M, Lagarde F, Maraloiu VA, Blanchin MG, Gendron F, Wilhelm C, Gazeau F (2010): Degradability of superparamagnetic nanoparticles in a model of intracellular environment: follow-up of magnetic, structural and chemical properties. Nanotechnology. 2010 Oct 1;21(39):395103. Epub 2010 Sep 6.

Liu *et al.* (2006): Analysis of gene expression and chemoresistance of CD133+ cancer stem cells in glioblastoma. Mol Cancer 5: 67

Lehrer S (2010): Anopheles mosquito transmission of brain tumor; Medical Hypotheses Volume 74, Issue 1, January 2010, Pages 167-168

McLeland CB, Rodriguez J, Stern ST (2011): Autophagy monitoring assay: qualitative analysis of MAP LC3-I to II conversion by immunoblot.
Methods Mol Biol. 2011;697:199-206.

Liu H, Liu Y, Liu S, Pang DW, Xiao G (2011): Clathrin-mediated endocytosis in living host cells visualized through quantum dot labeling of infectious hematopoietic necrosis virus. J Virol. 2011 Jul;85(13):6252-62. Epub 2011 Apr 27.

Li Y *et al.* (2004): In vivo release from a drug delivery MEMS device.
J Control Release 100:211-9

Li X, Du X, Huo T, Liu X, Zhang S, Yuan F. (2009): Specific targeting of breast tumor by octreotide-conjugated ultrasmall superparamagnetic iron oxide particles using a clinical 3.0-Tesla magnetic resonance scanner. Acta Radiol. Jul; 50(6):583-94

Liddell JR, Hoepken HH, Crack PJ *et al.* (2006): Gluthatione peroxidase 1 and gluthathione are required to protect mouse astrocytes from iron-mediated hydrogen peroxide toxicity. J Neurosci Res 84:578-586

Liddell JR, Dringen R, Crack PJ *et al.* (2006): Gluthatione peroxidase 1 and a high cellular gluthatione concentration are essential for effective organic hydroperoxide detoxification in astrocytes. Glia 54:873-879

Louis DN *et al.* 2007: The WHO classification of tumours of the central nervous system. Acta Neuropathologica. 114(2):97-109

Machesky L M, Mullins RD, Higgs HN, Kaiser DA, Blanchoin L, May RC, Hall ME and Pollard TD (1999): Scar, a WASp-related protein, activates nucleation of actin filaments by the Arp2/3 complex.
Proc. Natl. Acad. Sci. U.S.A. **96**, 3739–3744

Machesky LM and Insall RH (1998): Scar1 and the related Wiskott–Aldrich syndrome protein, WASP, regulate the actin cytoskeleton through the Arp2/3 complex. Curr. Biol. **8**, 1347–1356

Mastunaga T *et al.* (1996): Enhancement of magnetic particle production by nitrate and succinate fed-batch culture of Magnetospirillum sp. AMB-1.
Biotechnol. Tech. 10: 495-500

Matsunaga T, Okamura Y (2003): Genes and proteins involved in bacterial magnetic particle formation. Trends in Microbiol. Vol. 11: 536-541

van Meir *et al.* (2010): Exciting new advances in neuro-oncology: the avenue to a cure for malignant glioma.
CA Cancer J Clin. 60(3)166-193

Miki H, Suetsugu S and Takenawa T (1998): WAVE, a novel WASP-family protein involved in actin reorganization induced by Rac. EMBO J. 17, 6932–6941

Millard TH, Sharp SJ and Machewsky LM (2004): 1 Signalling to actin assembly via the WASP (Wiskott-Aldrich syndrome protein)-family proteins and the Arp2/3 complex; Biochem. J. 380, 1-17

Miller G (2009): Brain cancer. A viral link to glioblastoma? Science;323(5910):30–1

Möller W, Nemoto I, Matsuzaki T, Hofer T, Heyder J. (2000): Magnetic phagosome motion in J774A.1 macrophages: influence of cytoskeletal drugs.
Biophys J. 2000 Aug;79(2):720-30.

Mora CV, Davison M, Wild JM, Walker MM (2004): Magnetoreception and its trigeminal mediation in the homing pigeon. Nature 432:508-511.

Morawski AM, Lanza GA, Wickline SA (2005): Targeted contrast agents for magnetic resonance imaging and ultrasound. Curr. Opin. Biotechnol. 16(1): 89-92

Mucha B, Willumeit R, Lamszus K; Patentnummer WO 2011/058018; HZG Geesthacht, UK-Eppendorf

Naqvi S, Samim M, Abdin M, Ahmed FJ, Maitra A, Prashant C, Dinda AK (2010): Concentration-dependent toxicity of iron oxide nanoparticles mediated by increased oxidative stress. Int J Nanomedicine. 2010 Nov 16;5:983-9.

Nel A, Xia T, Mädler L and Li N (2006): Toxic Potential of Materials at the Nanolevel *Science 3 February 2006:Vol. 311 no. 5761 pp. 622-627*

Nikon 2009 Personal information of technician personal (Detlef Puetz and Christoph Hamers) Biotechnica

Norden AD, Young GS, Setayesh K, *et al.* (2008): Bevacuzimab for recurrent malignant gliomas; efficacy, toxicity and patterns of recurrence.

Neurology 70:779-787

Perls M (1867): Nachweis von Eisenoxyd in gewissen Pigmenten. *Virchows Archiv für pathologische Anatomie und Physiologie und für klinische Medizin* **39,** 42-48

Pollard TD, Borisy GG (2003): Cellular motility driven by assembly and self assembly of actin filaments, Cell 112 453-465

Rasouli– Nia A *et al.* (1994): Day 3rd, On the quantitative relationship between O^6methylguanine residues in genomic DNA and production of sister-chromatid exchanges, mutations and lethal events in a Mer-human tumor cell line, Mutat. Res. 314 99-113

Regis A, Vilchez MD, Kozinetz CA, Arrington AS, Madden CR and Butel JS (2003): Simian virus 40 in human cancers; The American Journal of Medicine Volume 114, Issue 8, 1 June 2003, Pages 675-684

Rohatgi, R, Ma L, Miki H, Lopez M, Kirchhausen T, Takenawa T and Kirschner MW (1999): The interaction between N-WASP and the Arp2/3 complex links Cdc42-dependent signals to actin assembly. Cell 97, 221–231

Sachdeva MS (1998): Drug targeting systems for cancer chemotherapy.
Expert Opin Investig Drugs. 7(11):1849-64.

Sakaguchi T *et al.* (2002): Desulvovibrio magnetics sp.nov. a Novel Sulfyae Reducing Bacterium That Produces Intracellullar Single-Domain-Sized Magnetite Particles. Int. J. Syst. Evol. Microbiol. 52, 215-221

Sampath P, Brem H (1998): Implantable slow release chemotherapeutics polymers for the treatment of malignant brain tumours. Cancer Control 5:130-137

Schneider T, Thalau H-P, Semm P, Wiltschko W (1994): Melatonin is crucial for the migratory orientation of pied flycatchers Ficedula hypoleuca pallas.
J Exp Biol 1994, 194:255-262.

Schulten K, Swenberg C, Weller A (1978): A biomagnetic sensory mechanism based on magnetic field modulated coherent electron spin motion. Z Phys Chem 1978, NF111:1-5.

Schultheiss D, Kube M, Schueler D (2004): Inactivation of the Flagellin Gene flaA in Magnetospirillum gryphiswaldense Results in Nonmagnetotactic Mutants Lacking Flagellar Filaments. Applied and environmental Microbiology: 3624-3631

Seregin SS, Amalfitano A (2011): Gene Therapy for Lysosomal Storage Diseases: Progress, Challenges and Future Prospects. Curr Pharm Des. 2011 Jul 21

Seong H *et al.* (2003): BCNU –loaded poly (d,l-lactide-co-glycolide) wafer and antitumor activity against XF-498 human CNS tumor cells in vitro. Int J Pharm 2003; 251:1-12

Singh S, Kumar A, Karakoti A, Seal A and Self WT (2010):
Unveiling the mechanism of uptake and sub-cellular distribution of cerium oxide nanoparticles. Mol Biosyst. 2010 October 1;6 (10): 1813-1820.

Spring S and Schleifer KH (1995): Diversity of Magnetotactic bacteria. Syst. Appl. Microbiol. 18, 147-153

Stark DD, Weissleder R, Elizondo G, Hahn PF, Saini S, Todd LE, Wittenberg J, and Ferrucci JT (1988): Superparamagnetic iron oxide: clinical application as a contrast agent for MR imaging of the liver. *Radiology August 1988 168:297-301*

Stieber VW, Mehta MP (2007): Advances in radiation therapy for brain tumours. Neurol Clin 2007; 25:1005-1033

Stormer F *et al.* (2009) Are the Astrocytes involved in magnetite based memory? medical hypotheses 73 (2009) 1072-1080

Stupp R, Mason WP, van den Bent MJ, *et al.* (2005): Radiotherapy plus concomitant and adjuvant temozolomide for glioblastoma. N Engl J Med 2005;352:987-996

Suzuki M, Honda H, Kobayashi T, Wakabayashi T, Yoshida J, Takahashi M. (1996): Development of a target-directed magnetic resonance contrast agent using monoclonal antibody-conjugated magnetic particles. Brain tumor Pathology 1996 Nov;13(2):127-32

Symons M, Derry JM, Karlak B, Jiang S, Lemahieu V, McCormick F, Francke U and Abo A (1996): Wiskott–Aldrich syndrome protein, a novel effector for the GTPase CDC42Hs, is implicated in actin polymerization. Cell **84**, 723–734

Tan YB, Wu XY, Zhang JF, Zhang MM (2010): [Magnetic resonance signal detection of superparamagnetic iron oxide nanoparticles and its biological effects on endothelial cells]. Zhejiang Da Xue Xue Bao Yi Xue Ban. 2010 Mar;39(2):118-24.

Torti FM, Torti SV, (2002): Regulation of Ferritin genes and protein,
Blood 99: 3505-3516

Tzima E, Kiosses WB, del Pozo MA and Schwartz MA (2003): Localized Cdcd42 Activation, detected using a novel assay, mediates microtubule organizing center positioning in endothelial cells in response to fluid shear stress, J of Bio Chem Vol. 278 No 33, 31020-31023

Valberg PA, Albertini DF (1985): Cytoplasmic motions, rheology, and structure probed by a novel magnetic particle method.
J Cell Biol. 1985 Jul;101(1):130-40.

Weller Prof. Dr. (2011) Personal talk at 28.07.2011 at the University Hamburg, Department for Chemistry

Wen Tien Chen (1981): Mechanism of retraction of the trailing edge during fibroblast movement, J. Cell Biol. 1981 July1 90(1) 187-200

Westphal M, Hilt DC, Bortey E *et al.* (2003): A phase 3 trial of local chemotherapy with biodegradable carmustine (BCNU) wafers (Gliadel wafers) in patients with primary malignant glioma. Neuro Oncol 2003;5:75-88

Wolf F and Kirchhoff F (2008): Imaging Astrocyte Activity Science Vol320, 2008

Wu X, Suetsugu S, Cooper LA, Takenawa T, Guan JL (2004): Focal adhesion Kinnase Regulation of N-WASP Subcellular Localization and Function,
J of Biol ChemVol. 279; 10:9965-9576

Xux et al (2006): BCNU loaded PEG-PLLA ultrafine fibers and their in vitro antitumor activity against glioma C6 cells. J Control Release 2006; 114:307-316

Xu H, Dai W, Han Y, Xiong F,Zhang Y and Cao JM J Nanosci (2010):
Differential internalization of superparamagnetic iron oxide nanoparticles in different types of cells. Nanotechnol. 2010 Nov; 10(11):7406-10

Zeiss 2009 Personal information of technician personal. Biotechnica

VII List of figures

VIII Abbreviations

ANOVA	Analysis of Variance
ADAMTS4+5	Disintegrins and metalloproteins with thrombospondin motifs 4+5
Arp 2/3	Actin related protein
ATP	Adenosintriphosphate
BBB	Blood Brain Barrier
BBS	Berliner Blue Staining
BCNU	Trade name for carmustine
CASY	Electric field cell counting system
Cdc42	Cell division cycle protein 42
cDNA	Complementary DNA
CFX	Computational Fluid Dynamics program
CNS	Central nervous system
DAPI	4´,6-diamindino-2-phenylindole
DMEM	Dulbecco´s Modified Eagle Medium
DMSO	Dimethyl Sulfoxid
DNA	Desoxyribonucleinacid
ER	Endoplasmic Reticulum
FAD	Photopigment flavin dehydrogenase
FCS	Fetal Calf Serum
GTP	Guanosine triphosphate
ICP-MS	Inductively coupled plasma mass spectrometry
IgG	Immunglobulin G
KCl	Potassiumchloride
KH_2PO_4	Monopotassiumphophate
Lyso	Lysosomes
MGMT	methylguanylmethyltransferase
MMB	Magnetotactic Multicellular Prokaryote
MPS	Mononuclear Phagocyte System
MRI	Magnetic Resonance Imaging
mT	Milli Tesla

MTOC	Microtubule organization center
Na_2HPO_4	Disodium Hydrogen Phosphate
NaCl	Sodiumchloride
NP-LA	Nanoparticles coated with lauricacid
NP-MA	Nanoparticles coated with myristicacid
OATZ	Oxic –anoxic transition zone
PBS	Phosphate buffered saline
pH	Measure of acidity or alkalinity
Rac	Monomere GTPases, Rho family
rcf	Relative centrifuge force
RF	Radio Frequency
Rho	GTPases
RNA	Ribonucleinacid
ROS	Reactive oxygen species
rRNA	Ribosomale RNA
RT-qPCR	Real-Time quantitative Poly Chain Reaction
Scar/WAVE 1	WASP-family protein
SV40	Simian Virus 40
TEM	Transmission Electron Microscopy
TfRC	Transferrin receptor C
VEGF	Vascular endothelial growth factor
WASP	Wiskott Aldrich Syndrom Protein
WHO	World Health Organization
µm	micrometer
3D	Three dimensional

IX Acknowledgements

This work was funded by the Helmholtz Russian Joint Research Group 016 and has been performed at the Institute of Materials Research, Department of Structural Research on Macromolecules, at the Helmholtz Centre Geesthacht.

First of all I want to thank my supervisor Prof. Regine Willumeit, I'm deeply indebted for having me offered the opportunity of research on this fascinating theme and for all the valuable discussions, the contribution of my work and the detailed proofreading. Not forgetting for all the other times she was "pushing" me forwards.
Prof. Ulrich Hahn I want to thank for the "official" supervising and all the answers he gave me.
I´m really appreciated that it was possible to accomplish the ICP-MS in the working group of Prof. Andreas Prange. Dr. Daniel Pröfrock gets my gratefulness for the help with the measurements. Prof. Horst Weller and Prof. Lothar Renwrantz I want to thank for their time and the interesting discussions about tricky little things called nanoparticles and lysosomes.
Special thanks as well to our nice cooperation partners Prof. Katrin Lamszus, Dr. Ladislaus Vekas, Dr. Mikhail Avdeev and all the others supporting this work, it was a pleasure to work with you.
I'm very grateful for Dr. Anna Schuster believing that mothers can do this and the never-ending motivation. Thank you, you are really a friend.
Dipl. Ing Gerhard Kozik and Bernhard Eltzschig were helping me constructing the magnets, Gerhard always risk his fingers, if the magnets had to be changed.
Dipl. Ing. Rudolf Zettler and Dr. Jonathan Paul: Thanks so much for the English proofreading, I'm starting to think English now.

My working group – WPS - I want to say: I had a great time with very special people, much cake, coffee and some barbecue, lab- party AND very nice support. Thank you, I was feeling home the last years. I have also received considerable assistance by our technician Gabriele Salamon, often starting incubations at the weekend.

Last but not least, I'm very grateful to my family, they were always catching me up, motivating and supporting me, when I lost believe. My husband I want to thank for living, loving and laughing with me during all this time.

Erklärung über frühere Promotionsversuche

Hiermit erkläre ich, dass vorher keine weiteren
Promotionsversuche unternommen worden sind, oder an einer anderen Stelle vorgelegt wurden.

Hamburg, den .....
……
(Unterschrift)

Eidesstattliche Versicherung

Hiermit erkläre ich an Eides statt, dass die vorliegende Dissertationsschrift selbständig und allein von mir unter den angegebenen Hilfsmitteln angefertigt wurde.

Hamburg, den …….
……
(Unterschrift)